

**Arctic spring and summertime aerosol optical depth baseline from
long-term observations and model reanalyses - Part 1: climatology
and trend**

Peng Xian¹, Jianglong Zhang², Norm T. O'Neill³, Travis D. Toth⁴, Blake Sorenson²,
Peter R. Colarco⁵, Zak Kipling⁶, Edward J. Hyer¹, James R. Campbell¹, Jeffrey S. Reid¹
and Keyvan Ranjbar^{3, a}

¹Naval Research Laboratory, Monterey, CA, USA.

²Department of Atmospheric Sciences, University of North Dakota, Grand Forks, ND

³Département de géomatique appliqué, Université de Sherbrooke, Sherbrooke, Québec,
Canada

⁴NASA Langley Research Center, Hampton, Virginia, USA.

⁵NASA Goddard Space Flight Center, Greenbelt, MD, USA.

⁶European Centre for Medium-Range Weather Forecasts, Reading, UK.

^anow at: Flight Research Laboratory, National Research Council Canada, Ottawa, ON,
Canada

Correspondence: Peng Xian (peng.xian@nrlmry.navy.mil)

Abstract

We present an Arctic aerosol optical depth (AOD) climatology and trend analysis for 2003-2019 spring and summertime periods derived from a combination of multi-agency aerosol reanalyses, remote sensing retrievals, and ground observations. This includes the U.S. Navy Aerosol Analysis and Prediction System ReAnalysis version 1 (NAAPS-RA v1), the NASA Modern-Era Retrospective Analysis for Research and Applications, version 2 (MERRA-2), and the Copernicus Atmosphere Monitoring Service ReAnalysis (CAMSRA). Space-borne remote sensing retrievals of AOD are considered from the Moderate Resolution Imaging Spectroradiometer (MODIS), the Multi-angle Imaging SpectroRadiometer (MISR), and Cloud-Aerosol Lidar with Orthogonal Polarization (CALIOP). Ground-based data include sun photometer data from Aerosol Robotic Network (AERONET) sites and oceanic Maritime Aerosol Network (MAN) measurements. Aerosol reanalysis AODs and space-borne retrievals show consistent climatological spatial patterns and trends for both spring and summer seasons over the lower-Arctic (60-70°N). Consistent AOD trends are also found for the high Arctic (north of 70°N) from reanalyses. The aerosol reanalyses yield more consistent AOD results than climate models, verify well with AERONET, and corroborate complementary climatological and trend analysis. Speciated AODs are more variable than total AOD among the three reanalyses, and a little more so for March-May (MAM) than for June-August (JJA). Black Carbon (BC) AOD in the Arctic comes predominantly from biomass burning (BB) sources in both MAM and JJA, and BB overwhelms anthropogenic sources in JJA for the study period.

AOD exhibits a multi-year negative MAM trend, and a positive JJA trend in the Arctic during 2003-2019, due to an overall decrease in sulfate/anthropogenic pollution, and a significant JJA increase in BB smoke. Interannual Arctic AOD variability is significantly large, driven by fine-mode, and specifically, BB smoke, with both smoke contribution and interannual variation larger in JJA than in MAM. It is recommended that climate models should account for BB emissions and BB interannual variabilities and trends in Arctic climate change studies.

1. Introduction

The Arctic is warming faster than the overall global climate, a phenomenon widely known as Arctic amplification (Serreze and Francis 2006; Serreze and Barry 2011). This has led to rapid changes in regional sea ice properties. September sea ice coverage is shrinking at an unprecedented rate (Comiso 2012; Meier et al., 2014). Younger and thinner ice is replacing thick multi-year sea ice (Kwok and Rothrock 2009; Hansen et al, 2013; Rosel et al. 2018). Mechanisms contributing to sea ice changes include increased anthropogenic greenhouse gases (Notz and Stroeve 2016; Dai et al., 2019), sea ice-albedo feedback (Perovich and Polashenski 2012), increased warm and moist air intrusion into the Arctic (Boisvert et al. 2016; Woods et al., 2016; Graham et al. 2017), radiative feedbacks associated with cloudiness and humidity (Kapsch et al. 2013; Morrison et al. 2018), and increased ocean heat transport (Nummelin et al., 2017; Taylor et al. 2018). However, one of the least understood factors of Arctic change is the impact of aerosols on sea ice albedo and concentration (IPCC 2021).

Atmospheric aerosol particles from anthropogenic and natural sources reach or can be found in the Arctic region as the result of long-range transport and local emissions respectively. This affects regional energy balance through both direct and indirect radiative processes (Quinn et al., 2008; Engvall et al., 2009; Flanner, 2013; Sand et al., 2013; Markowicz et al., 2021; Yang et al., 2018). Aerosol particles influence cloud microphysical properties as cloud condensation nuclei (CCN) and/or ice nucleating particles (INP), affecting cloud albedo, lifetime, phase, and probability of precipitation (e.g., Lubin and Vogelmann, 2006; Lance et al., 2011; Zamora et al, 2016; Zhao and Garrett 2015; Bossioli et al., 2021). Additionally, deposition of light-absorbing aerosol species such as dust and black/brown carbon on the surface of snow and ice can trigger albedo feedbacks and facilitate melting and prolong melting seasons (Hansen & Nazarenko, 2004; Jacobson, 2004; Flanner et al., 2007; Skiles et al., 2018; Dang et al., 2017; Kang et al., 2020). However, the impact of aerosol particles on polar climate change is still not well characterized, and their relative importance compared to other warming factors is difficult to isolate and quantify.

Climate modeling studies show that due to stronger feedback processes between the atmosphere-ocean-sea-ice-land the Arctic region is more sensitive to local changes in radiative forcing than tropical and mid-latitude regions (Shindell and Faluvegi 2009; Sand et al., 2013). Furthermore, there seems to be an emerging agreement on a higher sensitivity of Arctic clouds by aerosol particles than lower-latitude regions due to the very low aerosol amounts compared to lower latitudes (Prenni et al., 2007; Mauritsen et al. 2011; Birch et al., 2012; Coopman et al., 2018; Wex et al., 2019). Both underscore the important role aerosol particles may play in the Arctic weather and climate, and the urgency to better quantify the amount of aerosols in the Arctic.

A variety of atmospheric aerosol species exist in the Arctic region. Anthropogenic pollution contributes significantly to the formation of the Arctic haze, which generally occurs in later winter and spring due to wintertime build-up in the shallow boundary layer with effective transport and reduced removal (e.g., Law and Stohl, 2007; Quinn et al., 2008). Biomass burning (BB) smoke, originating from wildfires in boreal North America and Eurasia, are often observed and/or modeled being transported into the Arctic (Eck et al. 2009; Eckhardt et al. 2015; Stohl et al. 2007; Warneke et al. 2009; Iziomon et al., 2006; Evangeliou et al. 2016; Kondo et al., 2011; Brieder et al., 2014; Markowicz et al. 2016; Khan et al., 2017; Engelmann et al., 2021). Airborne dust, emitted from exposed sand or soils due to glacier retreat (Bullard et al., 2016; Groot Zwaaftink et al., 2016), are likely on the rise as the Arctic warms. Dust can also originate from lower latitude deserts, e.g., Sahara and Asia, and arrive in the Arctic through long-range transport (Stone et al, 2007; Breider et al., 2014; AboEl-Fetouh et al., 2020). As the Arctic sea-ice melts and the ice-free surface increases, emissions of sea salt and biogenic aerosols (e.g., from dimethylsulfide; Dall et al., 2017; Gabric et al., 2018) are expected to increase. There are also ultrafine particles nucleated from gaseous precursors, though in small amounts (Baccarini et al., 2021; Abbatt et al., 2019).

Because of the harsh surface environment endemic to the Arctic, aerosol field measurements are limited in comparison with the mid-latitude and tropical environments. Despite an increasing number of field campaigns carried out over the past two decades (e.g., review by Wendisch et al., 2019; and more recently the MOSAiC, <https://mosaic-expedition.org>) and their usefulness in improving process-level understanding, field measurement periods tend to be short and limited to certain areas and thus are not necessarily representative spatially and temporally of the whole Arctic. There are many Arctic-aerosol optical property studies that are based on long-term site measurements (e.g., Herber et al., 2002; Tomasi et al., 2007; Eck et al., 2009; Glantz et al., 2014; Ranjbar et al., 2019; AboEl-Fetouh et al., 2020). The number of sites is, however, limited and of irregular spacing (mostly located at the northern edge of the North American, Eurasian continents, and the Svalbard region).

Climate models that are not well constrained by observations exhibit large variations in basic aerosol optical properties: one finds, for example, an order of magnitude difference in simulated regional aerosol optical depth (AOD) and large differences in the simulated seasonal cycle of AOD over the Arctic (e.g., Glantz et al., 2014; Sand et al., 2017). Such results will not reduce the uncertainty in the radiative impact of aerosols through direct (including surface albedo effect) and indirect forcings in the Arctic climate. Impacts of aerosols and clouds, overall, constitute one of the largest sources of uncertainty in climate models (IPCC 2013). This is apparently exacerbated in a warming Arctic (Goosse et al., 2018). A modeling study by DeRepentigny et al. (2021) shows that

the inclusion of interannually varying BB emissions, compared with only climatological emissions, results in simulations of large Arctic climate variability and enhanced sea ice loss. This finding suggests the sensitivity of climate relevant processes to aerosol interannual variability in the Arctic.

In this paper, we present an AOD climatology and trend analysis for the 2003-2019 Arctic spring and summertime, based on a combination of multi-national interagency aerosol reanalyses, satellite remote sensing retrievals, and ground observations. We define the Arctic and the high-Arctic as regions north of 60°N and 70°N respectively. The lower-Arctic is defined as regions between 60°N-70°N. To reference lower-latitude source influences, the area of 50°N-90°N is included for context.

There are clear advantages to using aerosol reanalyses of chemical transport models in comparison with climate models for Arctic aerosol studies. Smoke emissions are frequently updated (hourly rather than monthly BB smoke emission sources for example) while satellite observations of both meteorological and aerosol data are also incorporated into those aerosol reanalyses through data assimilation. High-latitude fires are strongly influenced by weather patterns including large-scale transport patterns (e.g., Flannigan and Harrington 1998; Skinner et al. 1999). Thus, BB smoke in particular, is more realistically accounted for in aerosol reanalyses.

To our knowledge, this is the first time aerosol reanalysis products are evaluated and compared over the Arctic. The goal of the study is to provide a baseline of AOD distribution, magnitude, speciation, and interannual variability over the Arctic during the sea ice melting season. Statistics of Arctic extreme AOD events is provided in a companion paper (Part 2). The baseline can be used for evaluating aerosol models, calculating aerosol radiative forcing, and providing background information for field campaign data analysis and future field campaign planning in a larger climate context. This paper is organized as follows: Sect. 2 and 3 introduce the data sets and methods respectively. Sect. 4 verifies the reanalyses. Results are reported in Sect. 5. Discussions and conclusions are provided in Sect. 6 and 7.

2. Data

A combination of aerosol reanalyses, satellite-based aerosol remote sensing data, and ground-based aerosol measurements are used to describe source dependent AOD and its trend over the Arctic during spring (i.e., MAM) and summertime (i.e., JJA). The aerosol reanalyses include the Navy Aerosol Analysis and Prediction System reanalysis (NAAPS-RA; Lynch et al., 2016) developed at the Naval Research Laboratory, the NASA Modern-Era Retrospective Analysis for Research and Applications, version 2 (MERRA-2; Randles et al., 2017), and the Copernicus Atmosphere Monitoring Service ReAnalysis (CAMSRa; Inness et al., 2019) produced at ECMWF. The remote sensing

data include AOD retrievals from the Moderate Resolution Imaging Spectroradiometer (MODIS; Levy et al., 2013), the Multi-angle Imaging SpectroRadiometer (MISR; Kahn et al., 2010), and Cloud-Aerosol Lidar with Orthogonal Polarization (CALIOP). Sun photometer data from Aerosol Robotic Network sites and oceanic Maritime Aerosol Network measurements were employed as key validation components (respective citations of AERONET; Holben et al., 1998 and MAN, Smirnov et al., 2009). Overviews of remote sensing techniques for Arctic aerosols can be found in Tomasi et al. (2015) and Kokhanovsky et al. (2020). The analysis period is focused on 2003-2019, when all three aerosol reanalyses are available. A summary of the datasets is provided in Appendix A.

2.1 MODIS AOD

AOD data from MODIS on Terra and Aqua was based on Collection 6.1 Dark Target and Deep Blue retrievals (Levy et al., 2013). Additional quality control and some corrections were applied as described in Zhang and Reid 2006, Hyer et al. 2011, Shi et al. 2011, and Shi et al. 2013, and were updated for the Collection 6.1 inputs. The 550 nm quality-assured and quality-controlled MODIS C6 AOD data are a level 3 product that is produced at $1^\circ \times 1^\circ$ latitude/longitude spatial and 6-hrly temporal resolution. Those 6-hrly (averaged) MODIS AOD data were then monthly-binned in order to study long-term aerosol climatology and trends. Seasonally-binned (year to year) means and trends were derived only when the total count of $1^\circ \times 1^\circ$ degree and 6-hrly data exceeded 10 for a season.

2.2 MISR AOD

The MISR instrument onboard the Terra satellite platform provides observations at nine different viewing zenith angles across four different spectral bands ranging from 446 to 866 nm. These instrumental configurations facilitate AOD retrievals over bright surfaces, such as desert regions (Kahn et al., 2010). MISR Version 23 AOD data at 558 nm (Garay et al., 2020) were analyzed. No MISR AOD is available over Greenland due to snow and ice coverage. Monthly gridded MISR AOD data were created by averaging only MISR data with 100% clear pixels (as defined by each pixel's 'cloud screening parameter') at a spatial resolution of $1^\circ \times 1^\circ$ latitude/longitude. Only monthly grid cells whose number of MISR 100%-cloud-clear AODs was greater than 20 were used to derive the climatology and trend.

2.3 CALIOP AOD

Cloud-Aerosol Lidar with Orthogonal Polarization (CALIOP), the primary instrument on the Cloud-Aerosol Lidar and Infrared Pathfinder Satellite Observations (CALIPSO)

satellite, is a polarization-sensitive lidar that operates at two wavelengths (532 and 1064 nm; Winker et al. 2003). It has, since its launch in 2006, collected a continuity of vertical aerosol and cloud profiles. We primarily used daytime and nighttime 532 nm aerosol extinction coefficient data from the Version 4.2 (V4.2) Level 2 (L2) aerosol profile product (Kim et al., 2018). The product resolution is 5 km in horizontal and 60 m in vertical. The aerosol layer product was used for quality assurance (QA) procedures. The CALIOP aerosol profiles are rigorously QAed before analysis (Campbell et al. 2012; Toth et al. 2016; 2018). Only cloud-free CALIOP profiles are used: this was determined through the atmospheric volume description (AVD) parameter included in the aerosol profile product (i.e., we excluded CALIOP profiles with any range bin classified as cloud by the AVD parameter). A significant portion of CALIOP aerosol profile data consists of retrieval fill values (-9999s, or RFVs) that are, in part, due to the minimum detection limits of the lidar. In fact, over 80% of CALIOP profiles consist entirely of RFVs in some Arctic regions (Toth et al. 2018). These result in zero-valued column AODs: their inclusion in composites would artificially lower the mean AOD. They were thus excluded from our analysis. We also tested retaining AOD=0 values in our analysis and that did not change the AOD trends (see more discussions in section 6). Lastly, the cloud-free QAed profiles without AOD=0 profiles were used to compute mean CALIOP AODs at 2° x 5° latitude/longitude resolution. To ensure spatial and temporal representation, seasonally-binned means and trends were derived only when the total count of gridded data in any season exceeded 20.

2.4 AERONET

The AErosol ROBotic NETwork (AERONET) is a ground-based global sun photometer network. AERONET instruments measure sun and sky radiance in spectral bands ranging from the near-ultraviolet to the short-wave-infrared. This network has been providing daytime aerosol-property measurements since the 1990s (Holben et al., 1998; Holben et al., 2001). Only cloud-screened, quality-assured version 3 Level 2 AERONET data (Giles et al., 2019) are used in this study.

The 500 nm fine mode (FM) and coarse mode (CM) AODs from the Spectral Deconvolution Method (SDA) of O'Neill et al. (2003), along with the FM spectral derivative at 500 nm are used to extrapolate FM AOD to 550 nm (assuming equal CM AOD at 500 and 550 nm). Total AOD is simply the sum of FM and CM AODs. The SDA product is an AERONET product that has been verified using in situ measurements (see for example Kaku et al., 2014) and a variety of co-located lidar experiments (see, for example, Saha et al., 2010 and Baibakov et al., 2015). The FM and CM separation is effected spectrally: this amounts to a separation of the FM and CM optical properties associated with their complete FM and CM particle size distributions. This optical separation, characterized by the ratio of FM AOD to total AOD at 550 nm is referred to as the fine mode fraction (FMF). An analogous FM and CM AOD separation in terms of

a cutoff radius applied to a retrieved or measured particle size distribution is referred to as the sub-micron fraction (SMF; where the numerator of the SMF is the FM AOD associated with the AOD contribution of particles below a cutoff radius). The SMF is the basis for separating FM and CM components in the AERONET (AOD & sky radiance) inversion. The SDA algorithm and the AERONET inversion generate FM and CM AODs that are moderately different (see, for example, Sect. 4 of Kleidman et al., 2005). The advantage of the SDA is its significantly shorter intersampling time and thus retrieval numbers (~ 20 / hour vs ~ 1 / hour for the AERONET inversion), its independence from a variable cut off radius and its greater operational generality (being applicable to other networks such as the MAN sunphotometer network).

AERONET data were binned into 6-hr intervals centered at normal synoptic output times of the reanalyses (0, 6, 12, and 18 UTC) and then averaged within the bins. Monthly-mean temporal representativeness was rendered more likely by only including means with more than 18 6-hr data bins. Ten AERONET sites (Table 1, Fig. 1) were selected based on regional representativeness (coupled with the reality of the sparsity of AERONET sites in the Arctic), the availability of data records between Jan 2003 and Dec 2019, and for easier comparison with other Arctic studies (e.g., Sand et al., 2017). To explore the potential impact of different sampling resolutions on the results (e.g., Balmes et al., 2021), we generated daily AOD statistics (Table S1) that could be compared with Table 1 6 hrly statistics. In general, the mean and median of MAM or JJA AODs (including total, FM and CM AODs) at the ten AERONET sites change very slightly (mostly 0.00, or ≤ 0.01). The daily AOD standard deviation was less than its 6 hrly analogue.

We found that thin clouds could occasionally be identified and retrieved as CM aerosols in level 2, version 3 AERONET data. These retrievals were manually removed by identifying such thin clouds using Terra and Aqua visible-wavelength imagery from [NASA Worldview](#) and comparing 6-hrly NAAPS-RA with AERONET AODs. CM AODs greater than the 3-sigma level were then also removed (as per AboEl-Fetouh et al., 2020).

2.5 MAN AOD

The Marine Aerosol Network (MAN) is a hand-held Microtops sun photometer (research vessel based) counterpart to AERONET: ocean measurements are acquired where no-land based AERONET site can exist (Smirnov et al., 2009, 2011). The products share AERONET product nomenclature and data processing is similar to that of AERONET. Level 2 data above 70°N for were employed in this study. SDA-based FM and CM AOD at 550 nm were derived and averaged over 6-hr time bins.

286 2.6 NAAPS AOD reanalysis v1

287 The Navy Aerosol Analysis and Prediction System (NAAPS) AOD ReAnalysis (NAAPS-
288 RA) v1 provides 550 nm, global-scale, speciated AODs at 1°x 1° spatial and 6-hrly
289 temporal resolution for the years 2003-2019 (Lynch et al., 2016). This NAAPS-based
290 reanalysis incorporates assimilation of quality-controlled, MODIS and MISR AOD
291 retrievals (Zhang et al., 2006; Hyer et al., 2011; Shi et al., 2011). AODs from
292 anthropogenic and biogenic fine aerosol species (ABF; a non-BB sources mixture of
293 sulfate, black carbon or BC, organic aerosols and secondary organic aerosols), dust,
294 BB smoke, and sea salt aerosols are available. The aerosol source functions were
295 tuned to obtain the best match between the model FM and CM AODs and the
296 AERONET AODs for 16 regions globally. Wet deposition processes were constrained
297 with satellite-derived precipitation (Xian et al., 2009). The reanalysis reproduces the
298 decadal AOD trends found using standalone satellite products (e.g., Zhang et al., 2010;
299 2017 who excluded polar regions due to lack of verification data).

300 2.7 MERRA-2 AOD reanalysis

301 NASA Modern-Era Retrospective Analysis for Research and Applications, version 2
302 (MERRA-2) includes an aerosol reanalysis scheme that incorporates AOD assimilation
303 of a variety of remote sensing data sources, including MODIS and MISR after 2000. The
304 aerosol module used for MERRA-2 is the Goddard Chemistry, Aerosol Radiation and
305 Transport model (GOCART; Chin et al. 2000; Colarco et al., 2010). It provides
306 simulations of sulfate, black and organic carbon, dust and sea salt aerosols. A detailed
307 description and global validation of the AOD reanalysis product can be found in Randles
308 et al. (2017) and Burchard et al. (2017). Monthly mean speciated AODs and total AOD at
309 550 nm with 0.5° latitude and 0.625° longitude spatial resolution were used for this
310 study.

311 2.8 CAMSRA AOD reanalysis

312 The Copernicus Atmosphere Monitoring Service (CAMS) Reanalysis (CAMSRA) is a
313 new ECMWF-led global reanalysis of atmospheric composition (Inness et al., 2019). It
314 followed on the heels of the MACC reanalysis (Inness et al., 2013) and CAMS interim
315 reanalysis (Flemming et al., 2017). The dataset covers the period of 2003–2020 and is
316 being extended to subsequent years. The model is driven by the Integrated Forecasting
317 System (IFS) used at ECMWF for weather forecasting and meteorological reanalysis
318 (but at a coarser resolution). It incorporates additional modules activated for prognostic
319 trace gases and aerosol species, including dust, sea salt, organic matter, black carbon
320 and sulfate. Satellite retrievals of total AOD at 550 nm are assimilated from MODIS for
321 the whole period, and from the Advanced Along-Track Scanning Radiometer for 2003–
322 2012, using a 4D variational data assimilation system with a 12-hour data assimilation

window along with meteorological and trace gas observations. The speciated AOD products with monthly temporal resolution and a $\sim 0.7^\circ$ spatial resolution were used in this study. Model development has generally improved the speciation of aerosols compared with earlier reanalyses, and evaluation against AERONET globally is largely consistent over the period of the reanalysis.

2.9 Multi-reanalysis-consensus (MRC) AOD

All three of the individual reanalyses are largely independent in their underlying meteorology and in their aerosol sources, sinks, microphysics, and chemistry. They were also generated through data assimilation of satellite and/or ground-based observations of AOD. The assimilation methods, and the assimilated AOD observations, including the treatments of the observations prior to assimilation (quality control, bias correction, aggregation, and sampling, etc.), often differ. There is, on the other hand, consistent use of MODIS data with its daily global spatial coverage.

Based on the three aerosol reanalysis products described above, we made an MRC product following the multi-model-ensemble method of the International Cooperative for Aerosol Prediction (ICAP, Sessions et al., 2015; Xian et al., 2019). The MRC is a consensus mean of the three individual reanalyses, with a $1^\circ \times 1^\circ$ degree spatial and monthly temporal resolution. Speciated AODs and total AOD at 550 nm for 2003-2019 are available. This new product is validated here, along with the three component reanalysis members, using ground-based Arctic AERONET observations. Validation results in terms of bias, RMSE, and coefficient of determination (r^2) for monthly-mean total, FM and CM AODs are presented in Tables 2, 3, 4. The MRC, in accordance with the ICAP multi-model-consensus evaluation result, is found to generally be the top performer among all of the reanalyses for the study region.

2.10 Fire Locating and Modeling of Burning Emissions (FLAMBE) v1.0

FLAMBE is a biomass-burning emission inventory derived from a satellite-based active fire hotspot approach (Reid et al., 2009; Hyer et al., 2013). FLAMBE can take satellite fire products from either geostationary sensors, which offer faster refresh rates and observation of the full diurnal cycle, or polar orbiters, which have a greater sensitivity. There are significant daily sampling biases and additional artifacts induced by day to day shifts in the orbital pattern for polar-orbiting satellites (e.g., Heald et al., 2003, Hyer et al., 2013). However, the polar-only version of FLAMBE, which employed MODIS-based fire data, is more appropriate for reanalysis and trend analysis. This is because multiple changes in the geostationary constellation over the study period posed a challenge in terms of smoke source-function consistency. The FLAMBE MODIS-only smoke source was also used in the NAAPS-RA v1 because of the same temporal consistency requirement. FLAMBE shows similar BB emission trends as the yearly BB

emission time series for the Arctic region based on other inventories for a similar study period (using BC emission of Fig. 2 in McCarty et al., 2021). These inventories include the Global Fire Assimilation System (GFAS; Kaiser et al., 2012), and the Global Fire Emission Dataset (GFED; Randerson et al., 2006; van der Werf et al., 2006).

3. Method

The Arctic AOD climatology and trends are analyzed in this study using remote sensing products derived from MODIS, MISR, CALIOP, and AERONET (each sensor typically generating aerosol products of different native wavelengths). The 550 nm AOD was employed as the benchmark parameter since the three aerosol reanalyses AODs and the MODIS AOD are all available at 550 nm while the 558nm and 532nm AODs of MISR and CALIOP are appreciably close to 550 nm. AERONET and MAN modal AODs at 550 nm were derived using the SDA method as described in Sect. 2.4 and 2.5. Arithmetic means were employed for all the data processing in order to be consistent with the arithmetic statistics that are usually reported in the literature and with the arithmetic statistics of the monthly data from the aerosol reanalyses. Various studies have shown that geometric statistics are more representative of AOD histograms (see, for example, Hesaraki et al., 2017 and Sayer et al., 2019). However, Hesaraki et al. (2017) showed that arithmetic statistics could be employed to readily estimate geometric statistics¹. This option effectively renders the reporting of arithmetic or geometric statistics less critical.

The species of interest are BB smoke, ABF in NAAPS, and its analogue of sulfate for MERRA-2 as well as CAMSRA and dust and sea salt aerosols. Anthropogenic aerosol particles, as external climate forcers, have drawn some attention in climate studies (e.g., Wang et al., 2018; Ren et al., 2020; Yang et al., 2018; Sand et al., 2016; Eckhardt et al., 2015; Brieder et al., 2017). However, BB smoke, which can be both natural and anthropogenic in origin, has been shown to be the largest contributor (over the last two decades) to Arctic summer AOD and concentration (Evangelidou et al. 2016; Sand et al. 2017 for modelling studies and Eck et al. 2009; Eckhardt et al. 2015; Stohl et al. 2007; Warneke et al. 2009 for observational-based studies). Recent BC measurements in Arctic snow also show a strong association with BB based on modelled tracer correlations with measured optical properties of snow (Hegg et al., 2009; Doherty et al., 2010; Hegg et al., 2010; Khan et al., 2017). A climate modeling study recently found that much larger Arctic climate variability and enhanced sea ice melting were introduced using BB emissions with interannual variability as opposed to fixed climatological monthly-mean BB emissions (DeRepentigny et al., 2021), a result that underscored the importance of quantifying the magnitude and interannual variability of BB smoke in

¹ with an erratum: the equation (2) transformation to geometric mean should be $\tau_{g,x} = \frac{\langle \tau_x \rangle}{\exp\left(\frac{\ln^2 \mu_x}{2}\right)}$

Arctic climate forcing estimates. Thus BB smoke AOD is separated out from the total AOD as a singularly important species in this study.

The separation of species in this analysis is a bit arbitrary since the representation of different aerosol types and sources in each reanalysis is slightly different. The NAAPS model is unique compared to other reanalyses and operational models in that it carries aerosol species by source rather than chemical speciation. For example, biomass burning and ABF are carried as separate species and permit explicit hypothesis testing about the sources, sinks, and optical properties. Conversely, MERRA-2 and CAMSRA carry organic carbon (OC)/organic matter (OM), BC and various inorganic species combining a multitude of anthropogenic, biogenic and biomass burning source pathways. In this study the sum of OC/OM and BC AOD is used to approximate BB smoke AOD from CAMSRA and MERRA-2. The ratio of BC AOD to the sum of BC and OC/OM AOD is, on average, about 10% for areas north of 60°N for both MERRA-2 and CAMSRA for both MAM and JJA (the single exception to this is that the MERRA-2 ratio is about 18% in MAM). The ratios change little for area >70°N and area >80°N.

It is worth noting that the three reanalyses use either hourly or daily BB smoke emission inventories: inventories that employ dynamic smoke sources detected by polar-orbiting satellites. Examples include FLAMBE (Reid et al., 2009) for NAAPS-RA, Quick Fire Emissions Dataset (QFED) for MERRA-2 after 2010 (GFED with monthly BB emission before 2010 as per Randerson et al., 2006 and van derWerf et al., 2006), and Global Fire Assimilation System (GFAS, Kaiser et al., 2012) for CAMSRA. This is expected to yield a better spatial and temporal representation of BB smoke emissions compared to climate models which use monthly mean BB inventories (e.g., Sand et al., 2017).

We also assume all dust and sea salt are CM, while other model aerosol species, including ABF in NAAPS-RA, sulfate in MERRA-2 and CAMSRA, BB smoke in NAAPS-RA, BC and OC/OM in MERRA-2 and CAMSRA are FM aerosol particles. This approximation (the sequestering of dust and sea salt to the CM regime) is based on the fact that FM dust and sea salt only contribute a small portion of the total dust or sea salt AOD at 550 nm. For example, FM dust represents about 30% and 39% of total dust AOD globally in MERRA-2 and CAMSRA respectively. The numbers are 17% and 10% for sea salt. NAAPS-RA makes the simplifying microphysical assumption that all dust and sea salt are CM.

For verification purpose, bias, root-mean-square deviation (RMSE) and coefficient of determination (denoted r^2) of reanalysis AODs compared to AERONET/MAN AODs are calculated. r^2 equals the square of the Pearson correlation coefficient between the observed and the modeled AODs. When estimating contributions of individual species to total AOD interannual variability, r^2 is calculated as the square of the Pearson correlation coefficient between the seasonally-binned modeled speciated AOD and total

AOD. In that form, r^2 provides the percentage of “explained variance” of total AOD by a speciated AOD. The statistical definition and interpretation of r^2 can be found https://en.wikipedia.org/wiki/Coefficient_of_determination.

The significance test for trend analysis applies the same calculation method as in Zhang et al. (2010; 2017), an approach which, in turn, was based on the method of Weatherhead et al. (1998). This trend analysis method requires a continuous time series of data.

4. Comparison of AODs from aerosol reanalyses and AERONET

The number of AERONET observations are tied to the increase in the number of daylight hours and are therefore more numerous during the summer than in the spring. This translates to their generally being more temporally representative of 6 hr or daily means in JJA. As a consequence, we preferentially used a JJA climatology to illustrate reanalyses vs AERONET comparisons. Fig. 1 shows the mean JJA FM and CM AODs from AERONET and the speciated AODs from NAAPS-RA, MERRA-2, and CAMSRA. All three aerosol reanalyses appear to capture the total AOD magnitudes to varying extents. The AERONET retrievals show that total AOD during the Arctic JJA season is dominated by contributions from FM aerosols. Large FM AOD values (generally indicative of strong BB smoke influence) are found in Yakutsk and Tiksi in Siberia, and Bonanza Creek in Alaska. CM aerosols also contribute a substantial fraction, varying from a minimum of 15% in regions close to BB smoke sources to a maximum of ~25% at the Norwegian Sea and Greenland Sea coastal sites (Hornsund, Andenes, and Ittoqqortoormitt): these sites are likely impacted by sea salt aerosols lifted by North Atlantic cyclonic events. NAAPS-RA produces AERONET-comparable FM and total AODs in general while showing a tendency to overestimate CM AODs (see Table 2 for explicit biases). The other two reanalyses produce higher FM AOD and total AOD and lower CM AOD compared to AERONET (see also Table 2).

Differences exist between the three reanalyses with respect to the FM and CM partitioning of aerosol species. For example, sea salt aerosols always dominate in the CAMSRA (dust + sea salt) CM: this comment even applies to some inland sites (e.g., Bonanza-Creek) and implies a modeling issue. Dust is the dominant CM species in NAAPS-RA and MERRA-2. This is true at all AERONET site positions: it is likely attributable to elevated dust layers transported from lower latitudes (Stone et al, 2007; Jacob et al., 2010; Breider et al., 2014; Aboele-Fetouh et al., 2020). The proportional contribution of dust to total AOD is at its largest in NAAPS-RA: a result that could have contributed to its high bias in CM AOD (Table 2). The contribution of organic matter to FM AOD is generally larger in CAMSRA than in the other two reanalyses. On the whole, BB smoke is the largest contributing species to total JJA AOD over the Arctic. This is

consistent across all the reanalyses except for some sites in NAAPS-RA (e.g., Andenes, Hornsund, and Kangerlussuaq where ABF AOD is slightly larger than BB smoke AOD). This can be partially due to the different types of speciation employed in NAAPS-RA: ABF represents anthropogenic and biogenic pollution aerosols. The latter category includes sulfate, BC and (with the exception of BB aerosols) organic aerosols of all origins. It is also worth noting that mean AERONET AODs are, in general, higher (0.01-0.02, and can be ~0.1 higher for the sites close to BB sources) than their median counterparts (Table 1) as well as their geometric means. This is because AOD histograms are typically more lognormal than normal in form (asymmetric linear-AOD histograms with positively skewed tails as per, for example, Hesaraki et al., 2017): arithmetic means are, accordingly, often driven by extreme (>95% percentile for example) AOD events. Because these extreme events constitute an important part of the Arctic aerosol environment, the AOD means are presented here.

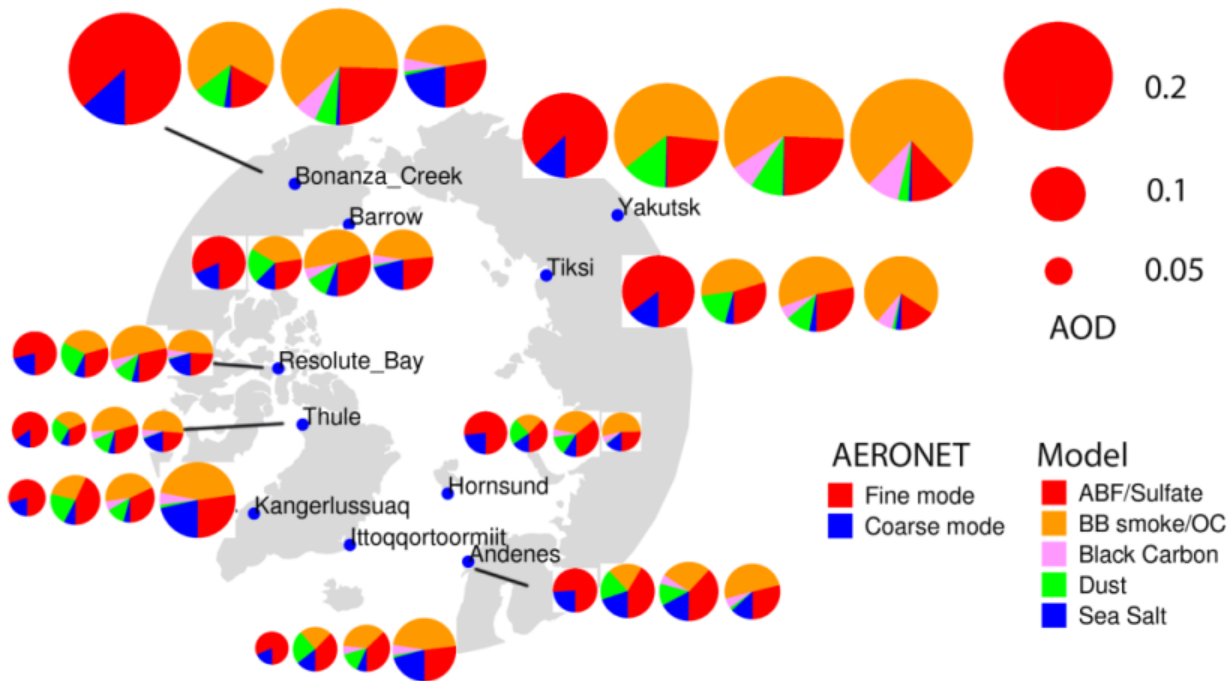


Figure 1. Polar projection map showing the locations of the AERONET Arctic sites (small solid blue circles) used in this study. Long-term (2003-2019) JJA-mean FM and CM AODs at 550 nm from AERONET (leftmost circle of each group of four circles) and respectively, the speciated pie-charts of 550 nm AODs from NAAPS-RA, MERRA2, and CAMSRA for each site. Warm colors (red, orange, and pink) represent FM and cool colors (green and blue) represent CM. Circle size varies with AOD magnitude (see the key to the top right).

Table 1. Geographical coordinates of AERONET sites used in this study and seasonally-binned mean, median and standard deviation of the total AOD and SDA-

derived FM and CM AOD at 550nm for MAM and JJA based on 2003-2019 data when available. “n” represents the number of 6-hrly AERONET data.

sites	latitude	longitude	elev (m)	region	MAM (mean median std)				MAM FMF		JJA (mean median std)				JJA FMF	
					total AOD	FM AOD	CM AOD	n	mean median	total AOD	FM AOD	CM AOD	n	mean median		
Hornsund	77.0°N	15.6°E	12	Svalbard	0.10 0.09 0.05	0.07 0.06 0.04	0.03 0.02 0.03	846	0.71	0.75	0.08 0.06 0.07	0.06 0.04 0.07	0.02 0.01 0.02	971	0.77	0.83
Thule	76.5°N	68.8°W	225	Greenland	0.08 0.07 0.05	0.06 0.05 0.03	0.03 0.01 0.04	1,009	0.75	0.81	0.07 0.05 0.07	0.06 0.04 0.06	0.01 0.01 0.02	1,509	0.85	0.88
Kangerlussuaq	67.0°N	50.6°W	320	Greenland	0.07 0.06 0.04	0.05 0.04 0.02	0.02 0.02 0.03	957	0.69	0.72	0.07 0.05 0.05	0.05 0.04 0.05	0.01 0.01 0.02	1,768	0.77	0.78
Ittoqqortoormiit	70.5°N	21.0°W	68	Greenland	0.06 0.05 0.04	0.04 0.04 0.02	0.02 0.01 0.03	545	0.72	0.78	0.06 0.04 0.04	0.05 0.03 0.05	0.01 0.01 0.02	1,280	0.80	0.81
Andenes	69.3°N	16.0°E	379	Norway	0.08 0.07 0.05	0.05 0.04 0.03	0.03 0.02 0.03	821	0.67	0.71	0.08 0.07 0.05	0.06 0.05 0.05	0.02 0.01 0.02	1,008	0.75	0.78
Resolute_Bay	74.7°N	94.9°W	35	Nunavut	0.10 0.08 0.05	0.07 0.06 0.04	0.03 0.02 0.03	520	0.73	0.78	0.08 0.05 0.10	0.06 0.04 0.10	0.02 0.01 0.03	1,178	0.78	0.83
Barrow	71.3°N	156.7°W	8	Alaska	0.11 0.09 0.07	0.08 0.06 0.05	0.03 0.02 0.04	605	0.73	0.77	0.10 0.07 0.15	0.08 0.05 0.15	0.02 0.01 0.02	1,155	0.79	0.82
Bonanza_Creek	64.7°N	148.3°W	353	Alaska	0.10 0.08 0.09	0.06 0.04 0.08	0.04 0.03 0.04	953	0.61	0.60	0.21 0.09 0.36	0.18 0.06 0.35	0.03 0.02 0.03	1,717	0.75	0.76
Tiksi	71.6°N	129.0°E	17	Siberia	0.10 0.10 0.03	0.08 0.08 0.03	0.02 0.01 0.02	39	0.80	0.82	0.13 0.08 0.18	0.11 0.07 0.17	0.02 0.01 0.02	449	0.80	0.85
Yakutsk	61.7°N	129.4°E	119	Siberia	0.15 0.11 0.15	0.11 0.08 0.13	0.04 0.02 0.04	1,516	0.76	0.80	0.16 0.09 0.24	0.14 0.07 0.24	0.02 0.01 0.02	2,579	0.81	0.84
MAN	>70°N	-	-	Arctic Ocean	0.11 0.10 0.06	0.06 0.06 0.04	0.04 0.04 0.03	85	0.62	0.62	0.06 0.05 0.07	0.04 0.03 0.07	0.02 0.02 0.01	435	0.66	0.67

The geographical coordinates of the ten AERONET sites are provided in Table 1, as well as the mean, median and standard deviation of the total, FM and CM AODs at 550 nm for both MAM and JJA based on available data (the availability of AERONET data can be appreciated from the monthly time series in Fig. 2). Analogous MAN statistics are provided in the last row of Table 1 (see also Fig. S1 for geographical distributions of MAN measurements). The seasonal mean total AOD for Resolute Bay, the Greenland sites, Hornsund and the MAN measurements are < ~ 0.1 (0.06-0.10) while the Alaskan and Siberian site values are >~ 0.1 (0.10 to 0.15 with Bonanza Creek displaying a substantially larger JJA value of 0.21). All sites, except Bonanza Creek, tend to have moderately higher median AOD in MAM: this is consistent with other Arctic sunphotometer studies (Tomasi et al., 2015; Xie et al., 2018). The lesser values in JJA, according to the reanalyses (Fig. 4 and 5), is related to higher FM ABF/sulfate and/or CM dust and sea salt in MAM. This AOD seasonal difference may have evolved in the past two decades with a decreasing trend in ABF/sulfate as discussed in Sect. 5.3. The mean AOD is greater in JJA than in MAM for Yakutsk, Tiksi and Bonanza Creek: this is likely due to strong FM AOD variations associated with BB smoke events (see, for example, the discussions concerning the seasonal competition between FM AOD smoke and FM AOD Arctic haze, in AboEl-Fetouh et al., 2020). The standard deviations of the total and FM AODs are also high for those three sites.

The Table 1 median and mean of the FMF vary, respectively, between 0.60 to 0.88 and 0.61 to 0.85 with higher FMF in JJA than in MAM. The MAN measurements have higher CM AODs and lower FMF compared to AERONET measurements, due to possible contributions from sea salt aerosols. The MAM to JJA increase in FMF for all sites and MAN is coherent with the month-to-month increase of AboEl-Fetouh et al., (2020) although their 550 nm arithmetic means tend to be larger (monthly-binned extremes of 0.81 to 0.98). Most, or at least a significant part of this difference is likely attributable to differences between our FMF (SDA) separation of the product and the SMF (AERONET-inversion) separation of AboEl-Fetouh et al.’s climatology. The SMF is

generally larger than the FMF because it tends to attribute a fraction of the CM particle size distribution and thus a fraction of the CM AOD to the FM AOD (see, for example, the 550 nm SMF vs FMF comparisons Section 4 of Kleidman et al., 2005). More discussions about the differences in terms of FMF vs. SMF and arithmetic vs. geometric statistics are available in the supplement material.

Table 2. Total, FM and CM AOD bias of CAMSRA, MERRA-2, NAAPS-RA and their consensus mean MRC compared to AERONET monthly data.

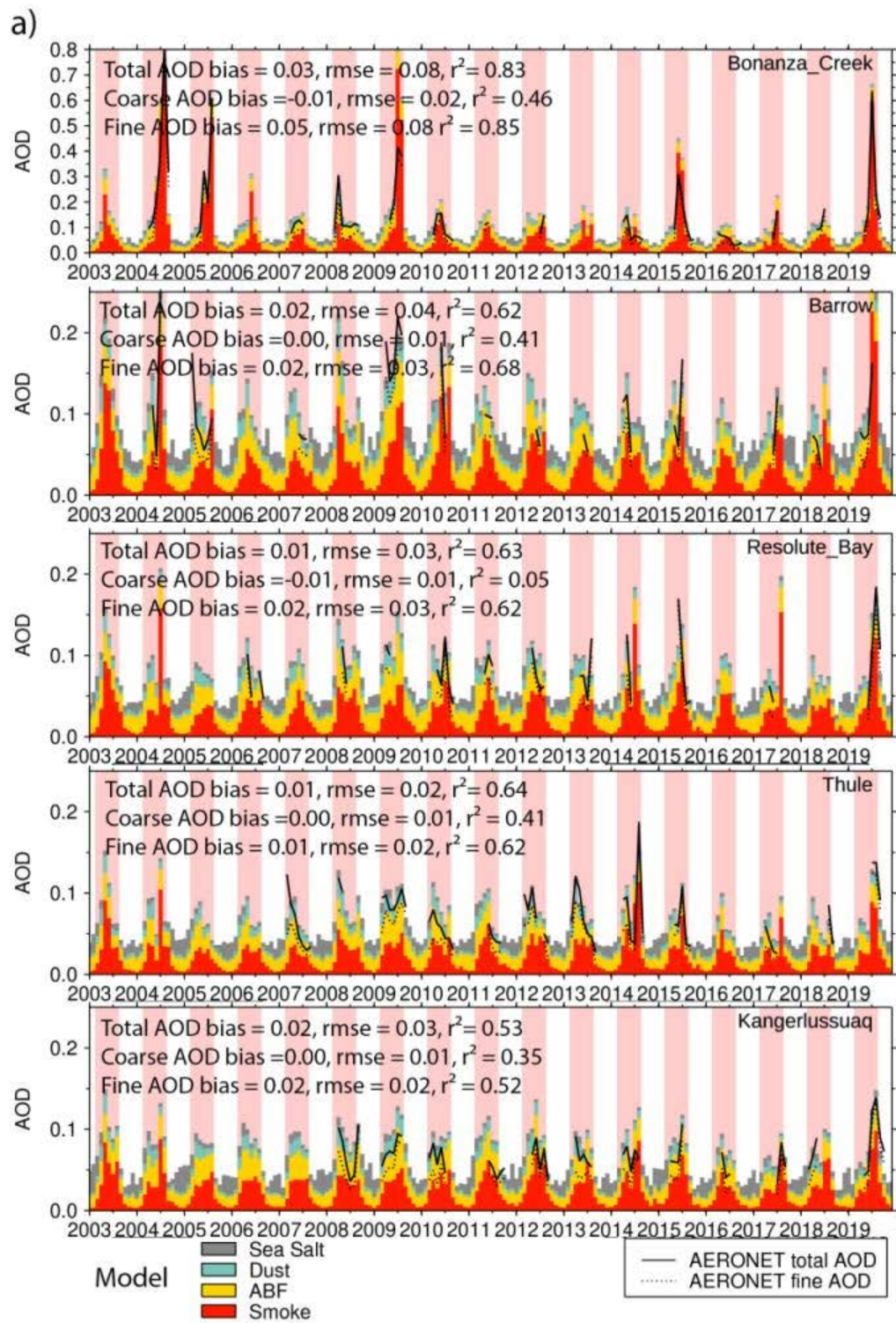
sites	Bias-total AOD				Bias-FM AOD				Bias-CM AOD			
	CAMSRA	MERRA2	NAAPS-RA	MRC	CAMSRA	MERRA2	NAAPS-RA	MRC	CAMSRA	MERRA2	NAAPS-RA	MRC
Hornsund	-0.02	0.01	0.00	0.00	-0.01	0.01	-0.01	0.00	-0.01	0.01	0.02	0.00
Thule	0.00	0.02	0.00	0.01	0.01	0.02	-0.01	0.01	-0.01	0.00	0.01	0.00
Kangerlussuaq	0.02	0.02	0.02	0.02	0.03	0.02	0.02	0.02	-0.01	0.00	0.02	0.00
Ittoqqortoormiit	0.04	0.03	0.02	0.03	0.04	0.02	0.00	0.02	0.00	0.01	0.02	0.01
Andenes	0.03	0.04	0.02	0.03	0.03	0.02	0.00	0.02	0.00	0.02	0.02	0.01
Resolute_Bay	0.01	0.02	0.01	0.01	0.03	0.02	0.00	0.02	-0.02	0.00	0.01	0.00
Barrow	0.02	0.03	0.00	0.02	0.04	0.03	-0.01	0.02	-0.02	0.00	0.02	0.00
Bonanza_Creek	0.06	0.04	0.00	0.03	0.09	0.05	0.00	0.05	-0.02	-0.01	0.00	-0.01
Tiksi	0.02	0.02	-0.01	0.01	0.04	0.02	-0.01	0.02	-0.02	0.00	0.01	0.00
Yakutsk	0.03	0.04	0.01	0.03	0.05	0.05	0.00	0.03	-0.02	0.00	0.01	-0.01
mean	0.02	0.03	0.01	0.02	0.04	0.03	0.00	0.02	-0.01	0.00	0.01	0.00
median	0.02	0.03	0.01	0.02	0.04	0.02	0.00	0.02	-0.02	0.00	0.02	0.00

Table 3. Same as Table 2, except for RMSE.

sites	RMSE-total AOD				RMSE-FM AOD				RMSE-CM AOD			
	CAMSRA	MERRA2	NAAPS-RA	MRC	CAMSRA	MERRA2	NAAPS-RA	MRC	CAMSRA	MERRA2	NAAPS-RA	MRC
Hornsund	0.04	0.02	0.02	0.02	0.03	0.02	0.02	0.02	0.02	0.01	0.02	0.01
Thule	0.02	0.03	0.02	0.02	0.03	0.03	0.02	0.02	0.02	0.01	0.02	0.01
Kangerlussuaq	0.03	0.03	0.03	0.03	0.04	0.02	0.02	0.02	0.01	0.01	0.02	0.01
Ittoqqortoormiit	0.04	0.03	0.02	0.03	0.05	0.03	0.01	0.02	0.01	0.01	0.02	0.01
Andenes	0.03	0.04	0.03	0.03	0.03	0.03	0.02	0.02	0.01	0.02	0.03	0.02
Resolute_Bay	0.03	0.04	0.02	0.03	0.04	0.04	0.02	0.03	0.02	0.01	0.02	0.01
Barrow	0.05	0.05	0.03	0.04	0.06	0.04	0.03	0.03	0.02	0.01	0.02	0.01
Bonanza_Creek	0.11	0.10	0.07	0.08	0.12	0.10	0.06	0.08	0.03	0.02	0.01	0.02
Tiksi	0.05	0.04	0.02	0.03	0.06	0.04	0.02	0.03	0.02	0.01	0.01	0.01
Yakutsk	0.07	0.07	0.04	0.06	0.08	0.07	0.04	0.06	0.03	0.01	0.01	0.01
mean	0.05	0.05	0.03	0.04	0.05	0.04	0.03	0.03	0.02	0.01	0.02	0.01
median	0.04	0.04	0.03	0.03	0.05	0.04	0.02	0.03	0.02	0.01	0.02	0.01

Table 4. Same as Table 2, except for r^2 .

sites	r2-total AOD				r2-FM AOD				r2-CM AOD			
	CAMSRA	MERRA2	NAAPS-RA	MRC	CAMSRA	MERRA2	NAAPS-RA	MRC	CAMSRA	MERRA2	NAAPS-RA	MRC
Hornsund	0.23	0.78	0.75	0.73	0.35	0.73	0.71	0.67	0.27	0.45	0.55	0.56
Thule	0.50	0.47	0.73	0.64	0.52	0.45	0.70	0.62	0.01	0.26	0.44	0.41
Kangerlussuaq	0.48	0.54	0.42	0.53	0.52	0.52	0.35	0.52	0.00	0.57	0.16	0.35
Ittoqqortoormiit	0.68	0.75	0.67	0.79	0.63	0.81	0.76	0.83	0.24	0.36	0.14	0.35
Andenes	0.67	0.63	0.68	0.71	0.68	0.66	0.64	0.71	0.10	0.23	0.21	0.21
Resolute_Bay	0.52	0.51	0.67	0.63	0.53	0.49	0.73	0.62	0.02	0.06	0.03	0.05
Barrow	0.33	0.68	0.70	0.62	0.45	0.76	0.69	0.68	0.05	0.27	0.41	0.41
Bonanza_Creek	0.81	0.78	0.80	0.83	0.83	0.79	0.82	0.85	0.06	0.43	0.45	0.46
Tiksi	0.77	0.80	0.87	0.84	0.82	0.82	0.90	0.86	0.02	0.20	0.10	0.15
Yakutsk	0.70	0.70	0.80	0.77	0.78	0.71	0.80	0.80	0.01	0.41	0.42	0.42
mean	0.57	0.66	0.71	0.71	0.61	0.67	0.71	0.72	0.08	0.32	0.29	0.34
median	0.60	0.69	0.72	0.72	0.58	0.72	0.72	0.70	0.04	0.32	0.31	0.38



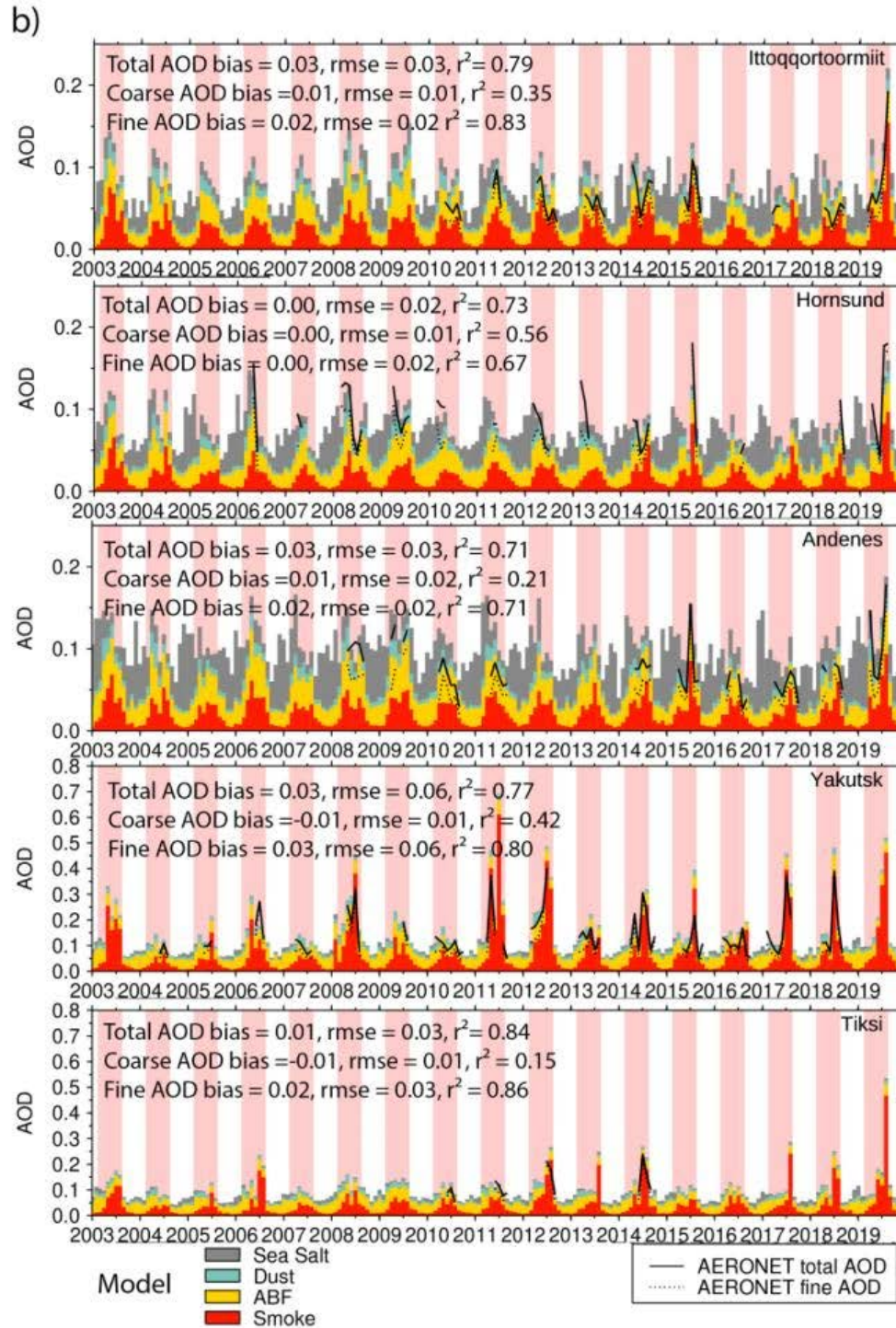


Figure 2. Monthly-binned time series of FM, CM, and total AERONET AODs and MRC speciated AOD at a) Bonanza Creek, Barrow, Resolute_Bay, Thule, Kangerlussuq, and b) Ittoqqortoormitt, Hornsund, Andenes, Yakutsk, and Tiksi sites. The JJA periods are highlighted with pink shading for easy reading. The legends of each time series show MRC bias, RMSE and r^2 .

The time series of monthly mean FM, CM and total AODs from the ten AERONET stations (CM AOD can be inferred from the difference between total AOD and FM AOD) and the speciated AODs from MRC are provided in Fig. 2. Bias, RMSE, and r^2 verification statistics versus AERONET for monthly-binned data of individual aerosol reanalysis members and the MRC are presented in Tables 2, 3, and 4 respectively. The MRC is consistently biased slightly high for FM AOD across all sites and about neutral for CM AOD for most. As a result, total AOD tends to bias slightly high, with biases ranging from 0.00 to 0.03. RMSE values range from 0.02 to 0.03 for most sites, except for Bonanza Creek, Yakutsk and Barrow with RMSE values of 0.06, 0.05 and 0.04 (driven mainly by FM variations). The r^2 values range from 0.53 to 0.84, with FM AOD r^2 values ranging from much higher to marginally higher than the CM AOD values. This is understandable as FM AOD displays large variabilities (which models are more capable of capturing) while CM AOD displays relatively low values and smaller absolute variabilities on seasonal and interannual time scales. Also, emissions of CM aerosols like dust and sea salt, are driven dynamically by model or reanalysis surface winds where the surface wind dependency increases exponentially in amplitude: the simulation of this dependency has been a challenge to all global aerosol models (Sessions et al., 2015; Xian et al., 2019).

Our previous experience with multi-reanalysis and multi-model ensembles indicates, in general, that the consensus of multi-reanalyses or multi-models show better verification scores than individual component members (Sessions et al., 2015; Xian et al., 2019; Xian et al., 2020). However, these studies are based on more global analyses for which the Arctic impact is relatively weak because of the sparsity of observational Arctic data. Tables 2, 3 and 4 indicate that the Arctic is rather unique inasmuch as the MRC is not necessarily the top AOD-estimation performer. NAAPS-RA generally has moderately better bias, RMSE and r^2 verification scores for the total and FM AODs compared to MERRA-2 and CAMSRA while CM AOD does not perform as well. In previous MRC and multi-model consensus evaluations, all component members either performed comparably in terms of AOD RMSE, bias and r^2 or the number of multi models was relatively larger (e.g., 5 to 6 for the International Cooperative for Aerosol Prediction multi-model consensus). This study is the first time that all three developing centers have systematically evaluated their AOD reanalysis performance on an Arctic-wide climate scale.

5. Seasonal Analysis

In this section we present spring and summertime Arctic AOD climatologies derived from space-borne remote sensing retrievals and aerosol reanalyses. We then present the seasonal cycle, interannual variability and trends of total and speciated AODs.

5.1 Spring and Summertime AOD Climatology for the Arctic

5.1.1 Space-based remote sensing AOD climatology

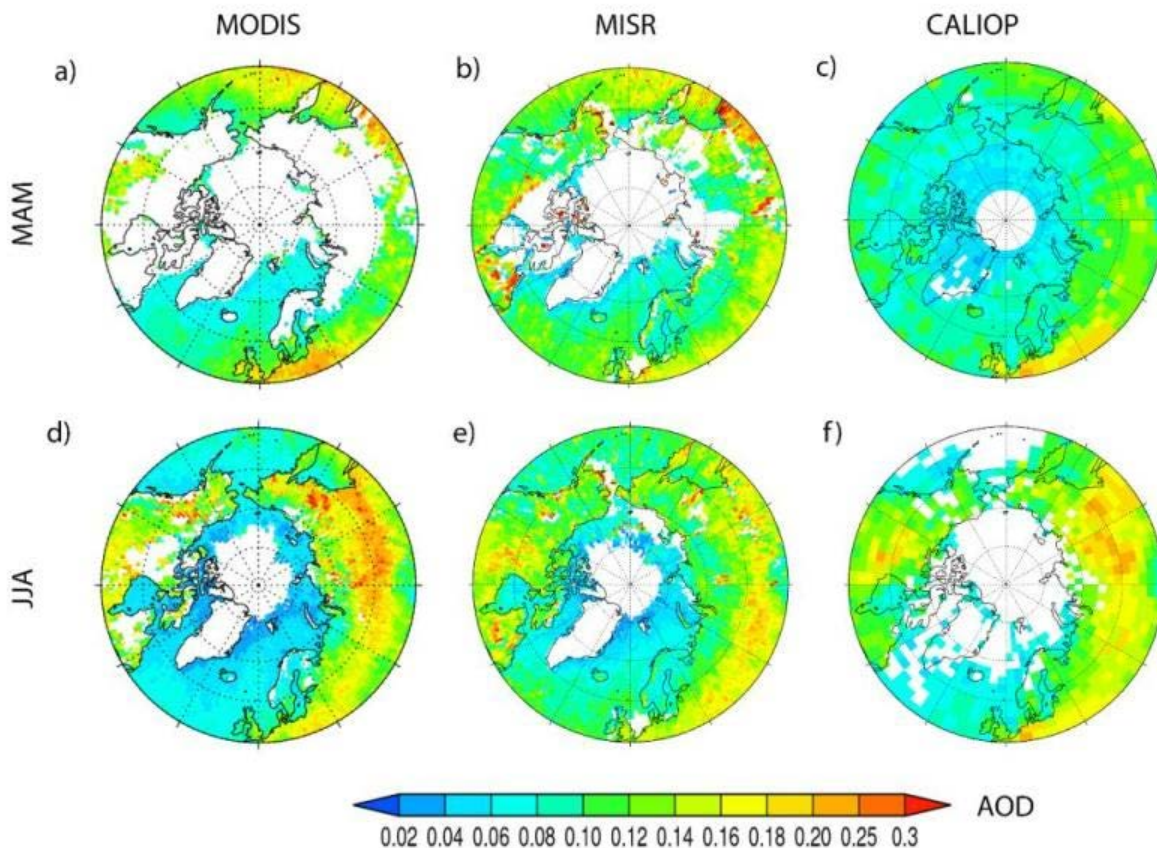


Figure 3. Satellite-derived, mean climatological MAM (upper) and JJA (lower) MODIS AOD at 550 nm (left), MISR AOD at 558 nm (middle), and CALIOP AOD at 532 nm (right). The averaging period for MODIS and MISR was 2003-2019 while the CALIOP period was 2006-2019. The white areas correspond to a lack of data. The latitude circles are at 50°, 60°, 70° and 80° N.

Bright, snow- and ice-covered surfaces, large solar zenith angles (SZA) and extensive cloud coverage result in limited (quality assured) Arctic AOD retrievals from sensors like MODIS and MISR. The latitude limit of an active, downward-looking, polar-orbiting sensor like CALIOP results in a polar region profile gap above 82°N. Known CALIOP issues of retrieval filled values (RFVs) (Toth et al., 2018) and low signal to noise over the Arctic during the summertime also limit its aerosol retrievals during the JJA season. These challenges translate to substantial data-free MAM and JJA areas in the high Arctic and Greenland as well as North America and Siberia in the MODIS, MISR, and CALIOP AOD climatology maps of Fig. 3. JJA shows significantly larger MODIS and MISR area coverage over higher latitudes as aerosol retrievals from MODIS and MISR are acquired in continuous or nearly continuous sunlight conditions. The summertime melt season

means a greater presence of ice- and snow- free ocean and land surfaces as required for passive satellite-based AOD retrievals. Nevertheless, the long operation time of these sensors (about two decades) provides sufficient data to construct an AOD climatology, as well as emissions climatology for the near Arctic and the midlatitude regions where most sources of Arctic aerosols reside.

In general, the Fig. 3 AOD patterns are similar for all three sensors. Higher AODs of 0.15-0.25 can be observed in the 50°N-65°N latitude belt over land. These are associated with large boreal and subarctic areas in Siberia, east and central Europe and North America in both spring and summer. AODs, mostly higher than 0.2 over Siberia in JJA are associated with biomass burning events. The average AOD over water is considerably lower, ranging from 0.02 to 0.12, with lower AOD over the north Atlantic and relatively higher AOD in the northeast Pacific influenced by outflows from the Eurasian Continent. The lowest AODs (0.02-0.06) occur over the Arctic Ocean. AOD over water is slightly higher in MAM than in JJA, which is consistent with other observation-based studies within the Arctic circle (e.g., Tomasi et al., 2015). This result is possibly related to higher pollution levels from the upstream continents in MAM. CALIOP AOD exhibits spatial patterns similar to MODIS and MISR. AODs over Greenland (unique to CALIOP) range from 0.02-0.06: these minimal values are attributable to its high elevations (nearly 2km on average). CALIOP-derived AODs over Siberia and North America are distinctively higher in JJA than in MAM. This seasonal difference (also seen by MISR) is attributable to seasonal boreal fire activities, i.e., boreal fire is generally more active in JJA than in MAM (Giglio et al., 2013). The seemingly larger JJA vs MAM CALIOP difference over Siberia and North American as compared with MODIS and MISR could also be associated with different averaging times (2006-2019 vs. 2003-2019) as well as data sampling rate. The swath for MODIS and MISR is on the order of a few hundred to a few thousand kilometers, while the “beam diameter” for CALIPSO is on the order of 70m (Winker et al., 2009; Colarco et al., 2014). While MODIS and MISR yield more valid retrievals during JJA than MAM, the CALIOP data samples more during MAM due to decreased signal to noise ratio during the summer (c.f. O’Neill et al., 2012).

5.1.2 Arctic AOD climatology derived from aerosol reanalyses

The spatial distributions of 2003-2019 mean total AOD and speciated AOD from the three aerosol reanalyses and their consensus mean for spring and summer respectively are shown in Figs. 4 and 5. Although there is limited AOD data available for data assimilation in the Arctic, lower latitude AODs that are assimilation constrained can affect Arctic AOD through transport and thus exert an indirect Arctic AOD constraint. Additionally, all the reanalyses use satellite-fire-hotspot-based BB emissions with fine temporal resolution (hourly to daily). This exerts a source constraint, especially temporally (emission magnitude differs more than timing among the different models).

As a result, there are significant similarities in the spatial distributions of total AODs among the three reanalyses. For example, MAM total AOD values are, for all reanalyses, high in the 50°N-65°N belt over the Eurasian continent and its downwind Pacific region (values of 0.16-0.30), low (of the order of 0.1 or less) for regions north of 70°N, and at a minimum over Greenland. The high AODs over boreal North America and the Siberian BB regions are more prominent in JJA compared to MAM. In general, we would note that the distribution patterns and total AOD magnitude are comparable to available retrievals from MODIS, MISR, and CALIOP.

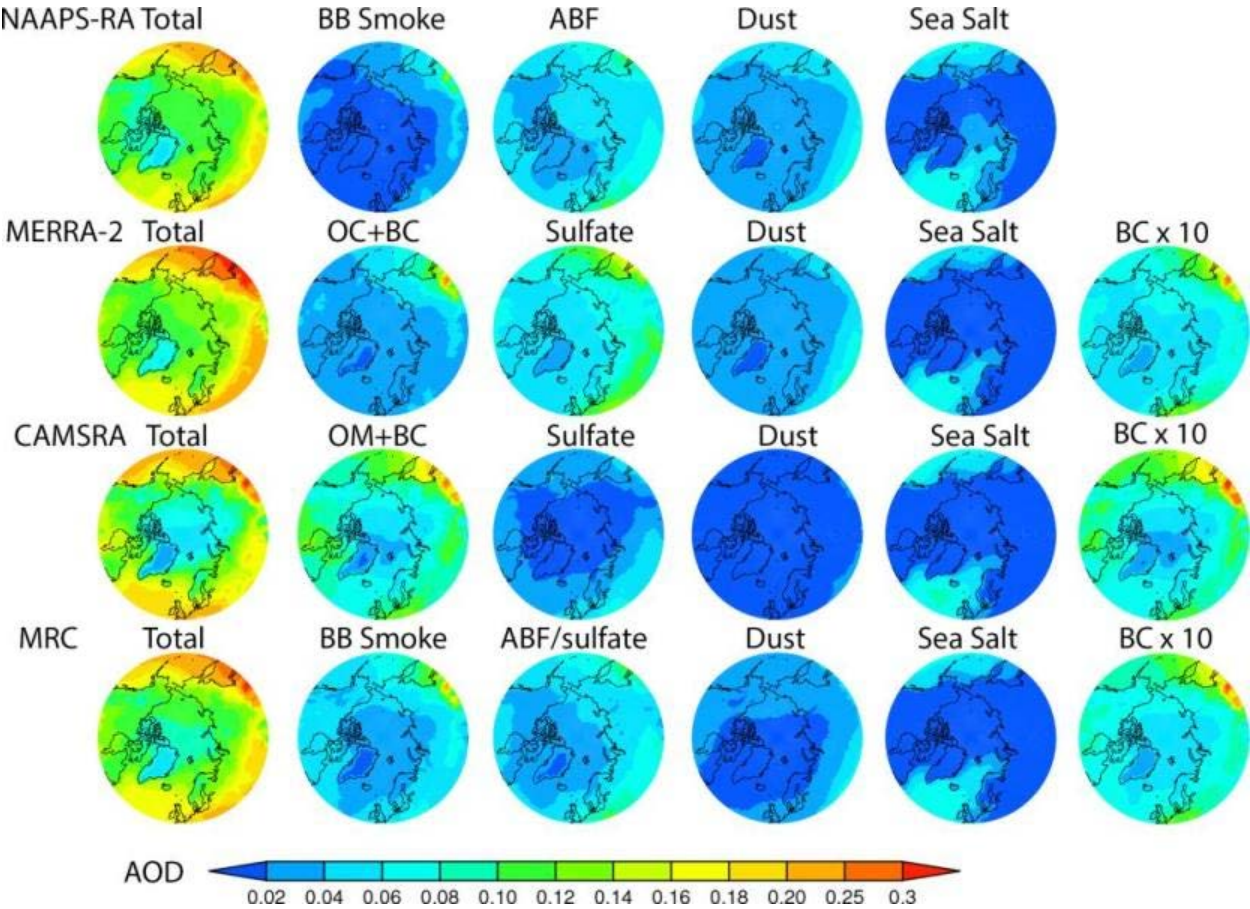


Figure 4. 2003-2019 Climatological MAM-mean total and speciated AOD at 550 nm from NAAPS-RA, MERRA-2 and CAMSRA over the Arctic.

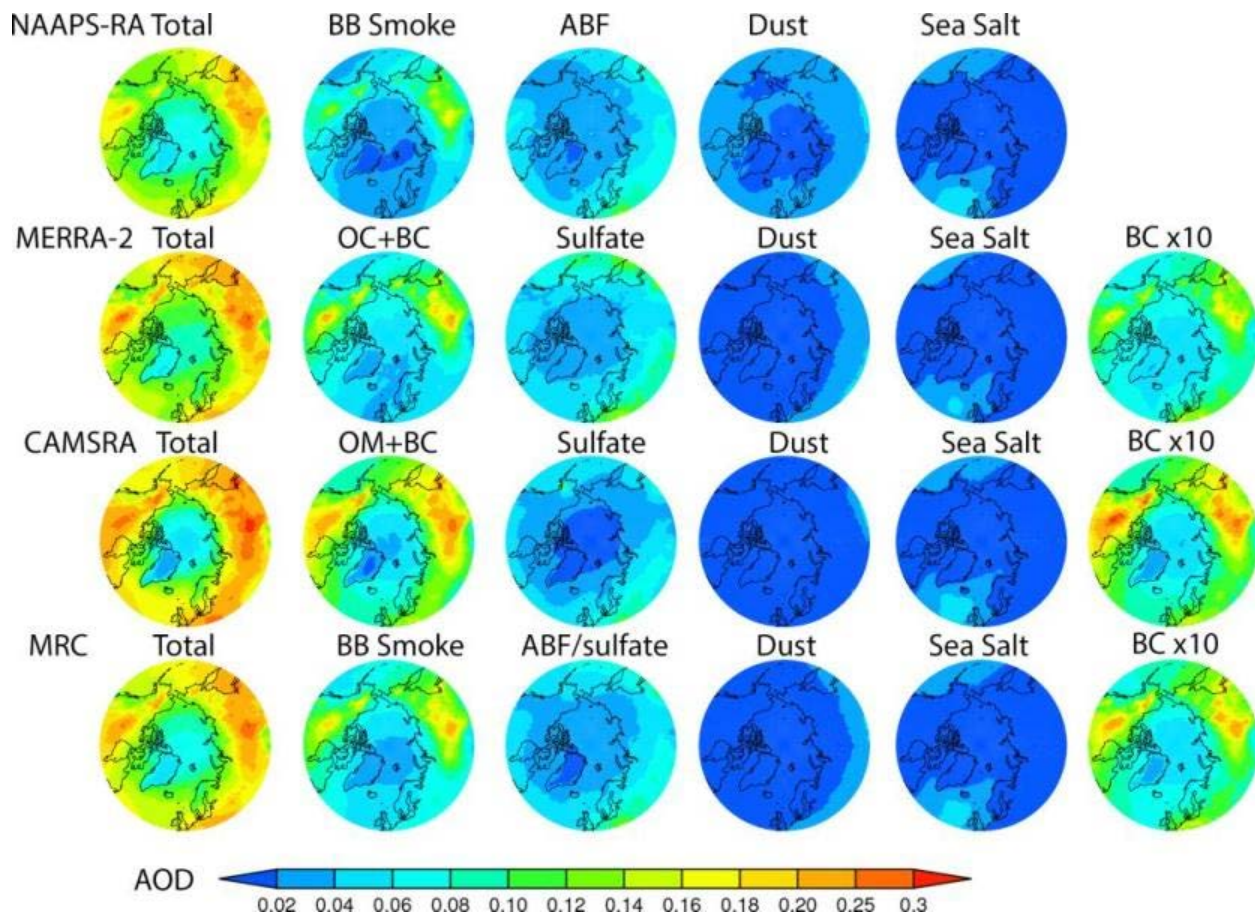


Figure 5. Same as Figure 4, except for JJA.

Speciated AODs have more variability than total AOD among the three reanalyses, and a little more so for MAM than for JJA as shown in Figs. 4, 5, 6. The lesser JJA variability follows because passive Arctic-AOD retrievals are more available in summer and reanalyses are therefore more constrained by those observations. The lesser total AOD variability is the result of it being constrained through data assimilation while speciated AOD is not: the latter AODs rely on model physics and boundary condition constraints. In general BB smoke and ABF/sulfate AODs largely dominate dust and sea-salt during MAM and JJA. The MRC MAM results show similar BB smoke and ABF/sulfate magnitudes. However, the NAAPS-RA and MERRA-2 results suggest an ABF/sulfate dominance over BB smoke while CAMSRA suggests the reverse. The high FM AOD vs AERONET bias of CAMSRA (Table 2) suggests OM and BC, and hence BB smoke overestimation. BB smoke becomes the dominant rival species over ABF/sulfate as summertime boreal BB activity increases. The increase in smoke AOD from spring to summer is a consistent feature across all the reanalyses (while CAMSRA, singularly, shows significantly higher BB smoke AOD and lower sulfate AOD in both seasons). All reanalyses show a June minimum in total AOD (Fig. 6). This is induced by general post-springtime ABF/sulfate, dust and sea salt AODs reductions coupled with increased July

and August BB activities. The spatial distributions of seasonal mean BC AOD from MERRA-2 and CAMSRA greatly resemble those of smoke AOD (arguably more so for JJA than MAM). This suggests a dominant role of BB sources over anthropogenic BC sources over the Arctic during spring and summer seasons. This also supports McCarty et al. (2021)'s BC emission estimate that wildfire emissions account for more than half of all BC yearly emissions north of 60°N (the author's noted much lower wintertime BB emissions when anthropogenic BC emission is at its maximum).

Figures 4, 5 and 6 indicate, for both seasons, that dust and sea salt are secondary contributors to the total AOD in the Arctic: noticeable influences of Saharan and Asian dust (c.f., for example, Stone et al., 2007; Brieder et al., 2014) as well as cyclonic-induced North Atlantic Greenland Sea, Norwegian Sea, and North Pacific sea salt are observable in Fig. 4. It is also noteworthy that dust AOD in CAMSRA is much lower than the other two models (<0.02) in the spring.

Monthly and latitudinally-segmented mean-AODs were found to gradually decrease from lower latitudinal belts to higher latitudinal belts (Fig. 7). Total AOD for the 60°-70°N belt increases, on average, from MAM to JJA due to the seasonality of BB activities. However, the total AOD for the 80°-90°N belt decreases slightly from MAM to JJA. This means the decreasing latitudinal gradient of total AOD is characterized by a larger amplitude in JJA than in MAM. This is most likely due to greater aerosol wet removal during transport from source regions to the high Arctic in summer (Garrett et al., 2010, 2011). It is also noted that the CAMSRA latitudinal AOD-gradient is larger than those of the two other reanalyses. This suggests stronger CAMSRA aerosol removal in the Arctic compared to MERRA-2 and NAAPS-RA.

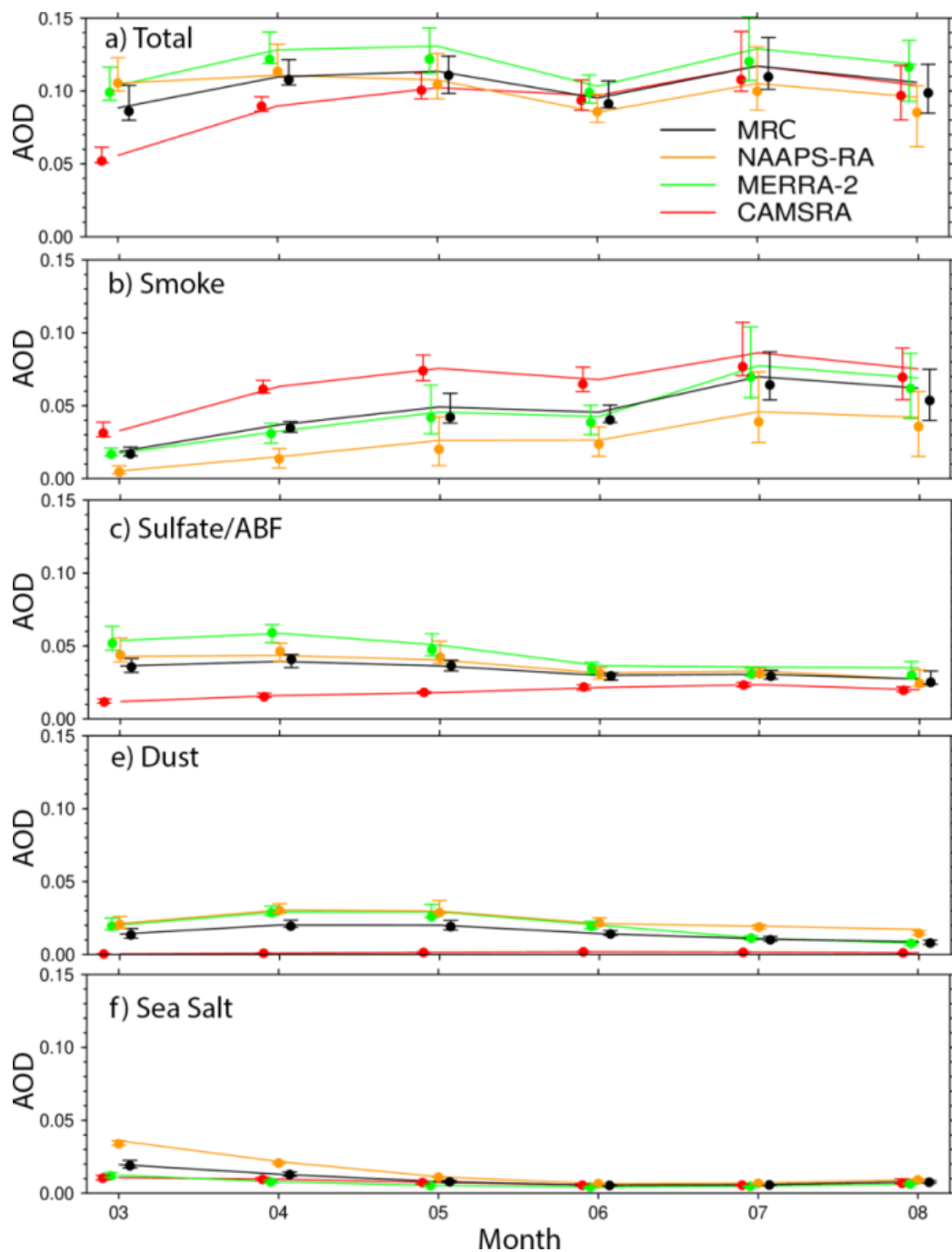


Figure 6. Climatological (2003-2019) seasonal cycle of Arctic (60°-90°N) average total and speciated AODs at 550 nm from the three aerosol reanalyses and the MRC. The top and bottom whiskers and the symbols represent, respectively, the 25% and 75% percentiles and the medians of monthly-binned AOD distributions.

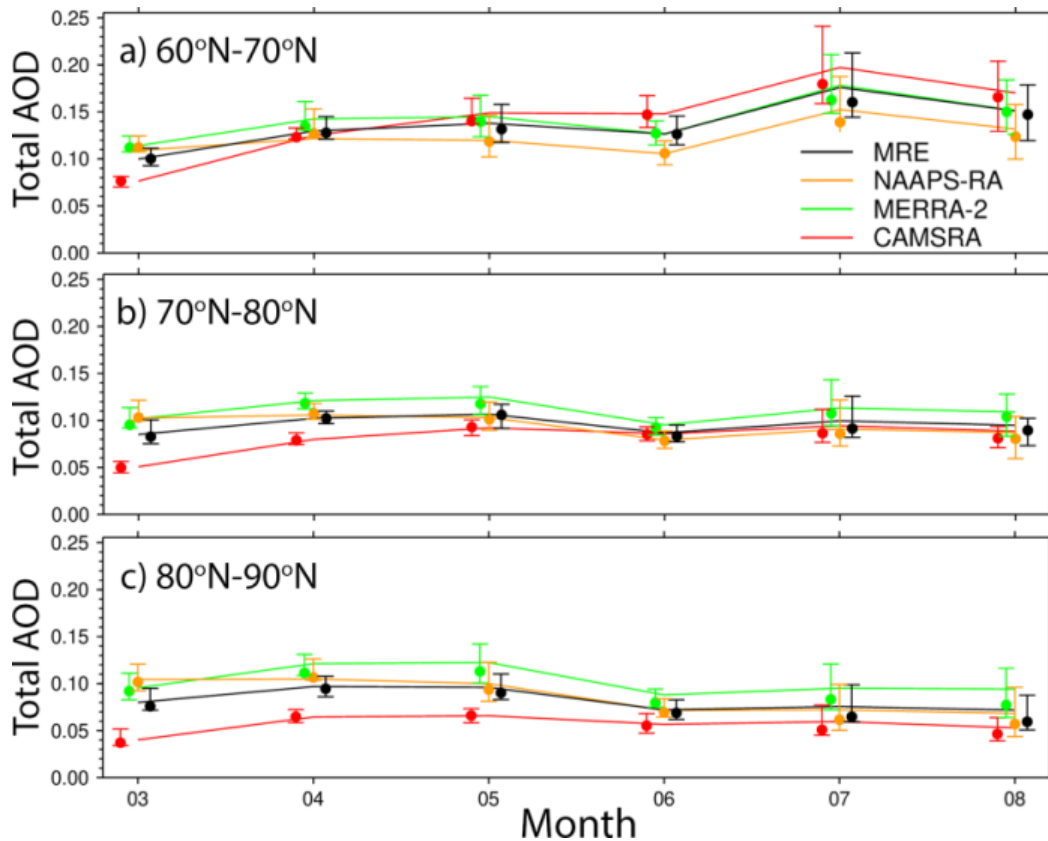


Figure 7. As per Figure 6, but for different latitudinal belts.

5.2 Interannual variability of AOD in the Arctic

5.2.1 General features of AOD Interannual variability

There are, as can be seen in Fig. 2 (and supported by the MAM/JJA discussion in Sec. 4), significant interannual AOD variabilities, especially for sites close to boreal fire sources. For example, the summertime peak of the total AERONET AOD at Bonanza Creek, Alaska, is around 0.6 - 0.8 in 2004, 2005, and 2019, while it is $< \sim 0.1$ -0.2 for other years. The year to year factor relating high- and low-amplitude summertime peak AOD values at Yakutsk, Siberia, can be 6 fold. The MRC shows that these large interannual variabilities are fairly consistent with AERONET FM AOD variabilities and are very likely attributable to interannual variabilities in BB smoke.

For sites far from smoke sources, such as Ittoqqortoormiit on the east coast of Greenland, Hornsund in Svalbard, and Thule on the northwest coast of Greenland, the high-amplitude peak AODs are about 2-3 times the low-amplitude peak AODs. The interannual spring/summer variability is largely associated with BB smoke as suggested by the MRC and the coherent variation of the AERONET FM AOD (c.f. Figures 6 and 7). Some of the strongest AOD events reported in previous studies have been shown to be associated with the long-range transport of BB smoke. For instance, the strong AOD peak in the summer of 2015 over Hornsund and Andenes was related to a series of

intense fires that originated in North America (Markowicz et al., 2016). The strong AOD peaks measured in August 2017 over Resolute Bay, Eureka and Thule were most probably related to intense-fire-induced pyroCB events in British Columbia and the long-range transport of high-altitude smoke (Ranjbar et al., 2019; Das et al., 2021). The high amplitude AOD peak in the spring of 2006 over Hornsund was traced to agricultural fires in Eastern Europe (Stohl et al., 2007). The summer, 2004 boreal fires in North America led to the maximum-amplitude AOD peaks (Fig. 2) for the two Alaskan sites and enhanced AOD on a pan-Arctic scale (Stohl et al., 2004). Some of the high-amplitude AOD peak events were recorded during intensive field campaigns. These included the ARCTAS/ARCPAC multi-platform campaign in the summer of 2008 (Matsui et al., 2011; Saha et al., 2010; McNaughton et al., 2011) and the NETCARE research vessel (Canadian Arctic) campaign in the spring of 2015 (Abbatt et al., 2019). Some of the BB smoke events cause short-term record-high AOD, and some lasted weeks to months, resulting in high monthly mean AOD. The statistics of extreme AOD events, and implications for the impact of regional biomass burning processes are provided in Part 2.

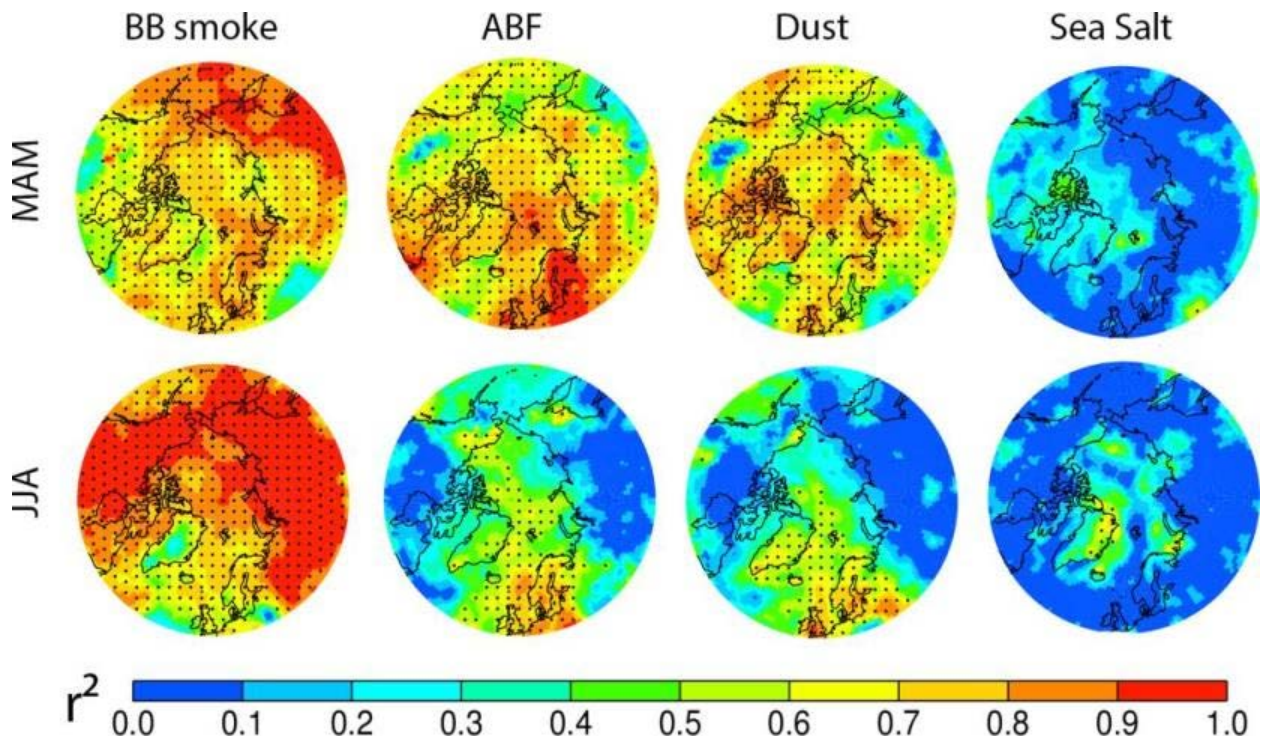


Figure 8. Percentage of interannual MRC variability of MAM (upper panel) and JJA (lower panel) seasonally-binned, total AOD at 550 nm explained by biomass-burning smoke AOD, ABF, dust, and sea salt aerosols respectively. Values in dotted area is statistically significant at the 95% level using a two-tailed Student *t* test.

5.2.2 Attribution of AOD interannual variability

It can be observed in Fig. 6 that the simulated interannual (60-90°N) AOD variability is mostly attributable to the large interannual variability of smoke AOD (interannual variability as measured by the size of the whisker bars). This is consistent across all the reanalysis products. For March and April, the contribution from sulfate/ABF is as important as BB smoke, if not larger. The interannual variation of dust AODs, as indicated with MERRA-2 and NAAPS-RA data, is non-negligible in MAM.

Regarding spatial distribution, Fig. 8 shows the percentage of interannual variabilities of spring and summer Arctic AOD explained by different aerosol species as computed from MRC AODs for 2003-2019. The fact that both MAM and JJA interannual variabilities are mostly explained by BB smoke (maximal r^2 values) is consistent with the correlation of monthly AOD time series shown in Fig. 2 and 6. The JJA r^2 values for BB smoke are generally larger than the MAM values and lower over the North Atlantic, the Norwegian Sea and Greenland than over North American and Eurasian sectors. Smoke explains 60%-80% of MAM and, with the exception of Greenland, about 80% of JJA AOD interannual variabilities north of 70°N. JJA values over the North American and Eurasian sectors (>60°N) represent about 100% explained variation. The second-largest contributor is ABF/sulfate and dust for MAM and to a lesser extent for JJA. Contribution from sea salt is weak and only statistically significant east of Greenland in JJA.

The explained variation by MAM ABF/sulfate is above 80% over the industry- and - population-concentrated European and northeast North American sectors and their outflow regions into the North Atlantic, Greenland Sea, Norwegian Sea, and the Arctic Ocean. Values decrease to above 60% over Europe in general and the European Arctic (including water). Dust, possibly from Asian and high-latitude sources, could explain some of the interannual AOD variabilities over some regions (e.g., Greenland and the Greenland Sea in JJA as well as the North Pacific and the Arctic ocean in MAM). However, there exist large uncertainties in this evaluation based on the weaker verification scores of CM compared to FM AOD (Tables 2,3,4) and, for example, only the CAMSRA reanalyses considers high-latitude dust. Co-variability of species e.g., BB smoke, ABF/sulfate, and dust, is discernible in Fig. 8: this is likely due to the same transport pathways being employed from the mid-latitudes to the Arctic. It is also possible that these species covary because of artifacts introduced by intrinsic treatment in AOD data assimilation for low AOD situations (Zhang et al., 2008).

5.3 Total and speciated AOD trends over 2003-2019

The total AOD springtime and summertime trends derived from MODIS and MISR over 2003-2019 as well 2006-2019 from CALIOP are presented in Fig. 9. Valid trend analysis is, because of the scarcity of valid Arctic retrievals, mostly limited to south of 70°N and the north Atlantic region (with less MODIS and MISR coverage in MAM than in JJA and, for reasons mentioned in Sect. 5.1, less CALIOP coverage in JJA than MAM).

5.3.1 AOD springtime trends

A generally negative total AOD MAM trend over the 50-60°N belt and the North Atlantic is shown in Fig. 9. The largest-amplitude negative trend of Fig. 9 (-0.06 to -0.10 AOD/decade) occurs over Europe: this is most likely due to a decrease in ABF/sulfate from decreased anthropogenic emissions (as we will see in the discussion surrounding the reanalyses of Fig. 10). The CALIOP trend is moderately more negative than the MODIS and MISR trends. This might, again, be attributable to the shorter length of the data record (where earlier and more polluted years of 2003-2006 for Europe and North America were not included) and/or the CALIOP daytime signal to noise issues. The Fig. 10 reanalyses all show a negative pan-Arctic total AOD trend (-0.01 to -0.02 AOD/decade) except for a near-zero CAMSRA trend over the Arctic ocean and a very slight positive trend over boreal North America. The reanalyses collectively suggest that the strong negative trend over the southeast Siberian and East Asian outflow region is associated with a decrease in BB smoke, and, perhaps, a more moderate decrease in ABF/sulfate from NAAPS-RA and MERRA-2. Other consistent features shared by the reanalyses include a negative ABF/sulfate trend over Europe due to decreased anthropogenic emissions (Breider et al., 2017), and a weak positive North Atlantic sea salt trend due possibly to an observed increase in cyclonic activities (Rinke et al., 2017; Waseda et al., 2021; Valkonen et al., 2021). It is notable that NAAPS-RA (and MERRA-2 after 2008) do not incorporate an ABF emission trend. This means that their ABF/sulfate trends are mostly driven by a negative AOD correction applied by the data assimilation systems. This corroborates the negative trend in ABF/sulfate.

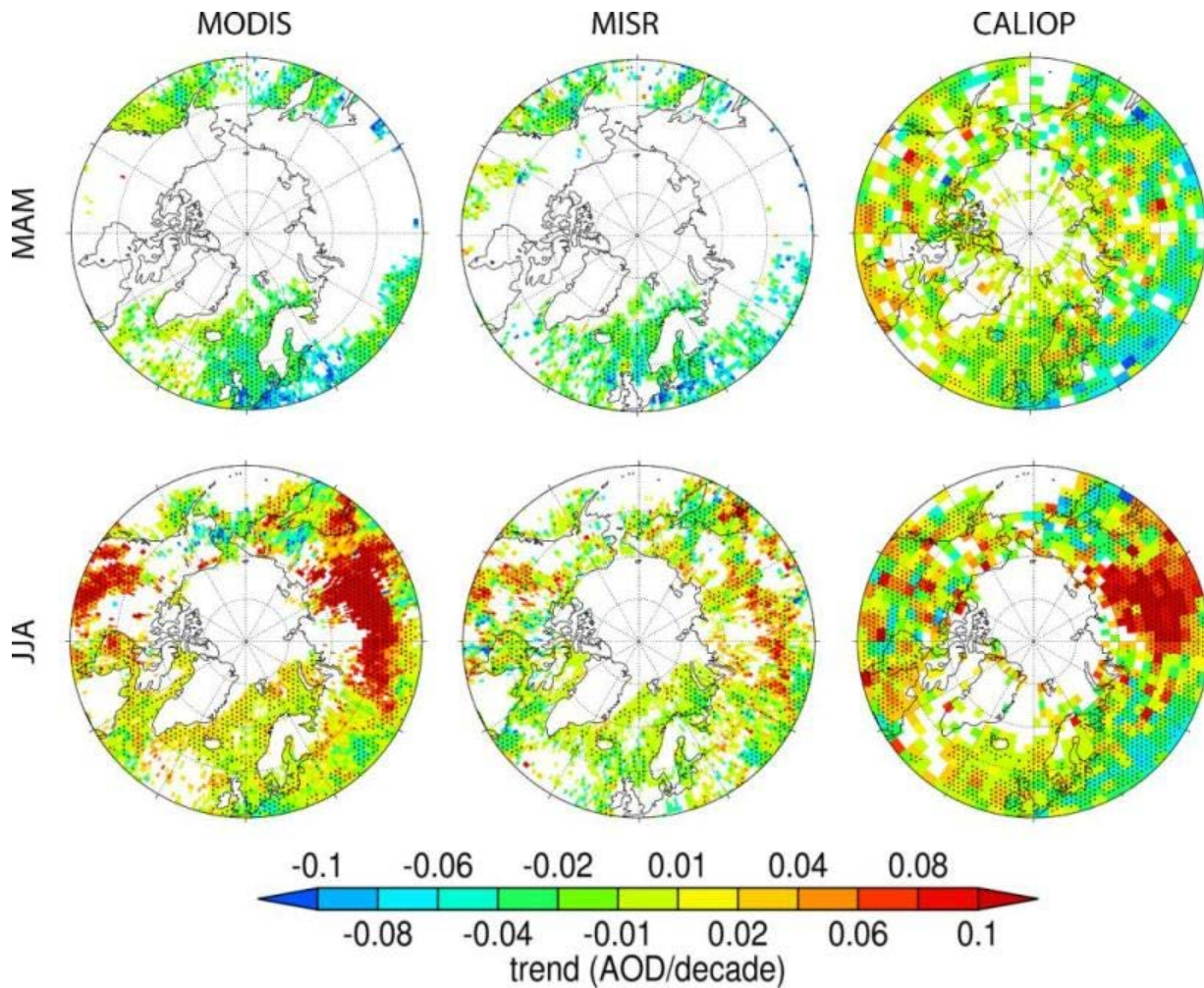


Figure 9. MODIS, MISR, and CALIOP MAM and JJA AOD trends for the time periods and AOD wavelengths given in the Figure 3 caption. Trends in the dotted areas are statistically significant.

5.3.2 AOD summertime trends

The most prominent Fig. 9 JJA feature is the strong and positive total AOD trend (> 0.10 AOD/decade) that appears, to a varying, sensor-dependent, spatial extent, over vast regions of Siberia and North America. All the reanalyses indicate that this trend is attributable to a significant increase in BB smoke AOD (Fig. 11). This is coherent with the FLAMBE-derived, MODIS-hotspot-based emission inventory of Fig. 12 that shows positive regional trends in BB emissions north of 50°N (and with other BB emission inventories such as GFED and GFAS inventories shown in Fig. 2 of McCarty et al., 2021). At the same time, there are negative trends in total AOD over Alaska, northeast of Russia, and the North Pacific from the reanalyses, which is seemingly consistent with the trend in remote sensing AODs (though for some satellite datasets the coverage is spotty in these regions). These trends are driven by BB smoke and smoke emission trends as suggested by all the reanalyses and FLAMBE. In addition, there is a

continued negative trend from MAM to JJA in ABF/sulfate over Europe, which is also reflected in total AOD trend, as shown in the reanalyses. This is consistent with the discernible negative though weak trend from the three sensors. JJA AOD trends in dust and sea salt are neutral from the reanalyses.

5.3.3 High Arctic AOD trends

For the high Arctic, AOD trends will hardly be seen with the same color scale as those for the lower latitudes because of lower AOD. Thus, they are shown separately in Fig. 13, where time series of MAM and JJA area-mean total, smoke, and ABF/sulfate AODs are shown individually and for all the reanalyses and the MRC over the 2003-2019 time period. There is a negative trend across models in MAM total AOD with -0.017 AOD/decade (-18% /decade), and a positive trend in JJA total AOD with 0.007 AOD/decade (8% /decade) based on the MRC. The largest contributor to the MAM negative trend is ABF/sulfate, and the smoke AOD trend is also negative. In the summertime, ABF/sulfate trend continues to be negative; however, smoke AOD trend turns positive, with a high positive trend of 0.010 AOD/decade (22% /decade). BC AOD trends from MERRA-2 and CAMSRA are dominantly driven by smoke AOD, and have similar trends with smoke AOD in percentage per decade. The negative trend in ABF/sulfate AOD is in line with the decreasing trend in surface sulfate mass concentrations measured over Arctic observational sites (e.g., Breider et al., 2017). The negative trend in MAM and positive trend in JJA for smoke AOD are consistent with the seasonally-binned and latitude-belt-binned mean BB emission trends shown in Fig. 12 (e,f). The trend magnitudes of the three aerosol reanalyses are different, but the signs are the same, corroborating the trend analysis results based on the MRC. These results are consistent with the trend analysis for lower latitude source regions as shown in Fig. 9-11. All these results also demonstrate that the Arctic aerosol baseline is changing quickly (Schmale et al., 2021), and the estimation here could contribute to the understanding and quantification of this new baseline.

5.3.4 Possible causes of BB smoke AOD trends

Besides rising surface temperature, climate phenomena such as the El Niño–Southern Oscillation (ENSO), Arctic Oscillation (AO), and Pacific Decadal Oscillation (PDO) have been reported as affecting fire activity in several key boreal fire source regions (Balzter et al., 2007; Macias Fauria and Johnson, 2007; Kim et al., 2020). However rising surface temperature, probably contributes more to the observed trend in BB emission in the high latitudes. With the rising surface temperature, lightning activity and lightning-caused wildfires in summertime high latitude regions were observed to increase in the past two decades (Zhang et al., 2021; Bieniek et al, 2020; Coogan et al., 2020). In addition, agricultural fire activity in Eastern Europe and European Russia (peaking at April to May) and central Asia and Asiatic Russian (peaking in August) (Korontzi et al,

2006; Hall et al., 2016) also affects the seasonality of total BB emissions. The MAM negative trend in BB smoke may be relevant to a strengthening of agriculture burning regulations in the later part of the time period. For example, the MAM BB emission maxima in 2003, 2006 and 2008 are all associated with wide-spread springtime agriculture burnings in high latitudes (Korontzi et al, 2006; Stohl et al., 2007; Saha et al., 2010). The aforementioned climate oscillations also modulate interannual variations of the transport of pollutants from the mid latitudes to the Arctic (e.g., Eckhardt et al., 2003; Fisher et al., 2010). Compared with the BB emission trend, trend in the atmospheric processes, e.g., transport and removals, probably plays a secondary role in the Arctic smoke AOD trend. This is illustrated by the similarity in spatial patterns of smoke AOD and BB emission trends, and the coincidence of peak years for emissions and the high Arctic area-mean smoke AODs. For example, 2012 and 2019 are associated with JJA peaks in emission and high Arctic smoke AOD, while 2003 and 2008 correspond to MAM peaks in both (Figs. 12 and 13).

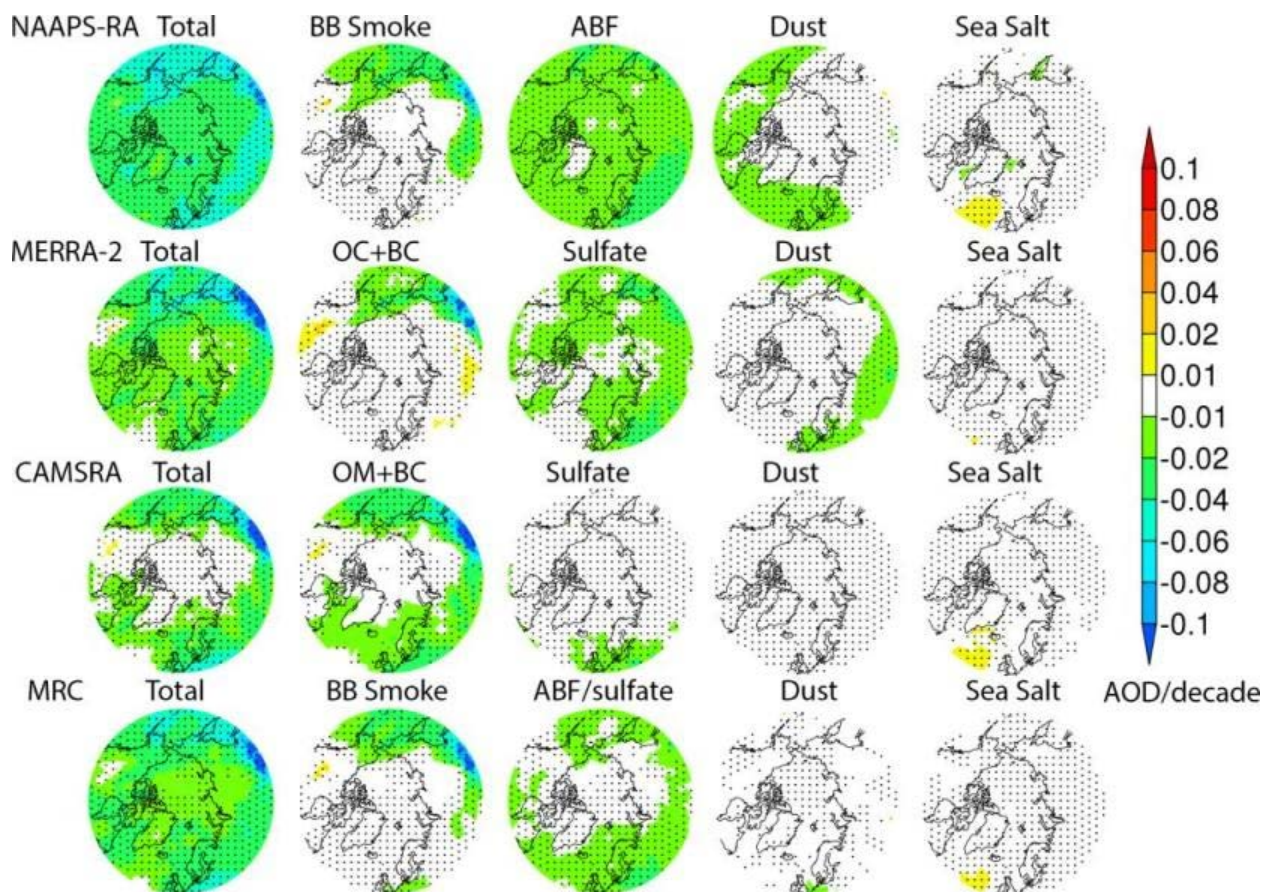


Figure 10. Trends of MAM 550 nm total AOD and contributions from BB smoke, ABF/Sulfate, dust and sea salt from NAAPS-RA, MERRA-2 and CAMSRA and the MRC.

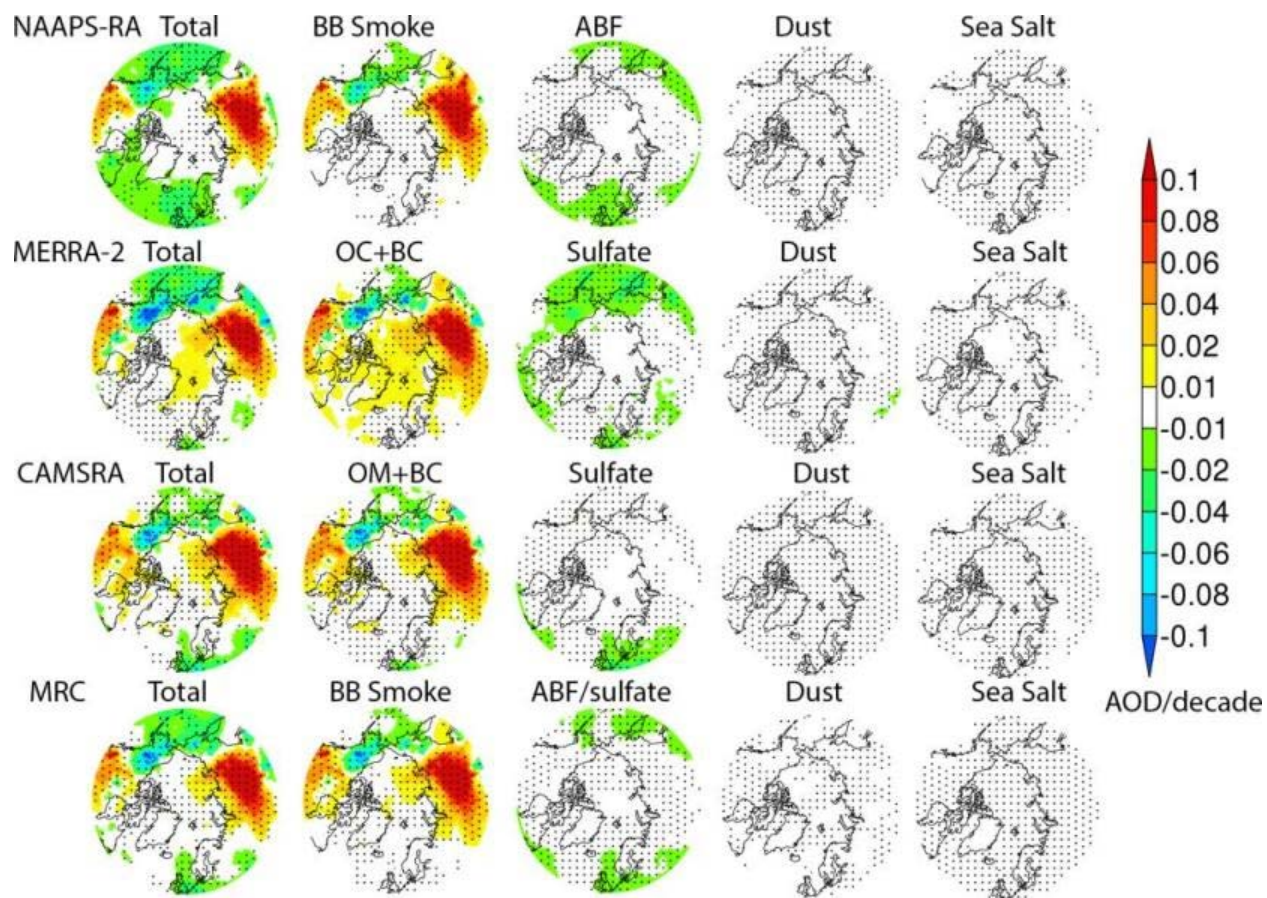


Figure 11. Same as Fig. 10, except for JJA.

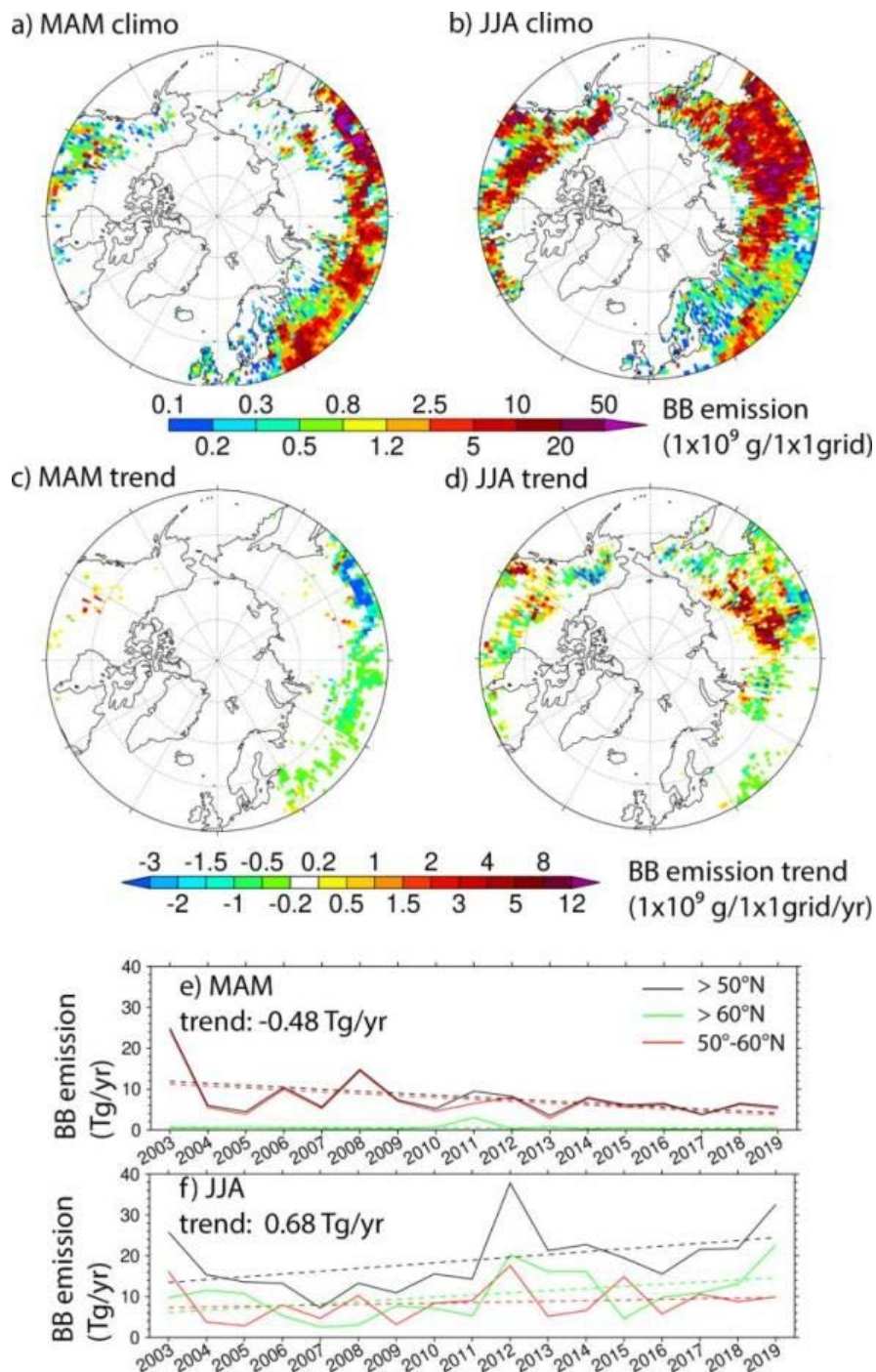


Figure 12. MAM/JJA seasonal total BB smoke particle emission climatology and trend for 2003-2019 derived from FLAMBE (a-d). e) and f) Time series of seasonally-binned area-means (>50°N, >60°N and 50°-60°N) BB smoke (PM_{2.5} particle) emissions for MAM and JJA respectively. Dashed lines represent linear trends, which are statistically significant with a confidence level of 95%. The trend for north of 50°N is displayed in the legends.

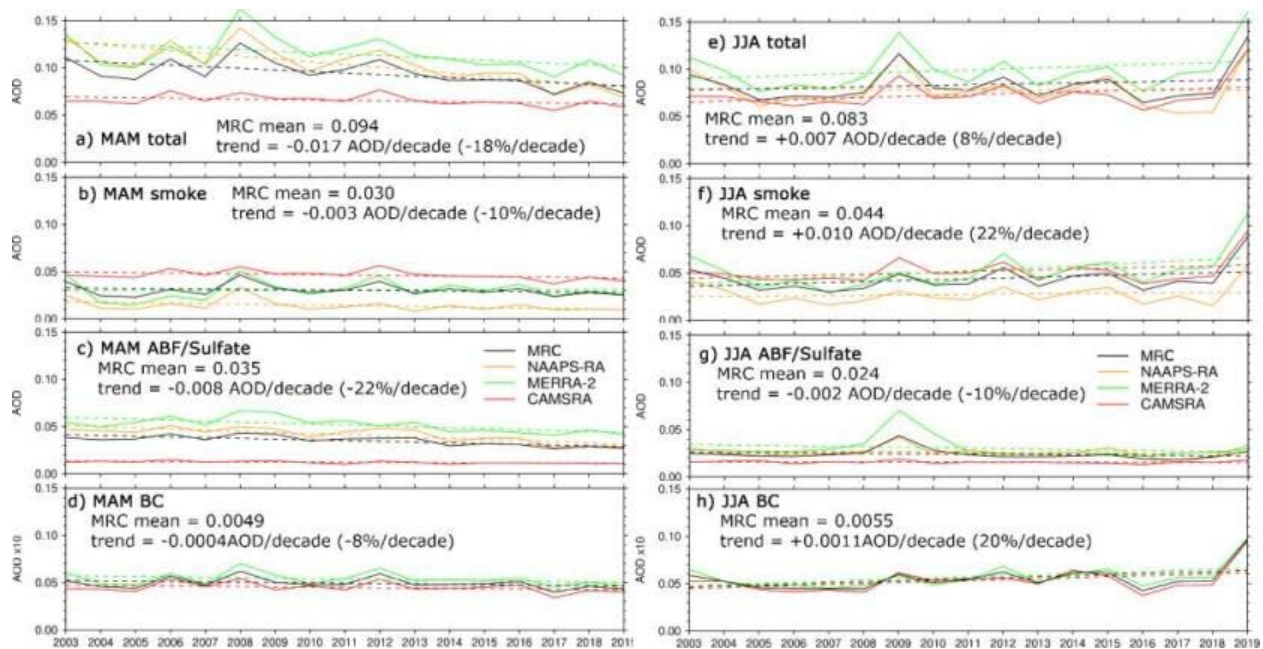


Figure 13. Time series of MAM and JJA 70°-90°N area mean total, BB smoke, ABF/sulfate and BC AODs from the reanalyses and the MRC. Solid lines are AODs, and dashed lines are linear regressions indicating trends. For easier visualization, BC AOD is multiplied by 10.

6. Discussion

The quality control processes applied on the AOD retrievals from MODIS, MISR, and CALIOP help to generate a consistent AOD climatology and trend near the Arctic. The cloud-clearing process on the MISR data and QA processes on the MODIS data removed a good volume of data (about 40% for MISR and MODIS). However, these QA processes help to retain only the best-quality data, which yield a closer magnitude of AOD for MODIS and MISR to AERONET AODs near the 70°N latitude circle (around or less than 0.1), compared to ~0.2 using regular level 3 MODIS and MISR data in Figs 20 and 23 of Tomasi et al., 2015, especially for springtime. The manual QA process on the AERONET AOD data also reveals more frequent cloud contamination in springtime than in summertime. Often artificial AOD values of zero are observed over the Arctic in CALIOP V4.2 L2 and L3 data, resulted partially from algorithmically setting altitude bins with retrieval filled values in the aerosol profile to zero, as these represent undetectable levels of faint aerosol (i.e., Toth et al., 2016; 2018). With AOD=0 values retained in the CALIOP V4.2 L2 data analysis (same processing in CALIOP V4.2 L3), the climatological seasonal mean AOD magnitude is much smaller (about half) than that shown in Fig. 3 and the AOD trends are slightly smaller than those in Fig. 9, although the spatial patterns of the seasonal AOD and trends are similar to those obtained with AOD data after removing the AOD=0 values (Fig. S2). After removing the pixels with filled and

zero values, CALIOP AOD seasonal spatial AOD distributions are similar to those from MODIS and MISR.

The total AOD at 550 nm from the three aerosol reanalyses are much more convergent in spatial distribution, magnitude, and seasonality in the Arctic compared to the climate models, and are similar to those from the remote sensors near the Arctic. For example, for AEROCOM models in Sand et al., 2017, MAM AODs averaged over nine Arctic AERONET sites (all included in this study) are an order of magnitude different for the highest and lowest AOD models, and peak AOD season varies among winter, spring and summer; In the CMIP5 models in Glantz et al., 2014, spring and summertime AODs over the Svalbard area also show an order of magnitude difference and there are different seasonality for some of the models. The possible reasons for the convergence of AOD in the reanalyses include 1) the hourly/daily resolved satellite-hotspot-based BB emissions used by these reanalyses apply fine-temporal and interannual-variability-resolved emission constraints; 2) despite that the commonly assimilated satellite AOD (e.g., MODIS AOD in all three reanalyses) has limited coverage in the Arctic due to retrieval challenges of dealing with bright surfaces and high cloud coverage, the observational constraint of model fields through assimilation of AOD in the lower latitudes is effective in constraining Arctic AOD to a good extent through transport; 3) more accurate meteorology representations. It is reasonable that the AOD spread among the three reanalyses increases with latitude, and into the early months (e.g., March) when retrieval coverage for lower latitudes is less than summer months.

Except for the chemical processes relevant to conversion of SO₂ to sulfate, the aerosol reanalysis products (or their underlying aerosol models) don't include other new particle formation processes that may be important over the Arctic open water/leads in Springtime or over packed ice during transitional summer to Autumn season (Abbatt et al., 2019; Baccarini et al., 2021). High latitude dust sources, e.g., glacier dust, which are present for some areas in the Arctic (Bullard et al., 2016), are only included in CAMSRA, despite that Arctic dust AOD in CAMSRA is much lower than those in the other two models (Fig. 6e).

To show the contribution of biomass burning on total AOD in the Arctic, we approximated BB smoke with the sum of BC and OC/OA from MERRA-2 and CAMSRA. This approximation is arguable: it is better suited for JJA than MAM, as the climatological seasonally-binned mean of Arctic AOD is dominated by BB smoke in JJA, which means that BC and OC/OA are mostly from BB sources, while the contribution of BC and OC/OA from anthropogenic sources is relatively higher in early spring (Figs. 4, 5). So smoke AOD is overestimated from MERRA-2 and CAMSRA and more so for MAM. This explains the larger difference in smoke AOD (ratio to total AOD) in MAM

than in JJA between the two reanalyses and NAAPS-RA, which explicitly tracks aerosol mass from BB sources (Figs. 4, 5, 6). While NAAPS-RA includes BC and OA from anthropogenic sources and sulfate into ABF, which is an arguably reasonable configuration for pollution species, as observational studies show a strong correlation between sulfate and elemental BC surface concentrations at pan-Arctic sites away from BB sources, indicating the sources contributing to sulfate and BC are similar and that the aerosols are internally mixed and undergo similar removal (Eckhardt et al., 2015). BB smoke is expected to have different vertical distributions from anthropogenic pollution if smoke is emitted above the boundary layer. Some estimates based on satellite observations near local noon have suggested that the fraction of smoke escaping the boundary layer is only ~10% (Val Martin et al., 2010), but taking account of the diurnal cycle of fire activity and potential for pyroconvection, the actual fraction of elevated smoke could be much larger (Fromm et al., 2010; Peterson et al., 2015; Peterson et al., 2017).

Stratospheric aerosols from volcanic eruptions can contribute to the total AOD in the Arctic, especially for the four years after the Mount Pinatubo eruption in 1991 (Herber 2002). For our study period, the eruptions of Kasatochi, Redoubt, Sarychev, and Eyjafjallajökull in August 2008, March 2009, July 2009, and March 2010, respectively, would have affected the stratospheric AOD and thus total column AOD. However, these eruptions are at least one order of magnitude smaller than that of Pinatubo. The stratospheric AOD contribution to the Arctic background AOD is estimated to be relatively small at ~0.01 (from Fig. 16 of Thomason et al., 2018; non-Pinatubo affected years in Fig. 5 of Herber 2002), despite that locally and over a short period the AOD contribution can be large (e.g., O'Neill et al., 2012). All the reanalyses have some sort of SO₂ and sulfate representation from volcanic degassing emissions, but a full representation for explosive volcanic sources is lacking (except that MERRA-2 has time-varying explosive and degassing volcanic SO₂ before December 31, 2010). The volcanic influence on Arctic AOD, if detectable, would be reflected in the ABF/sulfate AOD in the reanalyses, but its contribution would be much smaller than the anthropogenic counterpart for our study period. It is also worth noting that volcanic activities are not the only influence on the stratospheric aerosol budget: pyroCB-injected BB smoke can also contribute to stratospheric AOD, as discussed earlier. Stratospheric BB smoke was also detected over the Arctic with lidar measurements during the MOSAiC campaign (Engelmann et al., 2021). Stratospheric injection of BB smoke associated with pyroCB events are not represented in the reanalyses, despite that BB emission associated with these pyroCB events are included in the emission inventories with possible large bias in emission amount and height.

Arctic shipping is often brought up as a potentially important source of BC for the Arctic in the future. All of the reanalyses include shipping emissions, although little interannual trend is considered especially for the late period in 2003-2019. However “Arctic shipping is currently only a minor source of black carbon emissions overall” according to the recent Arctic Monitoring and Assessment Programme (AMAP) report (2021).

7. Conclusions

Using remote sensing AOD retrievals from MODIS, MISR and CALIOP, and AODs from three aerosol reanalyses, including NAAPS-RA, MERRA-2, and CAMSRA, and ground-based AERONET data, we have reported the Arctic/High-Arctic AOD climatology, and trend for spring and summer seasons during 2003-2019.

- 1) **Arctic AOD climatology:** The total AODs from space-borne remote sensing and the aerosol reanalyses show quite consistent climatological spatial patterns and interannual trends for both spring and summer seasons for the lower-Arctic, where remote sensing data is available. AOD trends for the high Arctic from the reanalyses have consistent signs too. Climatologically, FM AOD dominates CM AOD in the Arctic. Based on the reanalyses, BB smoke AOD increases from March to August associated with seasonality of BB activities in the boreal region ($>50^{\circ}\text{N}$); ABF AOD is slightly higher in MAM than in JJA; sea salt AOD is highest in March and decreases with time into later spring and summer; contribution of dust AOD to total AOD is non-negligible in April and May. The latitudinal gradient of AOD is larger in JJA than in MAM, consistent with observed more efficient removal in summertime (Garrett et al., 2011). Among aerosol species, BC is a very efficient light absorber, and climate forcing agent (e.g., Bond et al., 2013). We show that over the Arctic, the contribution of BC AOD from BB source overwhelms anthropogenic sources in both MAM and JJA, and more so in JJA during 2003-2019.
- 2) **Interannual AOD trend:** Total AOD exhibits a general negative trend in the Arctic in MAM, and strong positive trends in North Americas, Eurasia boreal regions (except Alaska and northeast Siberia) in JJA. For the high Arctic, the total AOD trend is $-0.017/\text{decade}$ ($-18\%/\text{decade}$) for MAM and $0.007/\text{decade}$ ($8\%/\text{decade}$) for JJA based on the MRC. The total AOD trends are driven by an overall decrease in sulfate/ABF AOD in both seasons ($-0.008/\text{decade}$, or $-22\%/\text{decade}$ for MAM and $-0.002/\text{decade}$ or $-10\%/\text{decade}$ for JJA), and a negative trend in MAM ($-0.003/\text{decade}$ or $-10\%/\text{decade}$) and a strong positive trend in JJA ($0.01/\text{decade}$ or $22\%/\text{decade}$) from biomass burning smoke AOD. The decreasing trend in sulfate in the Arctic in recent decades is in line with other

studies using surface concentration measurement (e.g., Eckhardt et al., 2015). The smoke AOD trends are consistent with MODIS fire-hotspot-based BB emission trends over the boreal continents.

- 3) **Impact of BB smoke on AOD interannual variability:** The interannual variability of total AOD in the Arctic is substantial and predominantly driven by fine-mode, and specifically BB smoke AOD in both seasons and more so in JJA than in MAM. For AERONET sites close to BB emission sources, the difference in monthly total AOD can be 6-fold for high versus low AOD years. For remote regions away from BB sources, the interannual variability of total AOD can also be explained mostly by smoke AOD.
- 4) **Overall performance of the aerosol reanalyses:** The aerosol reanalyses yield much more convergent AOD results than the climate models (e.g., AeroCOM models in Sand et al., 2017; CMIP5 models in Glantz et al., 2014) and verify with AERONET to some good extent, which corroborates the climatology and trend analysis. Speciated AODs appear more diverse than the total AOD among the three reanalyses, and a little more so for MAM than for JJA. NAAPS-RA and MERRA-2 total and FM AODs verify better in the Arctic than CAMSRA, which tends to have a high bias in FM overall. The reanalyses generally perform better in FM than CM. The three reanalyses exhibit different latitudinal AOD gradients, especially in summertime, indicating different removal efficiencies. The emerging capability of assimilating OMI Aerosol Index (AI) to constrain absorptive aerosol amount, could potentially fill in the observational gaps for aerosol data assimilation in reanalyses over the Arctic (Zhang et al., 2021). With more advanced retrieval algorithms on the current space-borne sensors for over snow/ice, new sensors on future satellites, improvements on the underlying meteorology and aerosol representations in models, improvements in aerosol reanalysis are expected.

The results presented here provide a baseline of AOD spatiotemporal distribution, magnitude, and speciation over the Arctic during spring and summer seasons for the recent two decades. This will help improve aerosol model evaluations and better constrain aerosol radiative and potentially indirect forcing calculation to evaluate aerosol impact in the Arctic amplification. For example, the contribution of reduction in sulfate to Arctic surface warming in recent decades (e.g., Shindell and Faluvegi, 2009; Breider et al., 2017) could potentially be better quantified, with the caveat that speciated AOD have larger uncertainties than total AOD in the reanalyses. The AOD statistics could also provide background information for field campaign data analysis and future field campaign planning in a larger climate context. It is also recommended that climate

models should take into account BB emissions besides anthropogenic climate forcers and BB interannual variabilities and trends in Arctic climate change studies.

Appendix A. Summary of data used in the study

Products	Data	resolution	time
MODIS (Moderate Resolution Imaging Spectroradiometer) C6.1L3	550nm AOD	1°x1° monthly	2003-2019
MISR (Multi-angle Imaging SpectroRadiometer) V23	558nm AOD	1°x1°, monthly	2003-2019
CALIOP (Cloud-Aerosol Lidar with Orthogonal Polarisation) V4.2L2	532nm AOD	2°x5°, monthly	2006-2019
AERONET (AErosol RObotic NETwork) V2L3	SDA total, FM, CM AOD at 550nm	6hrly, monthly	2003-2019
MAN (Marine Aerosol Network) Level2	SDA total, FM, CM AOD at 550nm	6hrly	2003-2019
MERRA-2 (Modern-Era Retrospective Analysis for Research and Applications, v2)	Total and speciated AOD at 550nm	0.5°lat x0.63°lon, monthly	2003-2019
CAMSRA (Copernicus Atmosphere Monitoring Service Reanalysis)	Total and speciated AOD at 550nm	0.7°x0.7°, monthly	2003-2019
NAAPS-RA v1 (Navy Aerosol Analysis and Prediction System reanalysis v1)	Total and speciated AOD at 550nm	1°x1°, 6hrly, monthly	2003-2019
MRC (Multi-Reanalysis-Consensus)	Total and speciated AOD at 550nm	1°x1°, monthly	2003-2019
FLAMBE (Fire Locating and Modeling of Burning Emissions) v1.0	BB smoke emission flux	1°x1°, monthly	2003-2019

Note: These are final form of data used in the result section. Some pre-processing and quality-control were applied to remote sensing data as described in the data section.

Code and Data Availability: All data supporting the conclusions of this manuscript are available either through the links provided below or upon request.

AERONET Version 3 Level 2 data: <http://aeronet.gsfc.nasa.gov>

MAN data: https://aeronet.gsfc.nasa.gov/new_web/maritime_aerosol_network.html

MODIS data-assimilation-quality AOD: https://nrlgodae1.nrlmry.navy.mil/cgi-bin/datalist.pl?dset=nrl_modis_l3&summary=Go

Or <https://modaps.modaps.eosdis.nasa.gov/services/about/products/c61-nrt/MCDAODHD.html>

MISR AOD: <ftp://15ftl01.larc.nasa.gov/misrl2l3/MISR/MIL2ASAE.003/>

CALIOP from NASA Langley Research Center Atmospheric Science Data Center:

https://doi.org/10.5067/CALIOP/CALIPSO/LID_L2_05kmAPro-Standard-V4-20 for the Version

4.2 CALIPSO Level 2 5 km aerosol profile and

https://doi.org/10.5067/CALIOP/CALIPSO/LID_L2_05kmALay-Standard-V4-20 for aerosol layer

products. Further QAed data are available upon request.

NAAPS RA AOD: [https://usgodae.org/cgi-](https://usgodae.org/cgi-bin/datalist.pl?dset=nrl_naaps_reanalysis&summary=Go)

[bin/datalist.pl?dset=nrl_naaps_reanalysis&summary=Go](https://usgodae.org/cgi-bin/datalist.pl?dset=nrl_naaps_reanalysis&summary=Go)

MERRA-2 AOD:

https://disc.gsfc.nasa.gov/datasets/M2TMNXAER_V5.12.4/summary?keywords=%22MERRA-2%22

CAMSRA AOD: <https://www.ecmwf.int/en/research/climate-reanalysis/cams-reanalysis>

FLAMBE BB smoke inventory is available upon request from U.S. NRL.

Author contributions: P.X. and J.Z designed this study. P.X. performed most of the data analysis and wrote the initial manuscript. T.T., B.S. and E.H. helped with

processing of CALIOP, MISR and MODIS AOD data respectively. All authors contributed to scientific discussion, writing and revision of the manuscript.

Competing interests: The authors declare that they have no conflict of interest.

Acknowledgments

We thank the NASA AERONET and MAN, and Environment and Climate change Canada AEROCAN groups for the sun-photometer data, and NASA MODIS, MISR and CALIOP teams for the AOD data used in the study. We acknowledge NASA GMAO, ECMWF and U.S. ONR and NRL for making the aerosol reanalysis products available. We acknowledge the use of imagery from the NASA Worldview application (<https://worldview.earthdata.nasa.gov>, last access: Sept 26 2021), part of the NASA Earth Observing System Data and Information System (EOSDIS).

Financial support

The authors acknowledge supports from NASA's Interdisciplinary Science (IDS) program (grant no. 80NSSC20K1260), NASA's Modeling, Analysis and Prediction (MAP) program (NNX17AG52G) and the Office of Naval Research Code 322. N.O. and K.R's work is supported by Canadian Space Agency, SACIA-2 project, Ref. No. 21SUASACOA, ESS-DA program.

References

- Abbatt, J. P. D., Leaitch, W. R., Aliabadi, A. A., Bertram, A. K., Blanchet, J.-P., Boivin-Rioux, A., et al. (2019). Overview paper: New insights into aerosol and climate in the Arctic. *Atmospheric Chemistry and Physics*, **19**(4), 2527– 2560. <https://doi.org/10.5194/acp-19-2527-2019>
- AboEl-Fetouh, Y., O'Neill, N. T., Ranjbar, K., Hesarakhi, S., Abboud, I., & Sobolewski, P. S. (2020). Climatological-scale analysis of intensive and semi-intensive aerosol parameters derived from AERONET retrievals over the Arctic. *Journal of Geophysical Research: Atmospheres*, **125**, e2019JD031569. <https://doi.org/10.1029/2019JD031569>
- AMAP, 2021. Impacts of Short-lived Climate Forcers on Arctic Climate, Air Quality, and Human Health. Summary for Policy-makers. Arctic Monitoring and Assessment Programme (AMAP), Tromsø, Norway. 20 pp
- Baccarini, A., Karlsson, L., Dommen, J. et al. Frequent new particle formation over the high Arctic pack ice by enhanced iodine emissions. *Nat Commun* **11**, 4924 (2020). <https://doi.org/10.1038/s41467-020-18551-0>
- Balzter, H., F. F. Gerard, C. T. George, C. S. Rowland, T. E. Jupp, I. McCallum, A. Shvidenko, S. Nilsson, A. Sukhinin, A. Onuchin, C. Schmullius, Impact of the Arctic Oscillation pattern on interannual forest fire variability in central Siberia. *Geophys. Res. Lett.* **32**, L14709 (2005).

- Baibakov, K., O'Neill, N. T., Ivanescu, L., Duck, T. J., Perro, C., Herber, A., Schulz, K.-H., and Schrems, O.: Synchronous polar winter starphotometry and lidar measurements at a High Arctic station, *AMT*, 8, 3789–3809, doi:10.5194/amt-8-3789-2015, 2015.
- Bieniek, P. A., Bhatt, U. S., York, A., Walsh, J. E., Lader, R., Strader, H., Ziel, R., Jandt, R. R., & Thoman, R. L. (2020). Lightning Variability in Dynamically Downscaled Simulations of Alaska's Present and Future Summer Climate, *Journal of Applied Meteorology and Climatology*, 59(6), 1139–1152.
- Birch, C. E., Brooks, I. M., Tjernström, M., Shupe, M. D., Mauritsen, T., Sedlar, J., Lock, A. P., Earnshaw, P., Persson, P. O. G., Milton, S. F., and Leck, C.: Modelling atmospheric structure, cloud and their response to CCN in the central Arctic: ASCOS case studies, *Atmos. Chem. Phys.*, 12, 3419–3435, <https://doi.org/10.5194/acp-12-3419-2012>, 2012.
- Boisvert, L.N., A.A. Petty and J.C. Stroeve, 2016: The Impact of the Extreme Winter 2015/16 Arctic Cyclone on the Barents–Kara Seas. *Monthly Weather Review*, **144** (11), 4279–4287, doi:10.1175/mwr-d-16-0234.1.
- Bossioli, E., Sotiropoulou, G., Methymaki, G., & Tombrou, M. (2021). Modeling extreme warm-air advection in the Arctic during summer: The effect of mid-latitude pollution inflow on cloud properties. *Journal of Geophysical Research: Atmospheres*, 126, e2020JD033291. <https://doi.org/10.1029/2020JD033291>
- Breider, T. J., Mickley, L. J., Jacob, D. J., Wang, Q., Fisher, J. A., Chang, R. Y. W., and Alexander, B.: Annual distributions and sources of Arctic aerosol components, aerosol optical depth, and aerosol absorption, *J. Geophys. Res.-Atmos.*, 119, 4107–4124, <https://doi.org/10.1002/2013JD020996>, 2014.
- Breider, T. J., Mickley, L. J., Jacob, D. J., Ge, C., Wang, J., Payer Sulprizio, M., Croft, B., Ridley, D. A., McConnell, J. R., Sharma, S., Husain, L., Dutkiewicz, V. A., Eleftheriadis, K., Skov, H., and Hopke, P. K.: Multidecadal trends in aerosol radiative forcing over the Arctic: Contribution of changes in anthropogenic aerosol to Arctic warming since 1980, *J. Geophys. Res.-Atmos.*, 122, 3573–3594, <https://doi.org/10.1002/2016JD025321>, 2017.
- Bullard, J. E., et al. (2016), High-latitude dust in the Earth system, *Rev. Geophys.*, 54, 447– 485, doi:10.1002/2016RG000518
- Campbell, J. R., Tackett, J. L., Reid, J. S., Zhang, J., Curtis, C. A., Hyer, E. J., ... & Winker, D. M. (2012). Evaluating nighttime CALIOP 0.532 μm aerosol optical depth and extinction coefficient retrievals. *Atmospheric Measurement Techniques*, 5(9), 2143–2160.

Colarco, P. R., R. A. Kahn, L. A. Remer, and R. C. Levy, 2014: Impact of satellite viewing-swath width on global and regional aerosol optical thickness statistics and trends. *Atmospheric Measurement Techniques*, **7**, 2313-2335.

Comiso, J. C., Large Decadal Decline of the Arctic Multiyear Ice Cover (2012). *J. Climate*, Vol., 25. 1176-1193. <https://doi.org/10.1175/JCLI-D-11-00113.1>

Coogan, S. C. P., Cai, X., Jain, P., and Flannigan, M. D. (2020) Seasonality and trends in human- and lightning-caused wildfires ≥ 2 ha in Canada, 1959–2018. *International Journal of Wildland Fire* **29**, 473-485. <https://doi.org/10.1071/WF19129>

Coopman, Q., Garrett, T. J., Finch, D. P., & Riedi, J. (2018). High sensitivity of arctic liquid clouds to long-range anthropogenic aerosol transport. *Geo-physical Research Letters*, 45, 372–381. <https://doi.org/10.1002/2017GL075795>

Dai, A., Luo, D., Song, M., & Liu, J. (2019). Arctic amplification is caused by sea-ice loss under increasing CO₂. *Nature Communications*, **10**(1), 121. <https://doi.org/10.1038/s41467-018-07954-9>

Dall'Osto, M., Beddows, D. C. S., Tunved, P., Krejci, R., Ström, J., Hansson, H.-C., et al. (2017). Arctic sea ice melt leads to atmospheric new particle formation. *Scientific Reports*, **7**(1), 3318. <https://doi.org/10.1038/s41598-017-03328-1>

Dang, C., S. G. Warren, Q. Fu, S. J. Doherty, M. Sturm, and J. Su (2017), Measurements of light-absorbing particles in snow across the Arctic, North America, and China: Effects on surface albedo, *J. Geophys. Res. Atmos.*, 122, 10,149–10,168, doi:10.1002/2017JD027070.

Das, S., Colarco, P. R., Oman, L. D., Taha, G., and Torres, O.: The long-term transport and radiative impacts of the 2017 British Columbia pyrocumulonimbus smoke aerosols in the stratosphere, *Atmos. Chem. Phys.*, 21, 12069–12090, <https://doi.org/10.5194/acp-21-12069-2021>, 2021.

DeRepentigny, P., Jahn, A., Holland, M., Fasullo, J., Lamarque, J.-F., Hannay, C., Mills, M., Bailey, D., Tilmes, S., and Barrett, A.: Impact of CMIP6 biomass burning emissions on Arctic sea ice loss, EGU General Assembly 2021, online, 19–30 Apr 2021, EGU21-9020, <https://doi.org/10.5194/egusphere-egu21-9020>, 2021.

Eck, T. F., et al. (2009), Optical properties of boreal region biomass burning aerosols in central Alaska and seasonal variation of aerosol optical depth at an Arctic coastal site, *J. Geophys. Res.*, 114, D11201, doi:10.1029/2008JD010870.

Eckhardt, S., A. Stohl, S. Beirle, N. Spichtinger, P. James, C. Forster, C. Junker, T. Wagner, U. Platt, and S. G. Jennings (2003), The North Atlantic Oscillation controls air pollution transport to the Arctic, *Atmos. Chem. Phys.*, 3(5), 1769–1778, doi:10.5194/acp-3-1769-2003.

Eckhardt, S., Quennehen, B., Olivié, D. J. L., Berntsen, T. K., Cherian, R., Christensen, J. H., Collins, W., Crepinsek, S., Daskalakis, N., Flanner, M., Herber, A., Heyes, C., Hodnebrog, Ø., Huang, L., Kanakidou, M., Klimont, Z., Langner, J., Law, K. S., Lund, M. T., Mahmood, R., Massling, A., Myriokefalitakis, S., Nielsen, I. E., Nøjgaard, J. K., Quaas, J., Quinn, P. K., Raut, J.-C., Rumbold, S. T., Schulz, M., Sharma, S., Skeie, R. B., Skov, H., Uttal, T., von Salzen, K., and Stohl, A.: Current model capabilities for simulating black carbon and sulfate concentrations in the Arctic atmosphere: a multi-model evaluation using a comprehensive measurement data set, *Atmos. Chem. Phys.*, 15, 9413–9433, <https://doi.org/10.5194/acp-15-9413-2015>, 2015.

Engelmann, R., Ansmann, A., Ohneiser, K., Griesche, H., Radenz, M., Hofer, J., Althausen, D., Dahlke, S., Maturilli, M., Veselovskii, I., Jimenez, C., Wiesen, R., Baars, H., Bühl, J., Gebauer, H., Haarig, M., Seifert, P., Wandinger, U., and Macke, A.: Wildfire smoke, Arctic haze, and aerosol effects on mixed-phase and cirrus clouds over the North Pole region during MOSAiC: an introduction, *Atmos. Chem. Phys.*, 21, 13397–13423, <https://doi.org/10.5194/acp-21-13397-2021>, 2021.

Evangeliou, N., Balkanski, Y., Hao, W. M., Petkov, A., Silverstein, R. P., Corley, R., Nordgren, B. L., Urbanski, S. P., Eckhardt, S., Stohl, A., Tunved, P., Crepinsek, S., Jefferson, A., Sharma, S., Nøjgaard, J. K., and Skov, H.: Wildfires in northern Eurasia affect the budget of black carbon in the Arctic – a 12-year retrospective synopsis (2002–2013), *Atmos. Chem. Phys.*, 16, 7587–7604, <https://doi.org/10.5194/acp-16-7587-2016>, 2016.

Fisher, J. A. *et al.* Sources, distribution, and acidity of sulfate-ammonium aerosol in the Arctic in winter-spring. *Atmos Environ* **45**, 7301–7318, <https://doi.org/10.1016/j.atmosenv.2011.08.030> (2011).

Fisher, J. A., et al. (2010), Source attribution and interannual variability of Arctic pollution in spring constrained by aircraft (ARCTAS, ARCPAC) and satellite (AIRS) observations of carbon monoxide, *Atmos. Chem. Phys.*, 10(3), 977–996, doi:10.5194/acp-10-977-2010.

Flanner, M. G., Zender, C. S., Randerson, J. T., & Rasch, P. J. (2007). Present-day climate forcing and response from black carbon in snow. *Journal of Geophysical Research*, 112(September 2006), D11202. <https://doi.org/10.1029/2006JD008003>

Flanner, M. G., C. S. Zender, P. G. Hess, N. M. Mahowald, T. H. Painter, V. Ramanathan, and P. J. Rasch (2009), Springtime warming and reduced snow cover from carbonaceous particles, *Atmos. Chem. Phys.*, 9(7), 2481–2497, doi:10.5194/acp-9-2481-2009.

Flannigan, M. D., and J. B. Harrington, 1988: A study of the relation of meteorological variables to monthly provincial area burned by wildfire in Canada (1953-1980). *J. Appl. Meteorol.*, **27**, 441-452.

Fromm, M., Lindsey, D. T., Servranckx, R., Yue, G., Trickl, T., Sica, R., Doucet, P., & Godin-Beekmann, S. (2010). The Untold Story of Pyrocumulonimbus, *Bulletin of the American Meteorological Society*, 91(9), 1193-1210.

Gabric, A., Matrai, P., Jones, G., & Middleton, J. (2018). The nexus between sea ice and polar emissions of marine biogenic aerosols. *Bulletin of the American Meteorological Society*, 99(1), 61– 81. <https://doi.org/10.1175/BAMS-D-16-0254.1>

Garay, M. J., and Coauthors, 2020: Introducing the 4.4 km spatial resolution Multi-Angle Imaging SpectroRadiometer (MISR) aerosol product. *Atmospheric Measurement Techniques*, 13, 593-628.

Garrett, T. J., Zhao, C., and Novelli, P.: Assessing the relative contributions of transport efficiency and scavenging to seasonal variability in Arctic aerosol, *Tellus B*, 62, 190–196, <https://doi.org/10.1111/j.1600-0889.2010.00453.x>, 2010.

Garrett, T. J., Brattström, S., Sharma, S., Worthy, D. E., and Novelli, P.: The role of scavenging in the seasonal transport of black carbon carbon and sulfate to the Arctic, *Geophys. Res. Lett.*, 38, L16805, <https://doi.org/10.1029/2011GL048221>, 2011.

Giglio, L., Randerson, J. T., and van der Werf, G. R.: Analysis of daily, monthly, and annual burned area using the fourth generation global fire emissions database (GFED4), *J. Geophys. Res.-Biogeo.*, 118, 317–328, <https://doi.org/10.1002/jgrg.20042>, 2013.

Giles, D. M., Sinyuk, A., Sorokin, M. G., Schafer, J. S., Smirnov, A., Slutsker, I., Eck, T. F., Holben, B. N., Lewis, J. R., Campbell, J. R., Welton, E. J., Korkin, S. V., and Lyapustin, A. I.: Advancements in the Aerosol Robotic Network (AERONET) Version 3 database – automated near-real-time quality control algorithm with improved cloud screening for Sun photometer aerosol optical depth (AOD) measurements, *Atmos. Meas. Tech.*, 12, 169–209, <https://doi.org/10.5194/amt-12-169-2019>, 2019.

Glantz, P., Bourassa, A., Herber A., Iversen T., Karlsson J., Kirkevåg, A., Maturilli, M., Seland, O., Stebel, K., Struthers, H., Tesche, M., and Thomason L., (2014), Remote sensing of aerosols in the Arctic for an evaluation of global climate model simulations, *J. Geophys. Res. Atmos.*, 119, 8169–8188, doi:10.1002/2013JD021279.

Goosse, H., Kay, J.E., Armour, K.C. *et al.* Quantifying climate feedbacks in polar regions. *Nat Commun* 9, 1919 (2018). <https://doi.org/10.1038/s41467-018-04173-0>

Graham, R.M. et al., 2017: Increasing frequency and duration of Arctic winter warming events. *Geophysical Research Letters*, 44 (13), 6974–6983, doi:10.1002/2017gl073395.

Groot Zwaafink, C. D., H. Grythe, H. Skov, and A. Stohl (2016), Substantial contribution of northern high-latitude sources to mineral dust in the Arctic, *J. Geophys. Res. Atmos.*, 121, 13,678–13,697, doi:10.1002/2016JD025482.

Hall, J. V., Loboda, T. V., Giglio, L., McCarty G. W. (2016), A MODIS-based burned area assessment for Russian croplands: Mapping requirements and challenges. *Remote Sensing of Environment*, Vol. 184, 506-521. <https://doi.org/10.1016/j.rse.2016.07.022>

Hansen J. and Nazarenko, L. (2004): Soot climate forcing via snow and ice albedos. *PNAS*, 101 (2). 423-428.

Hansen, E., Gerland, S., Granskog, M. A., Pavlova, O., Renner, A. H. H., Haapala, J., et al. (2013). Thinning of Arctic sea ice observed in Fram Strait: 1990–2011. *Journal of Geophysical Research: Oceans*, 118, 5202–5221. <https://doi.org/10.1002/jgrc.20393>

Herber, A., L. W. Thomason, H. Gernandt, U. Leiterer, D. Nagel, K. Schulz, J. Kaptur, T. Albrecht, and J. Notholt (2002), Continuous day and night aerosol optical depth observations in the Arctic between 1991 and 1999, *J. Geophys. Res.*, 107(D10), 4097, doi:10.1029/2001JD000536.

Hesarakis S, O'Neill NT, Lesins G, Saha A, Martin RV, Fioletov VE, Baibakov K, Abboud I. Comparisons of a chemical transport model with a four-year (April to September) analysis of fine-and coarse-mode aerosol optical depth retrievals over the Canadian Arctic. *Atmosphere-Ocean*. 2017 Oct 20;55(4-5):213-29.

Hyer, E. J., J. S. Reid, and J. Zhang, 2011: An over-land aerosol optical depth data set for data assimilation by filtering, correction, and aggregation of MODIS Collection 5 optical depth retrievals. *Atmospheric Measurement Techniques*, European Geophysical Union, 379-408.

Hyer, Edward J., Eric S. Kasischke, and Dale J. Allen. "Effects of source temporal resolution on transport simulations of boreal fire emissions." *Journal of Geophysical Research: Atmospheres* 112.D1 (2007). <https://doi.org/10.1029/2006JD007234>

Hyer EJ, Reid JS, Prins EM, Hoffman JP, Schmidt CC, Miettinen JI, [Giglio L.](#) : Patterns of fire activity over Indonesia and Malaysia from polar and geostationary satellite observations *Atmospheric Research*. 122: 504-519.
DOI: [10.1016/J.Atmosres.2012.06.011](https://doi.org/10.1016/J.Atmosres.2012.06.011) , 2013

Inness, A., Ades, M., Agustí-Panareda, A., Barré, J., Benedictow, A., Blechschmidt, A.-M., Dominguez, J. J., Engelen, R., Eskes, H., Flemming, J., Huijnen, V., Jones, L., Kipling, Z., Massart, S., Parrington, M., Peuch, V.-H., Razinger, M., Remy, S., Schulz, M., and Suttie, M.: The CAMS reanalysis of atmospheric composition, *Atmos. Chem. Phys.*, 19, 3515–3556, <https://doi.org/10.5194/acp-19-3515-2019>, 2019.

IPCC 2013 Chapter 8 by Myhre, G., D. Shindell, F.-M. Bréon, W. Collins, J. Fuglestad, J. Huang, D. Koch, J.-F. Lamarque, D. Lee, B. Mendoza, T. Nakajima, A. Robock, G. Stephens, T. Takemura and H. Zhang, 2013: Anthropogenic and Natural Radiative

Forcing. In: Climate Change 2013: The Physical Science Basis. Contribution of Working Group I to the Fifth Assessment Report of the Intergovernmental Panel on Climate Change [Stocker, T.F., D. Qin, G.-K. Plattner, M. Tignor, S.K. Allen, J. Boschung, A. Nauels, Y. Xia, V. Bex and P.M. Midgley (eds.)]. Cambridge University Press, Cambridge, United Kingdom and New York, NY, USA.

IPCC. (2021). Climate change 2021: The physical science basis. Contribution of working group I to the sixth assessment report of the intergovernmental panel on climate change [Masson-Delmotte, In V. P. Zhai, A. Pirani, S. L. Connors, C. Péan, S. Berger, N. Caud et al. (Eds.), Cambridge University Press. In Press.

Iziomon, M. G., U. Lohmann, and P. K. Quinn (2006), Summertime pollution events in the Arctic and potential implications, *J. Geophys. Res.*, 111, D12206, doi:10.1029/2005JD006223.

Jacob, D. J., J. H. Crawford, H. Maring, A. D. Clarke, J. E. Dibb, L. K. Emmons, R. A. Ferrare, C. A. Hostetler, P. B. Russell, and H. B. Singh (2010), The arctic research of the composition of the troposphere from aircraft and satellites (ARCTAS) mission: Design, execution, and first results, *Atmos. Chem. Phys.*, 10(11), 5191–5212.

Jacobson, M. Z. (2004), Climate response of fossil fuel and biofuel soot, accounting for soot's feedback to snow and sea ice albedo and emissivity, *J. Geophys. Res.*, 109, D21201, doi:10.1029/2004JD004945.

Kang S., Y. Zhang, Y. Qian, and H. Wang. 2020. "A review of black carbon in snow and ice and its impact on the cryosphere." *Earth - Science Reviews* 210. PNNL-SA-154137. doi:10.1016/j.earscirev.2020.103346

Kapsch, M.-L., R.G. Graversen and M. Tjernström, 2013: Springtime atmospheric energy transport and the control of Arctic summer sea-ice extent. *Nature Climate Change*, 3, 744, doi:10.1038/nclimate1884.

Khan, A. L., S. Wagner, R. Jaffe, P. Xian, M. Williams, R. Armstrong, and D. McKnight (2017), Dissolved black carbon in the global cryosphere: Concentrations and chemical signatures, *Geophys. Res. Lett.*, 44, 6226–6234, doi:10.1002/2017GL073485.

Kim, J. S., Kug, J. S., Jeong, S. J., Park, H., and Schaepman-Strub, G.: Extensive fires in southeastern Siberian permafrost linked to preceding Arctic Oscillation, *Sci. Adv.*, 6, eaax3308, <https://doi.org/10.1126/sciadv.aax3308>, 2020.

Kim, M. H., and Coauthors, 2018: The CALIPSO version 4 automated aerosol classification and lidar ratio selection algorithm. *Atmospheric Measurement Techniques*, 11, 6107-6135.

Kleidman, R. G., N. T. O'Neill, L. A. Remer, Y. J. Kaufman, T. F. Eck, D. Tanre', O. Dubovik, and B. N. Holben (2005), Comparison of Moderate Resolution Imaging Spectroradiometer (MODIS) and Aerosol Robotic Network (AERONET) remote-sensing

retrievals of aerosol fine mode fraction over ocean, *J. Geophys. Res.*, 110, D22205, doi:10.1029/2005JD005760.

Kokhanovsky, A., and Tomasi, C. (Eds.): *Physics and Chemistry of the Arctic Atmosphere*. Springer Nature Switzerland AG 2020. <https://doi.org/10.1007/978-3-030-33566-3>

Köllner, F., Schneider, J., Willis, M. D., Schulz, H., Kunkel, D., Bozem, H., Hoor, P., Klimach, T., Helleis, F., Burkart, J., Leaitch, W. R., Aliabadi, A. A., Abbatt, J. P. D., Herber, A. B., and Borrmann, S.: Chemical composition and source attribution of sub-micrometre aerosol particles in the summertime Arctic lower troposphere, *Atmos. Chem. Phys.*, 21, 6509–6539, <https://doi.org/10.5194/acp-21-6509-2021>, 2021.

Kondo, Y., et al. (2011), Emissions of black carbon, organic, and inorganic aerosols from biomass burning in North America and Asia in 2008, *J. Geophys. Res.*, 116, D08204, doi:10.1029/2010JD015152.

Korontzi, S., J. McCarty, T. Loboda, S. Kumar, and C. Justice (2006), Global distribution of agricultural fires in croplands from 3 years of Moderate Resolution Imaging Spectroradiometer (MODIS) data, *Global Biogeochem. Cycles*, 20, GB2021, doi:10.1029/2005GB002529.

Kwok, R. and Rothrock D. A. (2009) Decline in Arctic sea ice thickness from submarine and ICESat records: 1958-2008. *Geophys. Res. Lett.* 36 L15501.

Law, K. S. and A. Stohl, 2007: Arctic air pollution: Origins and impacts. *Science*, **315**, 1537–1540, doi:10.1126/science.1137695.

Lubin, D., and Vogelmann, A. M. (2006). A climatologically significant aerosol longwave indirect effect in the Arctic. *Nature*, 439, 453–456. <https://doi.org/10.1038/nature04449>

Lynch, P., J. S. Reid, D. L. Westphal, J. Zhang, T. Hogan, E. J. Hyer, C. A. Curtis, D. Hegg, Y. Shi, J. R. Campbell, J. Rubin, W. Sessions, J. Turk and A. Walker: An 11-year Global Gridded Aerosol Optical Thickness Reanalysis (v1.0) for Atmospheric and Climate Sciences. *Geosci. Model Dev.*, 9, 1489-1522, doi:10.5194/gmd-9-1489-2016, 2016.

Macias Fauria, M, E. A. Johnson, Large-scale climatic patterns control large lightning fire occurrence in Canada and Alaska forest regions. *J. Geophys. Res.* **111**, G04008 (2006).

Markowicz, K. M., et al. (2016), Impact of North American intense fires on aerosol optical properties measured over the European Arctic in July 2015, *J. Geophys. Res. Atmos.*, 121, 14,487–14,512, doi:10.1002/2016JD025310.

Markowicz, K.M., Lisok, J., Xian, P., Simulation of long-term direct aerosol radiative forcing over the arctic within the framework of the iAREA project, *Atmospheric Environment* (2021), doi: <https://doi.org/10.1016/j.atmosenv.2020.117882>.

Mauritsen, T., Sedlar, J., Tjernström, M., Leck, C., Martin, M., Shupe, M., Sjogren, S., Sierau, B., Persson, P. O. G., Brooks, I. M., and Swietlicki, E.: An Arctic CCN-limited cloud-aerosol regime, *Atmos. Chem. Phys.*, 11, 165–173, <https://doi.org/10.5194/acp-11-165-2011>, 2011.

McCarty, J. L., Aalto, J., Paunu, V.-V., Arnold, S. R., Eckhardt, S., Klimont, Z., Fain, J. J., Evangeliou, N., Venäläinen, A., Tchepakova, N. M., Parfenova, E. I., Kupiainen, K., Soja, A. J., Huang, L., and Wilson, S.: Reviews and syntheses: Arctic fire regimes and emissions in the 21st century, *Biogeosciences*, 18, 5053–5083, <https://doi.org/10.5194/bg-18-5053-2021>, 2021.

McNaughton, C. S., Clarke, A. D., Freitag, S., Kapustin, V. N., Kondo, Y., Moteki, N., Sahu, L., Takegawa, N., Schwarz, J. P., Spackman, J. R., Watts, L., Diskin, G., Podolske, J., Holloway, J. S., Wisthaler, A., Mikoviny, T., de Gouw, J., Warneke, C., Jimenez, J., Cubison, M., Howell, S. G., Middlebrook, A., Bahreini, R., Anderson, B. E., Winstead, E., Thornhill, K. L., Lack, D., Cozic, J., and Brock, C. A.: Absorbing aerosol in the troposphere of the Western Arctic during the 2008 ARCTAS/ARCPAC airborne field campaigns, *Atmos. Chem. Phys.*, 11, 7561–7582, <https://doi.org/10.5194/acp-11-7561-2011>, 2011.

Meier, W. N., Hovelsrud, G. K., van Oort, B. E. H., Key, J. R., Kovacs, K. M., Michel, C., et al. (2014). Arctic sea ice in transformation: A review of recent observed changes and impacts on biology and human activity. *Reviews of Geophysics*, **52**, 185– 217. <https://doi.org/10.1002/2013RG000431>

Morrison, A.L. et al., 2018: Isolating the Liquid Cloud Response to Recent Arctic Sea Ice Variability Using Spaceborne Lidar Observations. *Journal of Geophysical Research: Atmospheres*, **123** (1), 473–490, doi:10.1002/2017jd027248.

Notz D. and Stroeve, J. Observed Arctic sea-ice loss directly follows anthropogenic CO₂ emission (2016) *Science*. Vol. 354, Issue 6313, pp. 747-750 DOI: 10.1126/science.aag2345

Nummelin, A., C. Li and P.J. Hezel, 2017: Connecting ocean heat transport changes from the midlatitudes to the Arctic Ocean. *Geophysical Research Letters*, **44** (4), 1899–1908, doi:10.1002/2016GL071333.

O'Neill, N.T., T.F.Eck, B.N.Holben, A.Smirnov, O.Dubovik, and A.Royer (2001) Bimodal size distribution influences on the variation of Angstrom derivatives in spectral and optical depth space, *J. Geophys. Res.*, 106, 9787-9806.

O'Neill, N. T., Perro, C., Saha, A., Lesins, G., Duck, T. J., Eloranta, E. W., Nott, G. J., Hoffman, A., Karumudi, M. L., Ritter, C., Bourassa, A., Abboud, I., Carn S., A., Savastiouk, V. (2012) Properties of Sarychev Sulphate aerosols over the Arctic. *J. Geophys. Res. Atmos.* Vol. 117, D04203, <https://doi.org/10.1029/2011JD016838>

O'Neill, N. T., Perro, C., Saha, A., Lesin, G., Duck, T., Eloranta, E., Hoffman, M. L. Karumudi, A., Ritter, C., A. Bourassa, I. Aboud, S. Carn, V. Savastiouk, Impact of Sarychev sulphate aerosols over the Arctic, *Jour. Geophys. Res.*, VOL. 117, D04203, doi:10.1029/2011JD016838, 2012.

O'Neill, N. T., Eck, T. F., Smirnov, A., Holben, B. N., and Thulasiraman S. (2003) Spectral discrimination of coarse and fine mode optical depth. *J. Geophys. Res.*, 108, D05212, doi:10.1029/2002JD002975.

Peterson, D. A., Fromm, M. D., Solbrig, J. E., Hyer, E. J., Surratt, M. L., & Campbell, J. R. (2017). Detection and Inventory of Intense Pyroconvection in Western North America using GOES-15 Daytime Infrared Data, *Journal of Applied Meteorology and Climatology*, 56(2), 471-493.

Peterson, D. A., Hyer, E. J., Campbell, J. R., Fromm, M. D., Hair, J. W., Butler, C. F., & Fenn, M. A. (2015). The 2013 Rim Fire: Implications for Predicting Extreme Fire Spread, Pyroconvection, and Smoke Emissions, *Bulletin of the American Meteorological Society*, 96(2), 229-247.

Perovich, D. K., and C. Polashenski (2012), Albedo evolution of seasonal Arctic sea ice, *Geophys. Res. Lett.*, 39, L08501, doi:10.1029/2012GL051432

Prenni, A. J., Harrington, J. Y., Tjernstöm, M., DeMott, P. J., Avramov, A., Long, C. N., Kreidenweis, S. M., Olsson, P. Q., and Verlinde, J.: Can ice-nucleating aerosols affect arctic seasonal climate?, *B. Am. Meteorol. Soc.*, 88, 541–550, <https://doi.org/10.1175/BAMS-88-4-541>, 2007.

Quinn, P. K., et al. (2008), Short-lived pollutants in the Arctic: Their climate impact and possible mitigation strategies, *Atmos. Chem. Phys.*, 8(6), 1723–1735, doi:10.5194/acp-8-1723-2008.

Randles, C. A., daSilva, A. M., Buchard, V., Colarco, P. R., Darmenov, A., Govindaraju, R., et al.: The MERRA-2 aerosol reanalysis, 1980 onward. Part I: System description and data assimilation evaluation. *Journal of Climate*, 30(17), 6823-6850. <https://doi.org/10.1175/JCLI-D-16-0609.1>, 2017.

Randerson, J. T., and Coauthors, 2006: The impact of boreal forest fire on climate warming. *Science*, 314, 1130–1132, doi:10.1126/science.1132075.

Ranjbar, K., O'Neill, N. T., Lutsch, E., McCullough, E. M., AboEl-Fetouh, Y., Xian, P., et al. (2019). Extreme smoke event over the high Arctic. *Atmospheric Environment*, 218, 117002. <https://doi.org/10.1016/j.atmosenv.2019.117002>

Reid, J. S., Hyer, E. J., Prins, E. M., Westphal, D. L., Zhang, J., Wang, J., Christopher, S. A., Curtis, C. A., Schmidt, C. C., Eleuterio, D. P., Richardson, K. A., and Hoffman, J. P.: Global Monitoring and Forecasting of Biomass-Burning Smoke: Description of and Lessons from the Fire Locating and Modeling of Burning Emissions (FLAMBE) Program, *IEEE J. Sel. Top. Appl.*, 2, 144–162, JSTARS-2009-00034, 2009.

Reid, J. S., Koppmann, R., Eck, T. F., and Eleuterio, D. P.: A review of biomass burning emissions part II: intensive physical properties of biomass burning particles, *Atmos. Chem. Phys.*, 5, 799–825, <https://doi.org/10.5194/acp-5-799-2005>, 2005.

Rinke, A., Maturilli, M., Graham, R. M., Hatthes, H., Handorf, D., Cohen, L., Hudson, S. R. and Moore, J. C., (2017), Extreme cyclone events in the Arctic: Wintertime variability and trends. *Environ. Res. Lett.* **12** 094006

Rosel, A., Itkin, P., King, J., Divine, D., Wang, C., Granskog, M. A., Krumpen, T., and Gerland, S. (2018). Thin sea ice, thick snow and widespread negative freeboard observed during N-ICE2015 north of Svalbard. *J. Geophys. Res: Oceans*, 123, 1156–1176. <https://doi.org/10.1002/2017JC012865>

Saha, A., et al. (2010), Pan-Arctic sunphotometry during the ARCTAS-A campaign of April 2008, *Geophys. Res. Lett.*, 37, L05803, doi:10.1029/2009GL041375.

Sand, M., T. K. Berntsen, Ø. Seland, and J. E. Kristjánsson (2013), Arctic surface temperature change to emissions of black carbon within Arctic or midlatitudes, *J. Geophys. Res. Atmos.*, 118, 7788–7798, doi:10.1002/jgrd.50613.

Sand, M., Berntsen, T., Von Salzen, K., Flanner, M., Langner, J., and Victor, D.: Response of Arctic temperature to changes in emissions of short-lived climate forcers, *Nat. Clim. Change*, 6, 286–289, <https://doi.org/10.1038/nclimate2880>, 2016.

Sand, M., Samset, B. H., Balkanski, Y., Bauer, S., Bellouin, N., Berntsen, T. K., Bian, H., Chin, M., Diehl, T., Easter, R., Ghan, S. J., Iversen, T., Kirkevåg, A., Lamarque, J.-F., Lin, G., Liu, X., Luo, G., Myhre, G., Noije, T. V., Penner, J. E., Schulz, M., Seland, Ø., Skeie, R. B., Stier, P., Takemura, T., Tsigaridis, K., Yu, F., Zhang, K., and Zhang, H.: Aerosols at the poles: an AeroCom Phase II multi-model evaluation, *Atmos. Chem. Phys.*, 17, 12197–12218, <https://doi.org/10.5194/acp-17-12197-2017>, 2017.

Sayer, A. M. and Knobelspiesse, K. D.: How should we aggregate data? Methods accounting for the numerical distributions, with an assessment of aerosol optical depth, *Atmos. Chem. Phys.*, 19, 15023–15048, <https://doi.org/10.5194/acp-19-15023-2019>, 2019.

Serreze, M.C. and R.G. Barry, 2011: Processes and impacts of Arctic amplification: A research synthesis. *Global and Planetary Change*, **77** (1– 2), 85–96, doi:10.1016/j.gloplacha.2011.03.004.

Serreze, M.C., Francis, J.A. The Arctic Amplification Debate. *Climatic Change* **76**, 241–264 (2006). <https://doi.org/10.1007/s10584-005-9017-y>

Sharma, S., M. Ishizawa, D. Chan, D. Lavoué, E. Andrews, K. Eleftheriadis, and S. Maksyutov (2013), 16-year simulation of Arctic black carbon: Transport, source contribution, and sensitivity analysis on deposition, *J. Geophys. Res. Atmos.*, **118**, 943–964, doi:10.1029/2012JD017774.

Shi, Y., J. Zhang, J. S. Reid, E. J. Hyer, and N. C. Hsu, 2013: Critical evaluation of the MODIS Deep Blue aerosol optical depth product for data assimilation over North Africa. *Atmospheric Measurement Techniques*, **6**, 949-969.

Shi, Y., J. Zhang, J. S. Reid, B. Holben, E. J. Hyer, and C. Curtis, 2011: An analysis of the collection 5 MODIS over-ocean aerosol optical depth product for its implication in aerosol assimilation. *Atmos. Chem. Phys.*, **11**, 557-565.

Shindell, D. and Faluvegi, G.: Climate response to regional radiative forcing during the twentieth century, *Nat. Geosci.*, **2**, 294–300, <https://doi.org/10.1038/ngeo473>, 2009.

Schlosser, J. S., R. A. Braun, T. Bradley, H. Dadashazar, A. B. MacDonald, A. A. Aldhaif, M. A. Aghdam, A. H. Mardi, P. Xian, and A. Sorooshian (2017), Analysis of aerosol composition data for western United States wildfires between 2005 and 2015: Dust emissions, chloride depletion, and most enhanced aerosol constituents, *J. Geophys. Res. Atmos.*, **122**, 8951–8966, doi:10.1002/2017JD026547.

Skiles S. M., Flanner, M., Cook, J. M., Dumont, M. and Painter, T. (2018) Radiative forcing by light-absorbing particles in snow. *Nature Climate Change*, **8**, 964-971. <https://doi.org/10.1038/s41558-018-0296-5>

Skinner, W. R., B. J. Stocks, D. L. Martell, B. Bonsal, and A. Shabbar, 1999: The association between circulation anomalies in the mid- troposphere and area burned by wildland fire in Canada. *Theoretical and Applied Climatology*, **63**, 89-105.

Stohl, A., et al. (2006), Pan-Arctic enhancements of light absorbing aerosol concentrations due to North American boreal forest fires during summer 2004, *J. Geophys. Res.*, **111**, D22214, doi:10.1029/2006JD007216.

Stohl, A., et al. (2007), Arctic smoke—Record high air pollution levels in the European Arctic due to agricultural fires in eastern Europe in spring 2006, *Atmos. Chem. Phys.*, **7**(2), 511–534, doi:10.5194/acp-7-511-2007.

- Stone, R. S., G. P. Anderson, E. Andrews, E. G. Dutton, E. P. Shettle, and A. Berk (2007), Incursions and radiative impact of Asian dust in northern Alaska, *Geophys. Res. Lett.*, **34**, L14815, doi:10.1029/2007GL029878.
- Taylor, P., B. Hegyi, R. Boeke and L. Boisvert, 2018: On the Increasing Importance of Air-Sea Exchanges in a Thawing Arctic: A Review. *Atmosphere*, **9** (2), doi:10.3390/atmos9020041.
- Tomasi, C., Kokhanovsky, A. A., Lupi, A., Ritter, C., Smirnov, A., O'Neill, N. T., Stone, R. S., Holben, B. N., Nyeki, S., Wehrli, C., Stohl, A., Mazzola, M., Lanconelli, C., Vitale, V., Stebel, K., Aaltonen, V., de Leeuw, G., Rodriguez, E., Herber, A. B., Radionov, V. F., Zielinski, T., Petelski, T., Sakerin, S. M., Kabanov, D. M., Xue, Y., Mei, L., Istomina, L., Wagener, R., McArthur, B., Sobolewski, P. S., Kivi, R., Courcoux, Y., Larouche, P., Broccardo, S., & Piketh, S. J. (2015). Aerosol remote sensing in polar regions. *Earth-Science Reviews*, **140**, 108–157. <https://doi.org/10.1016/j.earscirev.2014.11.001>.
- Tomasi, C., Vitale, V., Lupi, A., Di Carmine, C., Campanelli, M., Herber, A., Treffeisen, R., Stone, R. S., Andrews, E., Sharma, S., Radionov, V., von Hoyningen-Huene, W., Stebel, K., Hansen, G. H., Myhre, C. L., Wehrli, C., Aaltonen, V., Lihavainen, H., Virkkula, A., Hillamo, R., Ström, J., Toledano, C., Cachorro, V. E., Ortiz, P., de Frutos, A. M., Blindheim, S., Frioud, M., Gausa, M., Zielinski, T., Petelski, T., & Yamanouchi, T. (2007). Aerosols in polar regions: a historical overview based on optical depth and in situ observations. *Journal of Geophysical Research, Atmospheres*, **112**, D16. <https://doi.org/10.1029/2007JD008432>.
- Thomason, L. W., Ernest, N., Luis, M. L., Rieger, L., Bourassa, A., Vernier, J.-P., Manney, G., Luo, B., Arfeuille, F., & Peter, T. (2018). A global space-based stratospheric aerosol climatology: 1979–2016. *Earth System Science Data*, **10**, 469–492. <https://doi.org/10.5194/essd-10-469-2018>.
- Torres, O., Bhartia, P. K., Taha, G., Jethva, H., Das, S., Colarco, P., Krotkov, N., Omar, A., and Ahn, C.: Stratospheric Injection of Massive Smoke Plume From Canadian Boreal Fires in 2017 as Seen by DSCOVR-EPIC, CALIOP, and OMPS-LP Observations, *J. Geophys. Res.-Atmos.*, **125**, e2020JD032579, <https://doi.org/10.1029/2020JD032579>, 2020.
- Toth, T. D., Campbell, J. R., Reid, J. S., Tackett, J. L., Vaughan, M. A., Zhang, J., & Marquis, J. W. (2018). Minimum aerosol layer detection sensitivities and their subsequent impacts on aerosol optical thickness retrievals in CALIPSO level 2 data products. *Atmospheric Measurement Techniques*, **11**(1), 499-514.
- Toth, T. D., Zhang, J., Campbell, J. R., Reid, J. S., & Vaughan, M. A. (2016). Temporal variability of aerosol optical thickness vertical distribution observed from CALIOP. *Journal of Geophysical Research: Atmospheres*, **121**(15), 9117-9139.

- Valkonen, E., Cassano, J., & Cassano, E. (2021). Arctic cyclones and their interactions with the declining sea ice: A recent climatology. *Journal of Geophysical Research: Atmospheres*, 126, e2020JD034366. <https://doi.org/10.1029/2020JD034366>
- van der Werf, G. R., J. T. Randerson, L. Giglio, G. J. Collatz, P. S. Kasibhatla, and A. F. Arellano Jr., 2006: Interannual variability in global biomass burning emissions from 1997 to 2004. *Atmos. Chem. Phys.*, 6, 3423–3441, doi:[10.5194/acp-6-3423-2006](https://doi.org/10.5194/acp-6-3423-2006).
- Warneke, C., Froyd, K. D., Brioude, J., Bahreini, R., Brock, C. A., Cozic, J., et al. (2010). An important contribution to springtime Arctic aerosol from biomass burning in Russia. *Geophysical Research Letters*, 37, L01801. <https://doi.org/10.1029/2009GL041816>
- Waseda, T., Nose, T., Kodaira, T., Sasmal, K and Webb, A. (2021) Climatic trends of extreme wave events caused by Arctic cyclones in the western Arctic Ocean. *Polar Science*. Vol 27, 100625, doi:10.1016/j.polar.2020.100625
- Wendisch, M., Macke, A., Ehrlich, A., Lupkes, C., Mech, M., Chechin, D., et al. (2019). The Arctic cloud puzzle: Using ACLOUD/PASCAL multiplatform observations to unravel the role of clouds and aerosol particles in Arctic amplification. *Bulletin of the American Meteorological Society*, 100, 841–871. <https://doi.org/10.1175/BAMS-D-18-0072.1>
- Wex, H., Huang, L., Zhang, W., Hung, H., Traversi, R., Becagli, S., Sheesley, R. J., Moffett, C. E., Barrett, T. E., Bossi, R., Skov, H., Hünnerbein, A., Lubitz, J., Löffler, M., Linke, O., Hartmann, M., Herenz, P., and Stratmann, F.: Annual variability of ice-nucleating particle concentrations at different Arctic locations, *Atmos. Chem. Phys.*, 19, 5293–5311, <https://doi.org/10.5194/acp-19-5293-2019>, 2019.
- Winker, D. M., Pelon, J. R., & McCormick, M. P. (2003). CALIPSO mission: spaceborne lidar for observation of aerosols and clouds. In *Lidar Remote Sensing for Industry and Environment Monitoring III* (Vol. 4893, pp. 1-11). International Society for Optics and Photonics.
- Winker, D. M., Vaughan, M. A., Omar, A., Hu, Y., Powell, K. A., Liu, Z., Hunt, W. H., and Young, S. A. (2009). Overview of the CALIPSO Mission and CALIOP Data Processing Algorithms. *J. of Atmos. Oceanic Tech.* Vol 26., 2310-2323, <https://doi.org/10.1175/2009JTECHA1281.1>
- Woods, C., & Caballero, R. (2016). The role of moist intrusions in Winter Arctic warming and sea ice decline. *Journal of Climate*, 29, 4473–4485. <https://doi.org/10.1175/JCLI-D-15-0773.1>
- Xian, P., Klotzbach, P. J., Dunion, J. P., Janiga, M. A., Reid, J. S., Colarco, P. R., and Kipling, Z.: Revisiting the relationship between Atlantic dust and tropical cyclone activity using aerosol optical depth reanalyses: 2003–2018, *Atmos. Chem. Phys.*, 20, 15357–15378, <https://doi.org/10.5194/acp-20-15357-2020>, 2020.

Xian, P., Reid J. S., Hyer, E., Sampson, C.R., Rubin, J., Ades M., et. al., Current state of the global operational aerosol multi-model ensemble: an update from the International Cooperative for Aerosol Prediction (ICAP), 2019, Quarterly J. of the Royal Met. Soc. <https://doi.org/10.1002/qj.3497>

Xian, P., J. S. Reid, J. F. Turk, E. J. Hyer and D. L. Westphal: Impact of models versus satellite measured tropical precipitation on regional smoke optical thickness in an aerosol transport model, *Geophys. Res. Lett.*, 36, L16805, doi:10.1029/2009GL038823, 2009.

Yang, Y., Wang, H., Smith, S. J., Easter, R. C., and Rasch, P. J.: Sulfate Aerosol in the Arctic: Source Attribution and Radiative Forcing, *J. Geophys. Res.-Atmos.*, 123, 1899–1918, <https://doi.org/10.1002/2017JD027298>, 2018.

Zamora, L. M., Kahn, R. A., Cubison, M. J., Diskin, G. S., Jimenez, J. L., Kondo, Y., McFarquhar, G. M., Nenes, A., Thornhill, K. L., Wisthaler, A., Zelenyuk, A., and Ziemba, L. D.: Aircraftmeasured indirect cloud effects from biomass burning smoke in the Arctic and subarctic, *Atmos. Chem. Phys.*, 16, 715–738, <https://doi.org/10.5194/acp-16-715-2016>, 2016.

Zhang, J. L., and J. S. Reid, 2006: MODIS aerosol product analysis for data assimilation: Assessment of over-ocean level 2 aerosol optical thickness retrievals. *J. Geophys. Res.-Atmos.*, 111.

Zhang, J. L., and J. S. Reid, D. L. Westphal, N. L. Baker, and E. J. Hyer, 2008: A system for operational aerosol optical depth data assimilation over global oceans. *J. Geophys. Res.*, 113, D10208, doi:10.1029/2007JD009065.

Zhang, J. and Reid, J. S.: A decadal regional and global trend analysis of the aerosol optical depth using a data-assimilation grade over-water MODIS and Level 2 MISR aerosol products, *Atmos. Chem. Phys.*, 10, 18879-18917, doi:10.5194/acpd-10-18879-2010, 2010.

Zhang J., Reid, J. S., Alfaro-Contreras, R., Xian P., Has China been exporting less particulate air pollution over the past decade?, *Geophysical Research Letters*, 10.1002/2017GL072617, 2017.

Zhang, J., Spurr, R. J. D., Reid, J. S., Xian, P., Colarco, P. R., Campbell, J. R., Hyer, E. J., and Baker, N. L.: Development of an Ozone Monitoring Instrument (OMI) aerosol index (AI) data assimilation scheme for aerosol modeling over bright surfaces – a step toward direct radiance assimilation in the UV spectrum, *Geosci. Model Dev.*, 14, 27–42, <https://doi.org/10.5194/gmd-14-27-2021>, 2021.

- 1796 Zhao, C., & Garrett, T. J. (2015). Effects of Arctic haze on surface cloud radiative
1797 forcing. *Geophysical Research Letters*, 42, 557–564.
1798 <https://doi.org/10.1002/2014GL062015>
1799
- 1800 Zhang, Z.; Wang, L.; Xue, N.; Du, Z. Spatiotemporal Analysis of Active Fires in the
1801 Arctic Region during 2001–2019 and a Fire Risk Assessment Model. *Fire* **2021**, 4, 57.
1802 <https://doi.org/10.3390/fire4030057>

Arctic spring and summertime aerosol optical depth baseline from long-term observations and model reanalyses - Part 2: Statistics of extreme AOD events, and implications for the impact of regional biomass burning processes

Peng Xian¹, Jianglong Zhang², Norm T. O'Neill³, Jeffrey S. Reid¹, Travis D. Toth⁴, Blake Sorenson², Edward J. Hyer¹, James R. Campbell¹, and Keyvan Ranjbar^{3, a}

¹Naval Research Laboratory, Monterey, CA, USA.

²Department of Atmospheric Sciences, University of North Dakota, Grand Forks, ND

³Département de géomatique appliqué, Université de Sherbrooke, Sherbrooke, Québec, Canada

⁴NASA Langley Research Center, Hampton, Virginia, USA.

^anow at: Flight Research Laboratory, National Research Council Canada, Ottawa, ON, Canada

Correspondence: Peng Xian (peng.xian@nrlmry.navy.mil)

Abstract

In a companion paper (Part I of the study), we present an Arctic aerosol optical depth (AOD) climatology and trend analysis for 2003-2019 spring and summertime periods derived from a combination of aerosol reanalyses, remote sensing retrievals, and ground observations. Continued from the previous discussion and as the second part of the study, we report the statistics and trends of Arctic AOD extreme events using the U.S. Navy Aerosol Analysis and Prediction System ReAnalysis version 1 (NAAPS-RA v1), the sun photometer data from the Aerosol Robotic Network (AERONET) sites, and the oceanic Maritime Aerosol Network (MAN) measurements. Here, extreme AOD events are defined as events with AOD exceeding the 95th percentile (denoted “AOD₉₅”) of AOD distributions for given locations using 6 hourly or daily AOD data. While AERONET and MAN data estimate that the Arctic median 550 nm AOD value to be 0.07, the 95th percentile value is 0.23. Such extreme events are dominant by fine-mode aerosol particles, largely attributable to biomass burning (BB) smoke events for the North American Arctic, the Asian Arctic, and most areas of the Arctic Ocean. However, extreme AOD events for the lower European Arctic is more attributable to anthropogenic/biogenic particles. The extreme-event occurrence dominance of sea salt is largely limited to the North Atlantic and Norwegian Seas. The extreme AOD amplitudes of anthropogenic and biogenic fine mode and sea-salt AOD are, however, significantly lower than those regions where extreme smoke AOD is dominant. Even for sites distant from BB source regions, BB smoke is the principle driver of AOD variation above the AOD₉₅ threshold.

Maximum AOD values in the high Arctic in 2010-2019 have increased compared to 2003-2009, indicating stronger extreme BB smoke influence in more recent years. The occurrence of extreme smoke events tended to be more equally distributed over all months (April-August) during the 2003-2009 period while being more concentrated in the late season (July-August) during the 2010-2019 period. The temporal shift of the occurrence of AOD extreme events is likely due to improved control of early-season agriculture burning, climate change related increases in summertime lightning frequencies, and a reduction in anthropogenic pollution over the 2010-2019 period.

1. Introduction

Warming faster than the rest of the world, the Arctic is a focal point for global warming (Serreze and Francis 2006; Serreze and Barry 2011). Interactions between the atmosphere, ocean, land surface, and sea ice, compounded by numerous human factors make the Arctic climate system challenging to predict, with large diversity between current numerical model outcomes (IPCC 2021). Aerosol particles from anthropogenic and natural sources affect regional energy balance through direct radiative processes and indirect cloud processes (Quinn et al., 2008; Engvall et al., 2009; Flanner, 2013; Sand et al., 2013; Markowicz et al., 2021; Yang et al., 2018). When deposited on the surface of snow and ice, light-absorbing aerosol particles, including dust and black/brown carbon from biomass burning and anthropogenic emissions, can trigger albedo feedbacks and accelerate melting (Hansen & Nazarenko, 2004; Jacobson, 2004; Flanner et al., 2007; Skiles et al., 2018; Dang et al., 2017; Kang et al., 2020).

Arctic aerosol concentrations are in general relatively low, with spring and summertime median/mean 550 nm aerosol optical depths (AOD) of 0.06 - 0.07 (e.g., Tomasi et al., 2007; Saha et al., 2010; AboEl-Fetouh et al., 2020) as compared to a global mean of roughly 0.20 over land and 0.12 over water (e.g., Levy et al., 2010; Lynch et al., 2016; Shutgers et al., 2020; Sogacheva et al., 2020). Extreme AOD events do occur within the Arctic, mostly associated with large-scale transport from lower latitudes. Biomass burning (BB) smoke from boreal wildfires, for example, can episodically result in record-high Arctic AOD (Myhre et al. 2007; Stohl et al., 2007; Markowicz et al., 2016; Ranjbar et al., 2019). Some strong smoke events were recorded during intensive field campaigns, including the ARCTAS/ARCPAC campaign in the summer of 2008 (Matsui et al., 2011; Saha et al., 2010; McNaughton et al., 2011) and the NETCARE research vessel (Canadian Arctic) campaign in the spring of 2015 (Abbatt et al., 2019). More extreme BB smoke cases in the Arctic can be found in Sec. 3.3.

Extreme AOD events cause large perturbations in regional energy balance (e.g., Myhre et al., 2007; Stone et al., 2008; Lisok et al., 2018). For example, a BB smoke transport event from North America to the High Arctic region of Svalbard in early July 2015 led to 500 nm AOD exceeding 1.2 at Spitsbergen (Markowicz et al., 2016). The two-day mean aerosol direct radiative forcing was estimated to cause overall cooling (-79 W/m^2 at the surface and -47 W/m^2 at the top of the atmosphere). However, a corresponding atmospheric heating rate profile was solved of up to 1.8 K/day within the BB plume (Lisok et al., 2018). Over bright snow and ice surfaces, or above clouds, top of the atmosphere BB smoke forcing can turn from negative to positive (i.e., warming) by reducing columnar albedo (Yoon et al., 2019; Markowicz et al., 2021).

Although the microphysical impacts of aerosol particles on Arctic clouds and precipitation processes are generally more difficult to measure and quantify, Arctic clouds are generally believed more sensitive to changes in the relatively low concentration of aerosols compared with the lower latitudes (Prenni et al., 2007; Mauritsen et al. 2011; Birch et al., 2012; Coopman et al., 2018; Wex et al., 2019). Extreme aerosol events correspond with an influx of relatively large concentrations of potential cloud condensation nuclei (CCN) and/or ice nucleating particles (INP), in what is otherwise a comparatively pristine background environment (Mauritsen et al. 2011; Leck et al., 2015). Such extreme events will accordingly have observable impacts on cloud albedo, lifetime, phase, and probability of precipitation (e.g., Lance et al., 2011; Zhao and Garrett 2015; Zamora et al, 2016; Bossioli et al., 2021) and further influence the regional energy budget. Dry deposition (and blowing snow processes), as well as wet deposition of BB smoke particles, can also trigger sustained surface radiative forcing by inducing surface snow discoloration and attendant surface albedo reduction (Warren and Wiscombe, 1980; Stohl et al., 2007; Hadley and Kirchstetter, 2012).

Extreme aerosol events, especially BB smoke events, often modulate the interannual variability of Arctic AOD (Part 1 of this study; Xian et al., 2022), as well as to the total annual aerosol budget in the Arctic. The modeling study by DeRepentigny et al. (2021) shows, in comparison with BB emissions characterized by a fixed annual cycle, that the inclusion of interannually varying BB emissions leads to larger Arctic climate variability and enhanced sea-ice loss. Their finding illustrates the unique sensitivity of climate-relevant processes to regional aerosol interannual variability, and further suggests that extreme aerosol events play an important Arctic climate role. It is accordingly important to understand how extreme aerosol-event statistics change with the changing Arctic climate to better inform climate simulations and our baseline understanding of how the region is poised to evolve.

This is the second of two papers examining spring and summertime Arctic AOD climatologies and their trends. In Part 1 (Xian et al., 2022), we report a baseline Arctic AOD climatology from AERONET, MAN, and satellite AOD data for those two seasons and the skill of three reanalysis AOD products in simulating those climatologies. The reanalyses and space-borne retrievals show consistent climatological spatial patterns and trends. Overall, AOD exhibits a multi-year negative trend for springtime and a positive trend for summertime during 2003-2019, due to an overall decrease in sulfate/anthropogenic pollution and a significant summertime increase in BB smoke. This second paper focuses on the statistics and trends of extreme Arctic AOD events. The data and methods we employ are described in Sec. 2, while results are provided in Sec. 3. Conclusions are presented in Sec. 4.

2. Data and Methods

2.1 AERONET

The AErosol RObotic NETwork (AERONET) is a federated ground-based sun photometer network with over 600 active sites across the globe. AERONET's Cimel photometers measure sun and sky radiance at several wavelengths, ranging from the near-ultraviolet to the near-infrared. While the exact set of bands depend on the model, all Cimel configurations include 440, 670, 870 and 1020 nm bands. All the sites used here also included 380 and 500 nm bands. The network has been providing high-accuracy daytime measurements of aerosol optical properties since the 1990s (Holben et al., 1998; Holben et al., 2001). Cloud-screened and quality-assured Version 3 Level 2 AERONET data (Giles et al., 2019) are used in this study.

Fine mode (FM) and Coarse mode (CM) AOD at 550 nm are derived based on the Spectral Deconvolution Method (SDA) of O'Neill et al. (2003) and averaged over 6 hr time bins. The same ten AERONET sites employed in Part 1, were selected (Fig. 1) for this study. Those sites had been chosen based on their regional representativeness as well as the availability of data records between Jan 2003 and Dec 2019 period of study.

Optically thin clouds, mostly cirrus, occasionally contaminate CM aerosol retrievals in Level 2, Version 3 AERONET data (Ranjbar et al., 2022). Data were manually inspected, and retrievals screened, using MODIS imagery at visible wavelengths from NASA Worldview (<https://worldview.earthdata.nasa.gov/> last accessed 15 May 2022) and by comparing 6-hrly NAAPS-RA with AERONET AODs. This step is likely an incomplete one, given the likely lesser sensitivity of MODIS imagers to thin clouds (Marquis et al., 2017). As such, CM AODs that deviate by more than the 3-sigma level from the background climatological mean were also removed (as per AboEl-Fetouh et al., 2020).

2.2 AERONET Marine Aerosol Network AOD Datasets

The Marine Aerosol Network (MAN) is part of the broader AERONET global network: in this case however, it is limited to AODs collected over open water. Hand-held Microtops sun photometers are deployed during research cruises of opportunity (Smirnov et al., 2009, 2011). Data processing is similar to that of AERONET with product nomenclature similar to AERONET. Level 2 data acquired above 70°N in the 2003-2019 period are used in this study. FM and CM AOD at 550 nm are derived using the SDA and averaged over 6 hr time bins.

2.3 NAAPS AOD reanalysis v1

The Navy Aerosol Analysis and Prediction System (NAAPS) AOD reanalysis (NAAPS-RA) v1 was developed at the U.S. Naval Research Laboratory. It provides speciated

AOD and concentrations at a global scale with $1^\circ \times 1^\circ$ degree latitude/longitude and 6 hr resolution for 2003-2019 (Lynch et al., 2016). NAAPS-RA is driven by the Navy Operational Global Analysis and Prediction System (NOGAPS; Hogan and Rosmond, 1991), with satellite precipitation applied within the tropics to mitigate model precipitation errors (Xian et al., 2009). NAAPS-RA features assimilation of quality-controlled AOD retrievals from MODIS and MISR (Zhang et al., 2006; Hyer et al., 2011; Shi et al., 2011). A first-order approximation of secondary organic aerosol (SOA) processes is adopted. Production of SOA from its precursors is assumed to be instantaneous and is included with the original anthropogenic species to form a combined anthropogenic and biogenic fine (ABF) species. In other words, ABF is a mixture of sulfate, BC, organic aerosols and secondary organic aerosols from non-BB sources. Monthly anthropogenic emissions come from a 2000-2010 average of the ECMWF MACC inventory (e.g., Granier et al., 2011). BB smoke is derived from Fire Locating and Modeling of Burning Emissions inventory (FLAMBE, Reid et al., 2009). This version of FLAMBE uses MODIS, near-real-time satellite-based thermal anomaly data to initialize the smoke source where corrections that minimize the impact of inter-orbit variations are applied to the MODIS data (Lynch et al., 2016). FLAMBE processing is applied consistently through the reanalysis time period while a smoke-particle emission climatology and its spring and summertime trends (both north of 50°N and 60°N) are provided in Fig. 12 of Part 1. Dust is emitted dynamically and is a function of modeled friction velocity to the fourth power, surface wetness, and surface erodibility. In this model run, erodibility is adopted from Ginoux, et al., (2001) with regional tuning. Sea-salt modeling is the same as Witek et al. (2007) and sea-salt emission is driven dynamically by sea surface wind.

Verification of monthly-binned NAAPS-RA total AODs at 550 nm using monthly-binned AERONET data from 10 Arctic sites (Table 1 and Fig. 2 of Part 1) shows that NAAPS-RA is able to capture the AOD interannual variability. The spatial distributions and magnitudes of climatological and seasonal AOD averages and their trends for 2003-2019 are also consistent with those derived from MODIS, MISR, and CALIOP (Part 1).

2.4 Data analysis methods

Our study period is Jan 2003 to Dec 2019, the same principal study period as used in Part 1. We define extreme events as those corresponding to AOD exceeding the 95th percentile mark in 6 hr or daily AOD data at a specific location or across a given region (the region north of 70°N for example). We employ 6 hr AERONET AODs as well as speciated daily and 6 hr NAAPS-RA AOD to depict the frequency and magnitude of the large FM AOD events. Pair-wised data are used for verification. “Pairwise” refers to those NAAPS-RA AODs that correspond to a resampled AERONET or MAN AOD whose $\pm 3\text{hr}$ bin contains at least one AERONET/MAN retrieval. Three independent

aerosol reanalysis products were used in the Part 1 of the study. For this study, the NAAPS-RA reanalysis was chosen given its slightly better performance in terms of FM and total AOD bias, RMSE, and r^2 scores (Part 1), as well as its capability of separating BB smoke from other aerosol species. To simplify some of the discussion below, we frequently employed the symbol “AOD_n” to represent the AOD associated with the n% percentile of its cumulative (histogram) distribution. One important application of this AOD_n formulation is to employ a particular value (AOD₉₅) as a threshold for the definition of extreme events (see Section 3.1 below). AOD₇₅, AOD₉₀, AOD₉₉, AOD_{99.5} and maximum AOD are also calculated to show AOD gradients for high AODs. A local extreme total AOD event for the NAAPS-RA means AOD > AOD₉₅ for the model grid cell of 1° x 1° (Latitude/Longitude). Again, we define the Arctic and the high-Arctic as regions north of 60°N and 70°N respectively. To reference source influences from lower-latitude, the area of 50°N-90°N is included for context.

3. Results

Regional statistics and trends of extreme AOD events are presented in this section: 6-hr AERONET AOD as well as speciated daily and 6-hr NAAPS-RA AOD are employed to characterize the frequency and magnitude of strong FM AOD events.

3.1 Verification of NAAPS-RA AOD over the Arctic

The reanalysis performance for 6-hr time bins was evaluated in order to study extreme events. Our choice of AOD₉₅ as an extreme event threshold was influenced by the fact that it was an upper-limit cumulative probability indicator that was robust. We reasoned, at the same time, that it should be comparable with the analog parameter derived from NAAPS-RA. Figure 1 displays NAAPS-RA AOD₉₅ overplotted with those from the ten selected AERONET sites for spring and summertime 2003-2019. NAAPS-RA appears to successfully capture the AOD₉₅ amplitude and spatial pattern, as well as those of FM AOD₉₅ and CM AOD₉₅. It also shows that FM is the main contributor to AOD₉₅ in the Arctic.

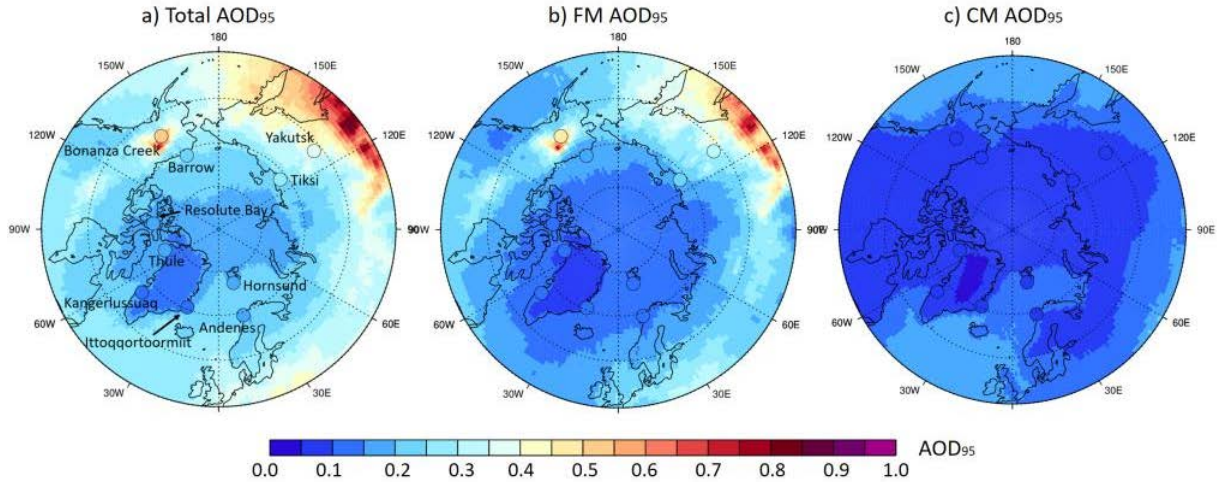


Figure 1. Total, FM and CM AOD at the 95th percentile (AOD_{95}) for the March-August time frame from the NAAPS-RA and the ten AERONET sites based on 6hrly data between 2003-2019.

Detailed geographical coordinates of the ten AERONET sites employed in our study are included in Table 1, as well as the simulation performance indicators of NAAPS-RA 550 nm total, FM and CM AOD. These AERONET parameters are an analogue to parameters used in the first part of the study and its Table 1 statistics, except that the averaging period extends across both the spring and summer seasons, as the averaging period is mostly confined to the April-August time frame. NAAPS-RA performance indicators relative to MAN data are shown in Fig. S1 and S2.

NAAPS-RA performance for this large averaging period is reasonable for FM and total AOD, though it is less skillful at predicting CM AOD. The FM AOD exhibits an average (Table 1) bias over all stations of -0.01, a root mean square error (RMSE) of 0.08 and a coefficient of determination (r^2) of 0.66. RMSE values for total and FM AOD are generally large for sites vulnerable to strong smoke influence, e.g. Bonanza Creek, Barrow, Tiksi and Yakutsk. Total AOD r^2 values are mostly between 0.5-0.7, except for Hornsund, Kangerlussuaq and Ittoqqortoormiit. FM AOD r^2 values exceed those of the total AOD for all sites except Kangerlussuaq. The 6-hr-binned Table 1 total AOD bias is similar to the monthly-binned NAAPS-RA bias results of Table 2, Part 1. This is due to the numerous 6-hr samples included in the AERONET bias averaging. In contrast, the Table 1 RMSE values are roughly doubled, and the r^2 values drop by about 30% relative to those of Tables 3 and 4 of Part 1. This suggests Table 1 model shortcomings in capturing finer temporal-scale AERONET-AOD variations. This is also consistent with model performance for regions other than the Arctic, and is generally a common result for numerical aerosol models (Lynch et al., 2016; Yumimoto et al., 2017)

The lesser CM vs FM skill of the NAAPS-RA might be a reflection of AERONET limitations as one approaches typical instrumental errors ~ 0.01 in total AOD or they could be a reflection of simulation and / or reanalysis limitations as one approaches very small values of CM AOD. The lack of model representation of CM smoke and possible soil particles associated with severe burning events may also contribute. At the same time, it must be recognized that residual cloud contamination in AERONET and MAN data cannot be ruled out as a “false” indicator of poor simulation skill. Cloud screening issues aside, a lesser CM vs FM correlation skill is a common feature of both the Table 1 and Table 4 (Part 1) reanalyses. However, modeled monthly CM AOD correlation is slightly more skillful than the averages derived from 6 hr data (Table 4 in Part 1 vs Table 1) inasmuch as the seasonal CM signal associated with dust and sea salt aerosols are apparently better resolved in the former case. The better model skill in seasonal CM simulation is likely due to the relative insensitivity of the model to the higher frequency components of the reference data in the latter case. It is also noted that the NAAPS-RA is generally less skillful in the Arctic region relative to global reanalyses (c.f. Fig. 7 in Lynch et al., 2016). This is understandable given that there is little satellite-based AOD data available to constrain the model through assimilation in the Arctic compared to lower latitudes. We note however that Zhang et al. (2021) attempted to address this problem with assimilation of Ozone Monitoring Instrument (OMI) Aerosol Index. To date, no remedy for aerosol data assimilation has yet been implemented in a larger RA-quality study.

Table 1. Geographical coordinates along with the total, FM and CM AOD statistics (2003-2019 depending on availability) for AERONET and 6-hrly NAAPS-RA 550 nm performance indicators versus AERONET. The last row shows the same statistics for MAN AODs acquired north of 70°N as the bias reference. These numbers are given as information: as indicated above the table statistics in Part 1 were explicitly computed using monthly binned data (which were, in turn, derived from the 6 hr data).

sites	latitude	longitude	elevation (m)	region	AERONET mean			total FM CM AOD									
					total	FM	CM	Bias			rmse			r ²			n
Hornsund	77.0°N	15.6°E	12	Svalbard	0.09	0.06	0.03	-0.01	-0.02	0.01	0.04	0.04	0.03	0.55	0.62	0.06	1,975
Thule	76.5°N	68.8°W	225	Greenland	0.07	0.06	0.02	0.00	-0.01	0.01	0.04	0.03	0.03	0.52	0.60	0.07	2,934
Kangerlussuaq	67.0°N	50.6°W	320	Greenland	0.07	0.05	0.02	0.02	0.00	0.01	0.05	0.04	0.03	0.32	0.30	0.03	3,066
Ittoqqortoormiit	70.5°N	21.0°W	68	Greenland	0.06	0.05	0.02	0.01	-0.00	0.01	0.04	0.03	0.03	0.41	0.49	0.04	2,041
Andenes	69.3°N	16.0°E	379	Norway	0.08	0.05	0.02	0.01	-0.01	0.01	0.04	0.03	0.03	0.54	0.56	0.16	2,222
Resolute_Bay	74.7°N	94.9°W	35	Nunavut	0.08	0.05	0.02	0.01	-0.01	0.01	0.06	0.05	0.03	0.55	0.62	0.02	1,876
Barrow	71.3°N	156.7°W	8	Alaska	0.10	0.08	0.02	-0.00	-0.02	0.01	0.09	0.08	0.04	0.53	0.61	0.07	1,920
Bonanza_Creek	64.7°N	148.3°W	353	Alaska	0.16	0.12	0.03	-0.02	-0.02	-0.00	0.16	0.15	0.04	0.69	0.70	0.07	3,177
Tiksi	71.6°N	129.0°E	17	Siberia	0.12	0.10	0.02	-0.01	-0.02	0.01	0.09	0.08	0.03	0.69	0.73	0.01	631
Yakutsk	61.7°N	129.4°E	119	Siberia	0.16	0.12	0.03	-0.01	-0.02	0.01	0.13	0.12	0.04	0.61	0.62	0.15	4,797
MAN	>70°N	-	-	Arctic Ocean	0.07	0.05	0.02	-0.00	-0.01	0.00	0.04	0.03	0.02	0.51	0.32	0.07	520
All AERONET sites	total FM CM median: 0.07 0.05 0.01				0.10	0.08	0.02	-0.00	-0.01	0.01	0.09	0.08	0.03	0.63	0.66	0.07	24,639

3.2 General statistics of extreme events

Shown in Figure 1 and Table 2 are NAAPS-RA and AERONET AOD₉₅ values for the March-August time frame and the 2003-2019 period. The values of AOD₉₅ are high (0.4~0.55) over Siberia and Alaska (and over the Yakutsk and Bonanza Creek AERONET stations) due to strong BB smoke influence. North of 70°N, the values are mostly between 0.15 to 0.25, with the exception of Greenland where they are largely below 0.15 (weak values that are attributable to the high terrain). It is also shown that (FM AOD)₉₅ has similar spatial distribution and magnitude as AOD₉₅, suggesting the dominant contribution of FM to AOD₉₅. Contribution of CM is relatively larger over the North Atlantic and European Arctic, though (CM AOD)₉₅ and (FM AOD)₉₅ are comparable in these regions.

The site-by-site, total, and FM AOD ranges are also shown in Fig. 2 from the 6-hr AERONET data for all 550 nm retrievals acquired between 2003-2019. In general, the NAAPS-RA largely captures the AERONET FM and total AOD range. This includes, for example, the AERONET AOD₅ to AOD₉₅ values (0.02 to > 0.10 for most sites), and the larger 0.02 to 0.4-0.6 range of sites with known strong BB influence (notably Bonanza Creek, Tiksi, and Yakutsk). Mean and median AODs are also comparable to AERONET values. Maximum AERONET FM AODs vary between 0.5 (Ittoqqortoormiit) to < 2.0 for most sites and around 3.0 for sites with strong BB smoke influence (see also Table 2). Maximum NAAPS-RA AOD values are often biased low, which is a common challenge for global aerosol models (e.g. Sessions et al., 2015; Xian et al., 2019).

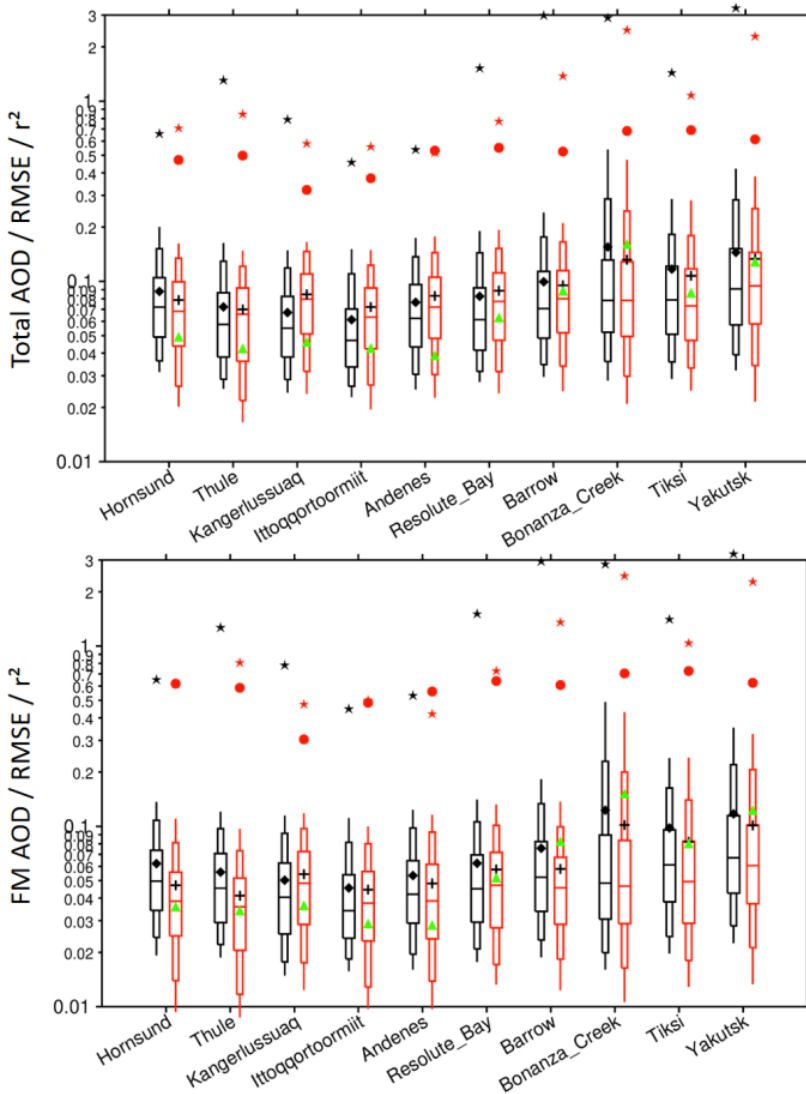
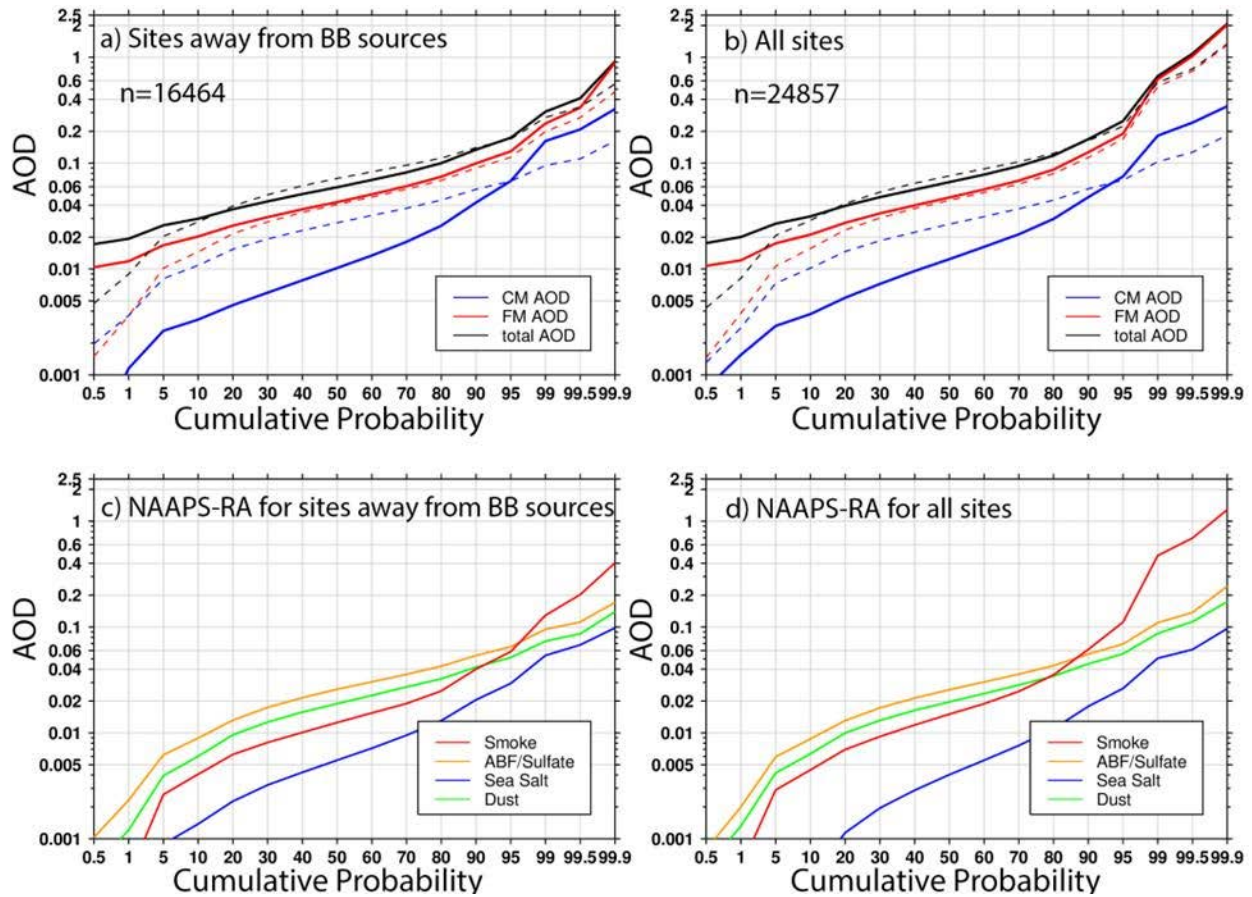


Figure 2. Comparison of the 6-hrly 550 nm total (top) and FM AOD (bottom) of the NAAPS-RA (red) at 95, 90, 75, 50, 25, 10, and 5% percentiles (respective, sequential features of the doubled spear-like symbols from the top tip to the bottom tip) with pairwise AERONET V3L2 data (black) for the ten AERONET sites of Table 1 and Fig. 1 for the 2003-2019 time period. Also shown are the site means of the NAAPS-RA and AERONET AODs (“+” and “♦” symbols respectively) and the NAAPS-RA RMSE (“▲”), the coefficient of determination (r^2) between the NAAPS-RA and AERONET (“•”) and the maximum AERONET and NAAPS-RA AODs (“★” and “★” respectively). Note that values greater than 3.0 are not shown.

309



310

311 **Figure 3.** Upper panes (a, b): cumulative probability distributions of 2003-2019, 6-hr
 312 total, FM and CM AOD at 550 nm for AERONET V3 L2 data (solid curves) and pair-wise
 313 NAAPS-RA (dashed curves). Lower panes (c,d): cumulative probability distributions for
 314 the corresponding speciated AOD from the NAAPS-RA. Left hand panes (a,c): AOD for
 315 sites that are distant from BB source regions, including Barrow, Resolute Bay,
 316 Kangerlussuaq, Thule, Andenes, Hornsund and Ittoqqortoormiit (see the discussion of
 317 Table 2 for emission considerations with respect to the particular site of Barrow). Right-
 318 hand panels (b,d) are all sites. “n” represents the total number of 6-hrly data points over
 319 the 2003-2019 period, including a small amount of AERONET data from September
 320 besides the March-August time frame.

321 The cumulative probability distributions of 6-hr total, FM and CM AODs are shown in
 322 Fig. 3 for AERONET and pair-wise NAAPS-RA total and modal AODs and speciated
 323 AODs. The median AOD for all AERONET sites in the Arctic (all sites north of 60°N) for
 324 2003-2019 is 0.07, while the AOD₉₅ extreme-event threshold is 0.23 with a dominant FM
 325 contribution. The CM AOD median for all measurements is 0.01, with a (CM AOD)₉₅
 326 threshold of only 0.07. NAAPS-RA total AOD bias is, due to a relatively large positive
 327 bias in CM AOD of 0.01 below the 95% threshold, slightly positive (<0.01) for all sites

north of 60°N, and for the 20%-80% cumulative probability range (a positive bias that is generally evident in Table 1).

The negative bias found at the largest CM AOD values could conceivably be associated with an underestimation of the CM AOD generated by sea-salt aerosols in the presence of strong winds or CM smoke and soil particles associated with severe burnings. We should, however, reemphasize this caveat: despite the quality-control measures taken to filter out cloud-contaminated AERONET data, the impact of CM residual clouds may still influence estimates of CM AOD.

It worth noting that BB smoke plays a dominant role compared to other aerosol species above our AOD₉₅ extreme-event threshold (see Fig. 3c, d in particular and note that Fig. 3a, b shows the expected dominance of FM AOD). Even for sites distant from BB source regions, including Resolute Bay, Kangerlussuaq, Thule, Andenes, Hornsund, Ittoqqortoormiit, BB smoke is the principal driver of AOD variations above the AOD₉₅ threshold. To some extent, Barrow can be categorized as being a site that is distant from BB emissions. However, it is also relatively close to the region of Alaska fires, depending on dominant upstream winds and trajectories (see Eck et al., 2009 for details).

Table 2. AERONET V2L3 FM, CM, and total AOD at 550nm at different percentiles for the listed Arctic sites along with maximum AOD values in the third last column. “N” represents the total number of 6-hr AODs for 2003-2019. The percentage of extreme FM events relative to the number of extreme total AOD events (using our AOD₉₅ extreme-event threshold) is also shown in the last column. The 2nd to last row shows MAN statistics for data acquired north of 70°N.

	Total FM CM AOD at 550nm							N	FM event
	Median	75%	90%	95%	99%	99.9%	maximum		
Hornsund	0.072 0.049 0.014	0.103 0.074 0.028	0.145 0.108 0.048	0.184 0.135 0.077	0.320 0.300 0.155	0.663 0.654 0.222	0.663 0.654 0.222	1975	67%
Thule	0.055 0.043 0.006	0.083 0.067 0.014	0.121 0.092 0.034	0.156 0.116 0.057	0.294 0.198 0.164	0.914 0.913 0.315	1.310 1.272 0.315	2934	59%
Kangerlussuaq	0.055 0.040 0.009	0.082 0.063 0.020	0.118 0.091 0.037	0.149 0.115 0.059	0.234 0.198 0.109	0.510 0.461 0.203	0.794 0.786 0.222	3066	75%
Ittoqqortoormiit	0.046 0.033 0.006	0.069 0.053 0.014	0.108 0.083 0.031	0.144 0.112 0.054	0.238 0.215 0.121	0.456 0.446 0.232	0.459 0.450 0.233	2041	73%
Andenes	0.062 0.042 0.014	0.096 0.064 0.027	0.136 0.098 0.049	0.172 0.123 0.072	0.274 0.210 0.148	0.451 0.432 0.249	0.541 0.534 0.258	2222	69%
Resolute Bay	0.061 0.045 0.011	0.092 0.069 0.021	0.143 0.106 0.039	0.187 0.140 0.059	0.409 0.389 0.152	1.530 1.516 0.379	1.530 1.516 0.379	1876	72%
Barrow	0.071 0.053 0.013	0.114 0.082 0.024	0.175 0.134 0.047	0.232 0.183 0.076	0.455 0.415 0.174	2.999 2.962 0.328	2.999 2.962 0.328	1920	81%
Bonanza Creek	0.078 0.048 0.022	0.130 0.089 0.036	0.280 0.230 0.057	0.532 0.497 0.083	1.713 1.643 0.186	2.619 2.591 0.341	2.908 2.857 0.345	3177	99%
Tiksi	0.079 0.061 0.011	0.121 0.096 0.021	0.182 0.163 0.040	0.286 0.239 0.060	0.936 0.915 0.123	1.442 1.413 0.238	1.442 1.413 0.238	631	97%
Yakutsk	0.094 0.069 0.014	0.153 0.119 0.027	0.272 0.221 0.053	0.400 0.345 0.089	0.980 0.963 0.201	3.018 2.972 0.317	3.296 3.259 0.340	4797	96%
MAN	0.052 0.029 0.021	0.090 0.062 0.031	0.126 0.097 0.042	0.164 0.118 0.052	0.281 0.253 0.085	0.777 0.761 0.234	0.777 0.761 0.234	520	92%
All AERONET sites	0.066 0.047 0.012	0.104 0.077 0.024	0.166 0.128 0.046	0.243 0.193 0.070	0.661 0.619 0.158	2.073 2.030 0.290	3.296 3.259 0.379	24639	86%

The modal and total AOD values at different percentile levels for the AERONET sites and MAN data collected north of 70° N are provided in Table 2. For sites closer to BB sources, including Bonanza Creek, Yakutsk, and Tiksi, the AOD₉₉ and (FM AOD)₉₉ values are larger than 1.0 while the maximum values are between 1.4-3.3. For the more distant sites, the AOD₉₉ and (FM AOD)₉₉ values vary between 0.23-0.46 while the maximum values are between 0.45-3.0 (1.5 for Resolute Bay and 3.0 for Barrow). FM event occurrences for the extreme total AOD events, range from 60-99%, with an

average of 86%, and accordingly dominate CM events statistically. Sites closer to the BB source regions show relative occurrences over 95%.

Large particles like ash and soil components emitted from vigorous burning during extreme BB smoke events (Reid et al., 2005; Schlosser et al., 2017) can likely be detected as AERONET CM AOD (see, for example, the correlation between the FM and “weak” CM particle size distributions for Bonanza Creek in Fig. 9a of Eck et al. [2009]). The extreme AOD events described above are likely dominated by smoke. For example, (FM AOD)₉₉ is 1.64 at Bonanza Creek and 0.94 at Tiksi in Table 2. For events with FM AOD greater than (FM AOD)₉₉, the associated CM AOD means at the two sites showed significantly larger values of 0.05 and 0.03, respectively (significantly larger relative to, for example, the CM AOD means in Table 1). The coherency of the associated CM AOD mean increase with the FM AOD mean increase suggests the presence of detectable CM smoke and/or soil particles induced by severe burning. The inability of the model to simulate potential CM smoke or soil components associated with severe burning could be a contributing reason as to why it performs less well in predicting CM AOD near BB sites.

3.3. Extreme biomass burning smoke AOD cases

A distinct class of extreme smoke cases comes from pyrocumulonimbus (pyroCb) events induced by intense biomass burning sources: these events inject smoke high into the troposphere or even well into the stratosphere (Fromm et al., 2010; Peterson et al., 2017). A significant pyroCb smoke event that occurred over British Columbia (BC) in August 2017 led to substantial increases in various optical measures of aerosol concentration in the lower Canadian and European Arctic (Peterson et al., 2018; Torres et al., 2020; Das et al., 2021). Ranjbar et al. (2019) showed that a specific Aug. 19, 2017 smoke event over the high Arctic PEARL observatory at Eureka, Nunavut was induced by the BC pyroCb fires and that it was a statistically significant extreme FM AOD event. More recent eastern Siberian fires in June - August 2021, induced more than a dozen cases of elevated smoke intrusion into the high Arctic with some smoke plumes reaching the North Pole and/or its vicinity. For example, on the 5th of August, 2021, operational NAAPS (common chemistry, physics, and BB emission sources with the NAAPS-RA) resolved a smoke plume north of 80°N (Fig. 4) with AOD values of 2-3. Smoke AOD over the source region was also 2 to >3 with a similar amplitude to AODs measured at Yakutsk. CALIOP data suggested a 1-6 km high smoke layer in the source region.

Other extreme or near-extreme smoke events in the Arctic have been reported. A series of intense fires originating in North America led to strong AOD peaks in the summer of 2015 over Svalbard (Markowicz et al., 2016; Lisok et al., 2018). Agricultural fires in

Eastern Europe in the spring of 2006 caused record-high AODs and pollution levels in the European Arctic (Stohl et al., 2007). The North American boreal fires in the summer of 2004 led to large-amplitude AOD peaks in Alaska and enhanced AODs on a pan-Arctic scale (Stohl et al., 2004).

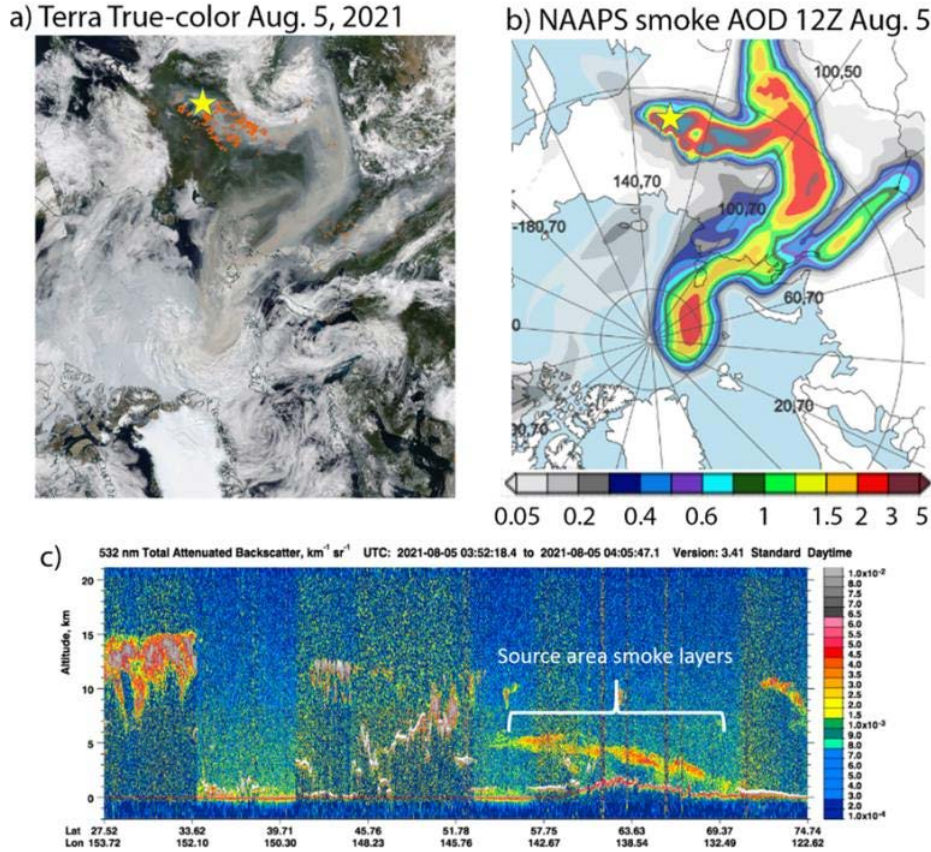


Figure 4. An August 5, 2021 example of BB smoke intrusion into the high Arctic from fires originating in eastern Siberia. a) Composite true-color Terra satellite imagery. The red dots represent satellite-detected fire hotspots. b) Operational NAAPS smoke AOD analysis at 12Z. c) CALIOP 532 nm attenuated backscatter coefficient showing the smoke layers around the source area. The yellow stars on a) and b) represent the location of Yakutsk, which experienced a daily mean total AOD (500 nm) of 2.0 (FM AOD ~ 1.9) and an intra-day peak around 2.5 based on AERONET V3L1.5 data. Sources: MODIS-Terra true-color satellite imagery and CALIOP-CALIPSO 532 nm attenuated backscatter coefficient profile (respectively <https://worldview.earthdata.nasa.gov/> and <https://www-calipso.larc.nasa.gov/>).

3.4 Geographic distribution of extreme AODs

The NAAPS-RA total-AOD map at different percentile levels locally for March-August 2003-2019 is shown in Fig. 5. We separated the study period into early (2003-2009) and

late (2010-2019) subperiods. The end-year of the first period was chosen as 2009 given the drop in ABF/sulfate emissions due to the civil Clean Air Acts enacted across the U.S. (e.g., Tosca et al., 2017; Kaku et al., 2018) as well as Europe and China, and the attendant decrease in ABF/sulfate AOD in these countries/regions (Lynch et al., 2016; Zhang et al., 2017). This ABF/sulfate AOD decrease was also observed in the Arctic, as shown in Fig. 13 of Part 1. The median Arctic AOD (less than 0.1 as compared with 0.07 for the AERONET sites from Fig. 3 and Table 2) are an order of magnitude smaller than the maximum AODs. Clear BB smoke features in the North American and Asian boreal burning regions start to emerge in the AOD₉₅ maps (see also Fig. 1). The maximum AOD is high (greater than 2.0) while being relatively low over the Arctic Ocean (~ 0.3 - 1.0) and the North Atlantic, with the lowest values over the generally high-elevation Greenland landmass. The maximum AOD is associated with peak burning activities and generally occurs in July and August. The exception is the Norwegian Sea area, where the maximum AODs occurs in March-May. This is possibly associated with a combined high AOD level from anthropogenic pollutions, marine aerosols and springtime agriculture fires.

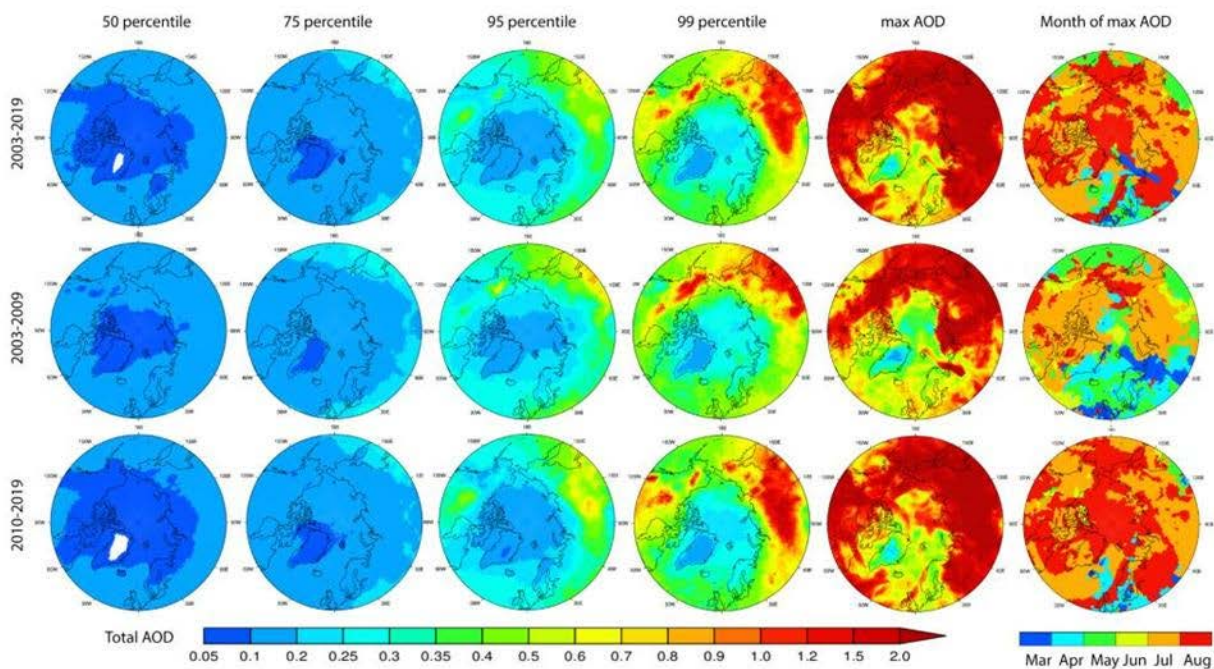


Figure 5. NAAPS-RA daily (550 nm) total-AOD maps at different percentile levels for the March-August time frame, the maximum AOD and (rightmost column) the month that the maximum AOD occurred. The three rows represent respectively, the sampling periods of 2003-2019, 2003-2009, and 2010-2019. The AOD₉₅ value for 2003-2019 is the same as that of Fig. 1 despite of different color scales.

The occurrence of different aerosol species relative to the occurrence of total AOD for total AOD extreme events (March-August time frame) are shown in Fig. 6. The occurrence maps accordingly indicate which aerosol species are numerically dominant for extreme AOD events. As expected, BB smoke is the prevailing extreme event contributor over the North American and Asian Arctic, especially near the boreal source regions and associated transport pathways, as well as most of the Arctic ocean (except the Barents Sea and the Norwegian Sea). ABF occurrence dominates the low European Arctic. Sea-salt particles and, to a lesser extent, ABF are the most significant occurrence contributors, in the North Atlantic and the Norwegian Sea. Dust occurrences to extreme AOD events are very small (0-10%) except over the predominantly high-elevation region of Greenland where the relative occurrence of high-altitude African dust dominates the relative occurrence of the other species.

In terms of AOD amplitudes for total AOD extreme events (Fig. 7), BB smoke AOD shows dominant contributions, especially in the areas near the boreal source regions and transport pathways, including most areas of the high Arctic. ABF and sea salt show slightly higher extreme-event AODs than BB smoke over the North Atlantic and European Arctic. The regional extreme AODs are not, however, as large as the extreme AODs in the BB smoke-dominant regions.

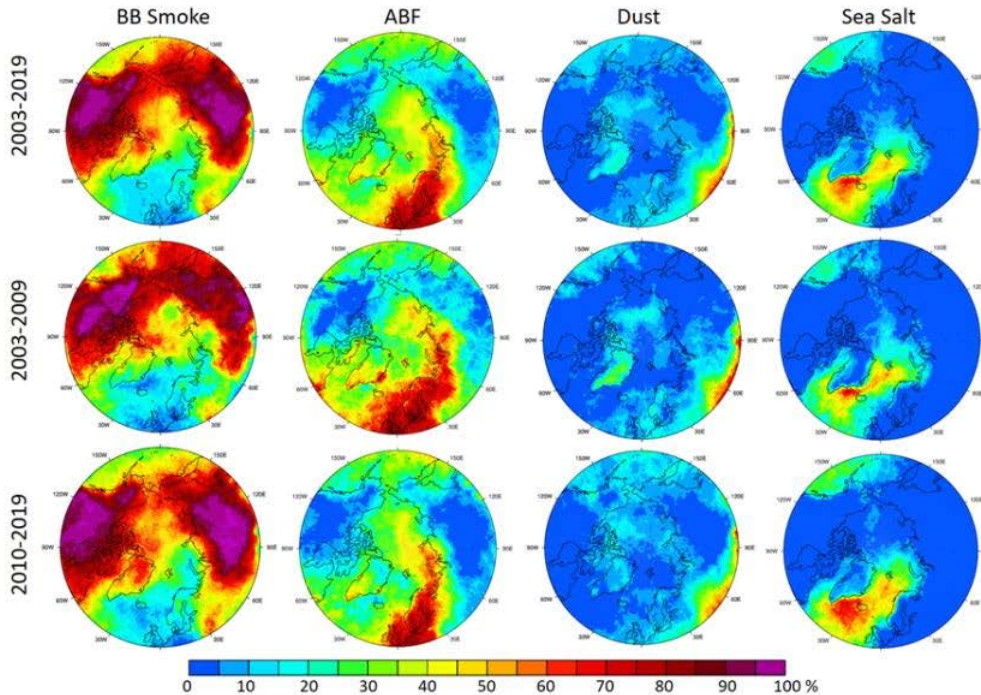
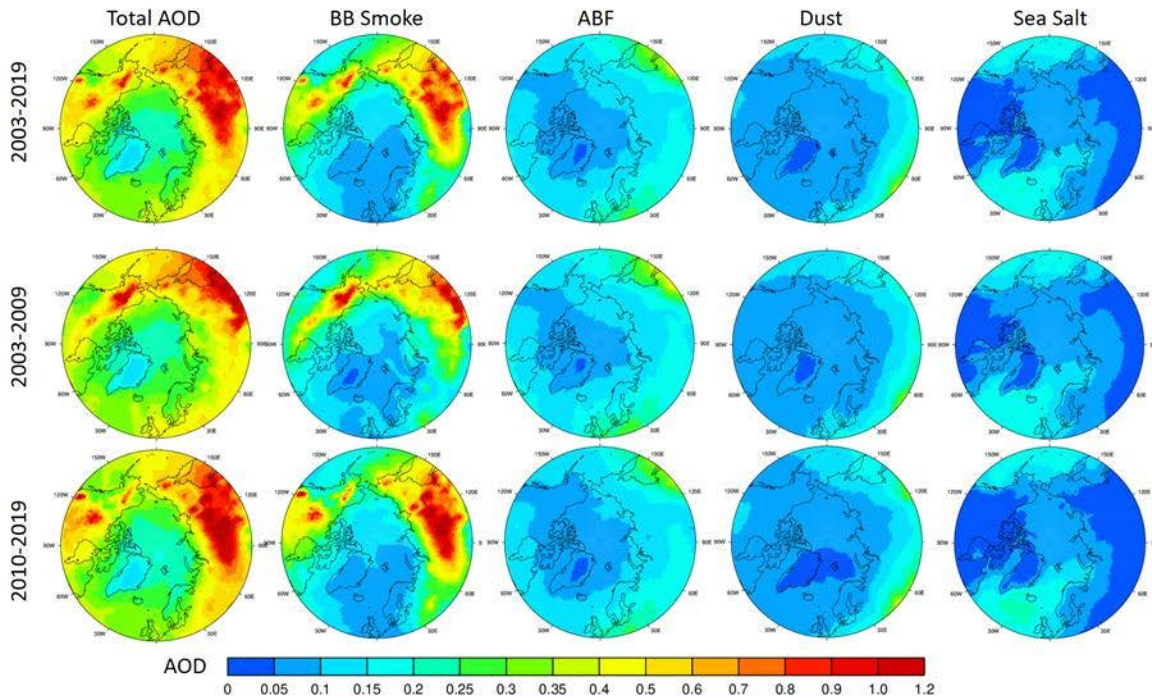


Figure 6. Occurrence of different aerosol species (expressed as a percent) relative to the occurrence of total AOD extreme events (daily total AOD > AOD₉₅ locally) for the March-August time frame. The sampling periods are the same as in Fig. 5.



460 **Figure 7.** Mean speciated and total AODs averaged for days with speciated AOD or
 461 total AOD > AOD₉₅ (i.e. the mean value of the top 5% AOD data) for the March-August
 462 time frame. The sampling periods are the same as in Figs. 5 and 6.

463 3.5 Seasonality of extreme AOD events

464 The NAAPS-RA seasonal cycle of total and speciated AOD are shown in Figure 8 for
 465 daily averages across the area north of 70° N (a latitude limit which largely excludes BB
 466 source regions). The seasonal cycle of monthly mean total AOD shows relatively higher
 467 values in Mar-Apr-May (MAM) compared with the lower AODs in Jun-Jul-Aug (JJA), and
 468 a minimum in June. The spread of the ABF AOD seasonal values is moderately stable,
 469 with a relatively higher mean/median in MAM than JJA (see the Figure 9 caption for a
 470 definition of spread). Sea-salt AOD and its spread are relatively higher in the earlier
 471 months (March and April). Dust AOD and spread are generally stable through the
 472 season, with a visibly higher mean/median in April and May. Smoke AOD amplitude and
 473 spread exhibit the greatest inter-species seasonal variations with the lowest mean and
 474 spread in March, increased means and spreads in April, and significantly higher mean
 475 and spread in later months. July and August appear to have the largest mean, spread
 476 and maximum smoke AODs (a smoke importance statement that is generally consistent
 477 with the results of Fig.6). These smoke features significantly contribute to the
 478 seasonality of total AOD extremes. It is also noted that the MAM total and smoke AOD
 479 means approximately equal their medians, but that the JJA means are greater than their

medians (and that this is especially true for August). The greater number of smoke AOD extremes in the later season and the attendant consequence of greater positive histogram skewness would explain those relative increases in the mean.

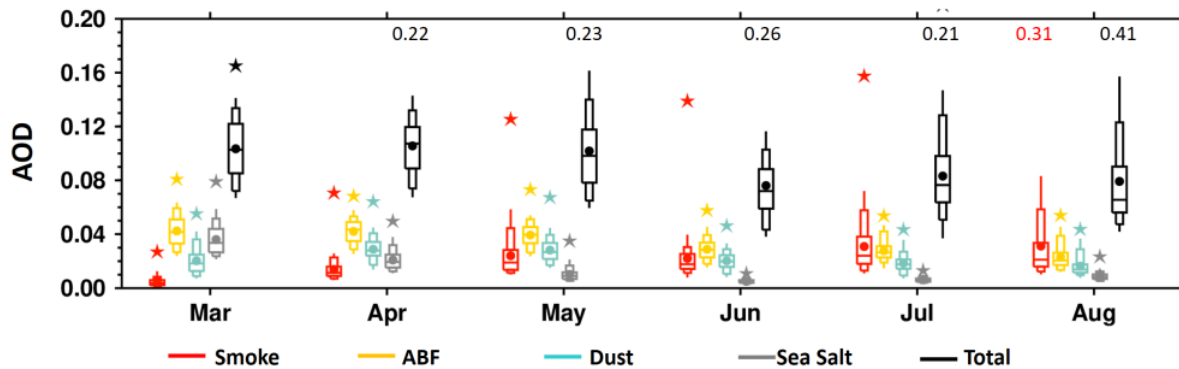


Figure 8. Box and whisker plot of daily and area-averaged (70°N-90°N) speciated AOD at 550 nm from NAAPS-RA (2003-2019) for different months. The box and whiskers represent AOD at 95, 90, 75, 50, 25, 10, and 5 percentiles. Mean total AODs are shown as solid black circles and maximum AODs as stars. Maximum AOD values appear as appropriately colored numerical values if they extend beyond the 0.2 plot maximum.

3.6 Trends of extreme AOD events

There is, as shown in Part 1 of the study, a multi-year decreasing MAM trend and an increasing JJA trend for total AOD in the Arctic over the 2003-2019 sampling period. This was attributed to an overall decrease in MAM and JJA sulfate/ABF AOD coupled with a negative trend in MAM, and a strong positive trend in JJA for biomass-burning smoke AOD. In terms of extreme event trends, AOD₉₅ (Fig. 5) and the average AOD above AOD₉₅ (Fig. 6) generally increased over the boreal continents from the 2003-2009 to 2010-2019 period (with the notable exception of Alaska and northeastern Siberia in 2010-2019). This is consistent with the positive BB emission trends in JJA north of 50°N and 60°N (for which the JJA trend dominated the MAM trend inasmuch as JJA was associated with much higher BB emissions; Part 1).

The negligible or slight decrease in high Arctic AOD₅₀, AOD₇₅ and AOD₉₅ values from the 2003-2009 to the 2010-2019 period (Figure 5), is likely associated with the generally weak ABF decrease seen in Figure 7. However, the increase in the maximum AOD value (Fig. 5) and the contribution of BB smoke to AOD extreme events (Fig. 7) in the latter period is an indication of stronger extreme BB smoke influence in more recent years. It is also noted that the maximum high-Arctic AOD occurred later in the season (mostly August) in 2010-2019 compared with the more balanced variation occurring in March through August in 2003-2009. This is likely attributable to overall lower ABF levels in the 2010-2019 period (especially in MAM), and a shift in extreme smoke events to

later in the season (Fig. 9). Specific counts of extreme BB smoke days for different months and years and yearly cumulative extreme AODs also support the seasonal shift of extreme smoke events (Table S1).

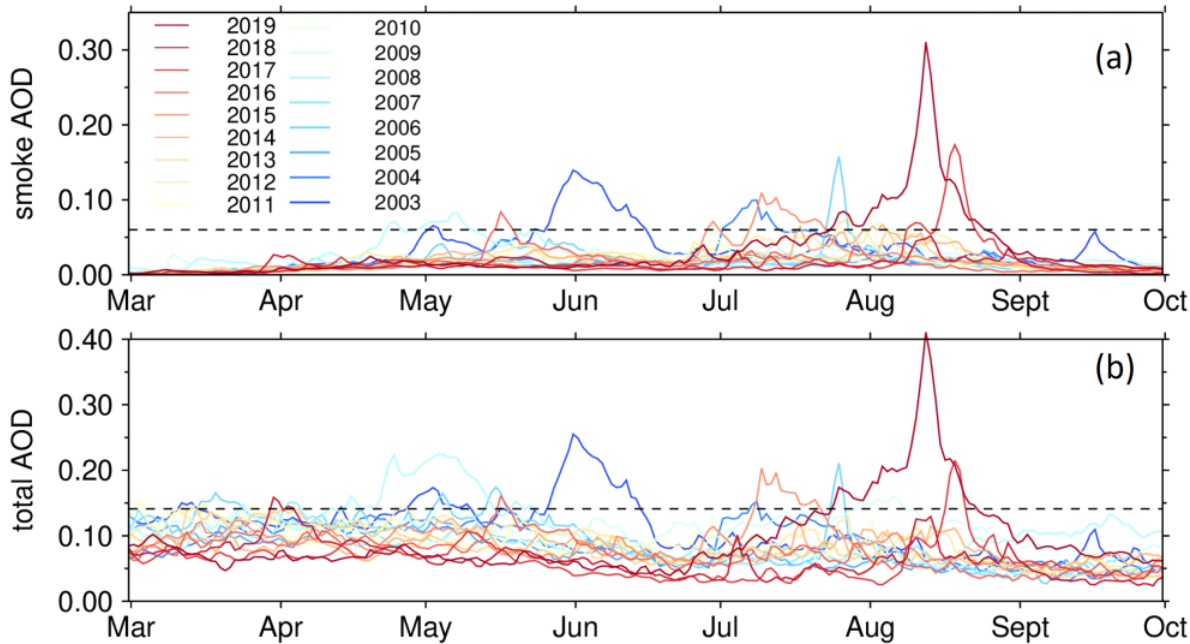


Figure 9. Seasonal (March to September) time series of daily-mean AODs averaged over the (70°N-90°N) high-Arctic area for each individual year of the 2003-2019 period: (a) BB smoke AOD, and (b) total AOD. The years before 2010 are shown as cold colors, and years after 2010 are shown as warm colors. The dashed horizontal lines show the smoke AOD₉₅ value of 0.06 and the total AOD₉₅ value of 0.14 respectively during the study period.

The time series of high-Arctic-averaged daily-mean BB smoke and total AOD from March to September for all years between 2003-2019 is shown in Fig. 9. The extreme total AOD variation is largely dictated by BB smoke. There is also a discernible 2003-2009 to 2010-2019 springtime reduction in extreme total AOD: this, as discussed in the previous paragraph, is likely due to an overall reduction in ABF AOD. The occurrence of extreme smoke events tended to be more equally distributed over all months (April-August) during the 2003-2009 period while being more concentrated in the late season (July-August) during the 2010-2019 period. The extreme smoke and total AOD trends resembled the extreme-smoke occurrence trends: more seasonally balanced during the 2003-2009 period and summertime dominance during the 2010-2019 period.

The occurrence of extreme high-Arctic smoke events thus demonstrates a clear smoke and total AOD shift from a more balanced spring and summer to the late season

(notably the months of July and August; see also Table S1). This is consistent with the temporal shift of fire activity to a later time in Siberia over 2003-2018 (Liu et al., 2020), and the projection of emerging pan-Arctic fire regimes marked by increases in the likelihood of extreme fires later in the growing season (McCarty et al., 2021). An earlier fire season in the boreal region normally suggests a better-managed forest/land with fewer large and destructive fires, while a later fire season indicates the opposite.

The shift of boreal fire activity, and the resulting BB smoke AOD extremes in the Arctic from early season to late season, is probably related to early-season strengthening of agriculture burning regulations and increased summertime lightning frequencies with climate change in the latter decade. For example, the springtime BB smoke AOD peak values in 2003, 2006 and 2008 are all associated with agricultural activity (resulting in fires burning out of control) and widespread high-latitude burning (Korontzi et al, 2006; Stohl et al., 2007; Saha et al., 2010). At the same time, with climate change, lightning activity and lightning-caused wildfires in summertime high-latitude regions were observed to increase in the past two decades (Zhang et al., 2021; Bieniek et al, 2020; Coogan et al., 2020). Also noted is a lengthening of growing season in boreal regions, which infers lengthening of fire season as well (Park et al., 2016). These factors aside, climate oscillations, including the Arctic Oscillation, ENSO and Pacific Decadal Oscillation, also affect boreal fire activities (Balzter et al., 2007; Macias Fauria and Johnson, 2007; Kim et al., 2020). These climate factors modulate interannual variations and possibly the transport dynamics of pollutants from the mid-latitudes to the Arctic region (e.g. Eckhardt et al., 2003; Fisher et al., 2010).

The dominant contributor, ABF, to regional extreme AOD occurrence and magnitude in the lower European Arctic decreased slightly from 2003-2009 to 2010-2019 (Fig. 6 and 7): This observation is generally coherent with the Part 1 results showing a pan-Arctic ABF AOD decrease in the 2003-2019 period and Fig. 9. Extreme total-AOD events dominated by sea-salt contributions in the North Atlantic and Norwegian Sea increased slightly in 2010-2019. This was possibly due to the observed increase in cyclonic activities (Rinke et al., 2017; Waseda et al., 2021; Valkonen et al., 2021). Although the model simulation of CM AOD is not as skillful as that of FM, trend analysis of CM AOD which is based on relative change is arguably significant.

4. Summary

AOD data from the NAAPS-RA, the ground-based AERONET, and MAN were employed in analyzing the 2003-2019 statistics and trends of extreme Arctic-AOD events for spring and summer seasons. Extreme AODs are defined as any AOD greater than the 95th percentile (AOD_{95}) for any given distribution of AODs, whether that distribution is generated by the ensemble of AODs representing the time series of a

specific location or of a regional average. Total, FM and CM AODs at 550 nm from 6-hr resolution NAAPS-RA were first validated against AERONET and MAN AOD data. NAAPS-RA was shown to be capable of largely capturing FM and total AOD ranges and variability. The NAAPS-RA performance in simulating CM AOD was significantly better if the temporal resolution of the all-season statistics was less sensitive to high frequency dust and sea-salt events (i.e. the use of temporal resolution bins of a month rather than 6 hr). Statistics of the 6-hr Arctic AOD and extreme AOD events were analyzed. Finally, trends of extreme AOD in the Arctic were presented and analyzed.

Baseline statistics for 6hrly AOD: The median of 6-hr total AODs at 550 nm for all Arctic AERONET sites and MAN retrievals over the 2003-2019 period is 0.07 while AOD₉₅ is 0.23. Both the median and AOD₉₅ values show a dominant FM AOD contribution. The CM AOD median is 0.01 while AOD₉₅ is 0.07. The maximum AOD over the 2003-2019 period varies between 0.5-3.0 for measurements made away from BB source regions, and 1.5 to greater than 3.0 for measurements made closer to BB source regions. The seasonal NAAPS-RA spread of smoke AOD is much higher than other speciated AODs, including ABF, dust, and sea salt AODs, for all months between May and August: the spread is especially large in July and August. These late-season smoke features significantly contribute to the seasonality and interannual variabilities of extremes in total AOD.

Extreme AOD events: Extreme AOD events using the Arctic spring and summer data are largely attributable to FM AOD events, and notably BB smoke transport events in general. Extreme Arctic AOD events show large seasonal and interannual variability, with the interannual AOD variability largely modulated by BB smoke. Extreme AOD occurrences in the North American Arctic, the Asian Arctic, and the high Arctic are dominated by BB smoke events. The occurrence of regionally extreme AOD events is attributed more to ABF in the lower European Arctic. The extreme-event occurrence dominance of sea salt aerosols is largely limited to the North Atlantic and Norwegian Seas. The extreme AOD amplitudes of ABF and sea-salt AOD are, however, significantly lower than those regions where extreme-AOD smoke AOD is dominant. Even for sites distant from BB source regions, BB smoke is the principal driver of AOD variation above the AOD₉₅ threshold.

Shift of extreme AOD events from spring-summer to summer season: There is an overall increase in the maximum AOD values in the high Arctic in 2010-2019 compared to 2003-2009, suggesting stronger extreme BB smoke influence for more recent years. Extreme AOD events are observed to occur in a more balanced fashion over the entire April-August season during 2003-2009 while being more concentrated in the latter part of the season (i.e., July and August) during 2010-2019. The seasonal shift in extreme smoke AOD events is consistent with the multi-year negative MAM trend and positive

JJA trend in BB emissions (north of 50°N, Part 1). These trends are likely attributable to early season agricultural burning controls, and increased lightning activity and lightning-caused wildfires in summertime in the boreal high-latitude regions on top of the overall lower level, especially in spring, of 2010-2019 vs 2003-2009 anthropogenic aerosols. The shift in extreme smoke events is consistent with a general multi-year decreasing springtime trend and an increasing summertime trend of BB emissions north of 50°N (Part 1).

Global warming is expected to continue generating drier conditions and increased wildfire activities in the high latitudes (McCarty et al., 2021) and thus render the Arctic more susceptible to extreme smoke events. These events can significantly change the regional aerosol budget by bringing large amounts of smoke aerosols into the Arctic. These extreme smoke events will likely play an increasingly important Arctic aerosol budget role given the decreasing (Part 1) baseline in anthropogenic pollution aerosols over the 2003-2019 period. Smoke aerosols are, notably, much more light-absorbing than anthropogenic sulfate. As well, their different physical and chemical properties relative to anthropogenic aerosols will translate into different efficiencies in their role as CCN and INP. When deposited on surface snow and ice, they impact the surface radiative forcing budget by reducing surface albedo. The climate impacts of BB smoke would, accordingly, differ and possibly counteract the dynamics of anthropogenic aerosols. Therefore, the baseline AOD trends reported in Part 1 and the trends in extreme AOD events reported here are important in terms of implications for the changing Arctic climate. The greater sensitivity of Arctic climate to aerosol forcings relative to other regions of the globe (e.g. Wang et al., 2018), the impact of the extreme BB smoke events and their interannual variability and trends on Arctic climate warrants further exploration. The statistics of extreme AODs reported here are expected to help in the formulation of climate sensitivity experiments and improve our knowledge of the relative importance of aerosol processes compared to other factors of the changing Arctic climate.

Code and Data Availability: All data supporting the conclusions of this manuscript are available through the links provided below.

AERONET Version 3 Level 2 data: <http://aeronet.gsfc.nasa.gov>

MAN data: https://aeronet.gsfc.nasa.gov/new_web/maritime_aerosol_network.html

NAAPS RA AOD: https://usgodae.org/cgi-bin/datalist.pl?dset=nrl_naaps_reanalysis&summary=Go

Author contributions: P.X. designed this study, performed most of the data analysis and wrote the initial manuscript. All authors contributed to scientific discussion, revision and editing of the manuscript.

Competing interests: The authors declare that they have no conflict of interest.

Acknowledgments

We thank the NASA AERONET, and MAN, and Environment and Climate change Canada (ECCC) AEROCAN group for the sun-photometer data. We acknowledge the use of imagery from the NASA Worldview application (<https://worldview.earthdata.nasa.gov>, last access: Mar 11, 2022), and NASA CALIPSO website (<https://www-calipso.larc.nasa.gov/>).

Financial support

The authors acknowledge support from NASA's Interdisciplinary Science (IDS) program (grant no. 80NSSC20K1260), NASA's Modeling, Analysis and Prediction (MAP) program (NNX17AG52G) and the Office of Naval Research Code 322. N.O. and K.R.'s work was supported by the Canadian Space Agency, SACIA-2 project, Ref. No. 21SUASACOA, ESS-DA program.

References

- AboEl-Fetouh, Y., O'Neill, N. T., Ranjbar, K., Hesaraki, S., Abboud, I., & Sobolewski, P. S. (2020). Climatological-scale analysis of intensive and semi-intensive aerosol parameters derived from AERONET retrievals over the Arctic. *Journal of Geophysical Research: Atmospheres*, 125, e2019JD031569. <https://doi.org/10.1029/2019JD031569>
- Balzter, H., F. F. Gerard, C. T. George, C. S. Rowland, T. E. Jupp, I. McCallum, A. Shvidenko, S. Nilsson, A. Sukhinin, A. Onuchin, C. Schmullius, Impact of the Arctic Oscillation pattern on interannual forest fire variability in central Siberia. *Geophys. Res. Lett.* **32**, L14709 (2005).
- Baibakov, K., O'Neill, N. T., Ivanescu, L., Duck, T. J., Perro, C., Herber, A., Schulz, K.-H., and Schrems, O.: Synchronous polar winter starphotometry and lidar measurements at a High Arctic station, *AMT*, 8, 3789-3809, doi:10.5194/amt-8-3789-2015, 2015.
- Bieniek, P. A., Bhatt, U. S., York, A., Walsh, J. E., Lader, R., Strader, H., Ziel, R., Jandt, R. R., & Thoman, R. L. (2020). Lightning Variability in Dynamically Downscaled Simulations of Alaska's Present and Future Summer Climate, *Journal of Applied Meteorology and Climatology*, 59(6), 1139-1152.

- Birch, C. E., Brooks, I. M., Tjernström, M., Shupe, M. D., Mauritsen, T., Sedlar, J., Lock, A. P., Earnshaw, P., Persson, P. O. G., Milton, S. F., and Leck, C.: Modelling atmospheric structure, cloud and their response to CCN in the central Arctic: ASCOS case studies, *Atmos. Chem. Phys.*, 12, 3419–3435, <https://doi.org/10.5194/acp-12-3419-2012>, 2012.
- Boisvert, L.N., A.A. Petty and J.C. Stroeve, 2016: The Impact of the Extreme Winter 2015/16 Arctic Cyclone on the Barents–Kara Seas. *Monthly Weather Review*, **144** (11), 4279–4287, doi:10.1175/mwr-d-16-0234.1.
- Bossioli, E., Sotiropoulou, G., Methymaki, G., & Tombrou, M. (2021). Modeling extreme warm-air advection in the Arctic during summer: The effect of mid-latitude pollution inflow on cloud properties. *Journal of Geophysical Research: Atmospheres*, 126, e2020JD033291. <https://doi.org/10.1029/2020JD033291>
- Coogan, S. C. P., Cai, X., Jain, P., and Flannigan, M. D. (2020) Seasonality and trends in human- and lightning-caused wildfires ≥ 2 ha in Canada, 1959–2018. *International Journal of Wildland Fire* **29**, 473-485. <https://doi.org/10.1071/WF19129>
- Coopman, Q., Garrett, T. J., Finch, D. P., & Riedi, J. (2018). High sensitivity of arctic liquid clouds to long-range anthropogenic aerosol transport. *Geo-physical Research Letters*, 45, 372–381. <https://doi.org/10.1002/2017GL075795>
- Dang, C., S. G. Warren, Q. Fu, S. J. Doherty, M. Sturm, and J. Su (2017), Measurements of light-absorbing particles in snow across the Arctic, North America, and China: Effects on surface albedo, *J. Geophys. Res. Atmos.*, 122, 10,149–10,168, doi:10.1002/2017JD027070.
- Das, S., Colarco, P. R., Oman, L. D., Taha, G., and Torres, O.: The long-term transport and radiative impacts of the 2017 British Columbia pyrocumulonimbus smoke aerosols in the stratosphere, *Atmos. Chem. Phys.*, 21, 12069–12090, <https://doi.org/10.5194/acp-21-12069-2021>, 2021.
- DeRepentigny, P., Jahn, A., Holland, M., Fasullo, J., Lamarque, J.-F., Hannay, C., Mills, M., Bailey, D., Tilmes, S., and Barrett, A.: Impact of CMIP6 biomass burning emissions on Arctic sea ice loss, EGU General Assembly 2021, online, 19–30 Apr 2021, EGU21-9020, <https://doi.org/10.5194/egusphere-egu21-9020>, 2021.

Eck, T. F., et al. (2009), Optical properties of boreal region biomass burning aerosols in central Alaska and seasonal variation of aerosol optical depth at an Arctic coastal site, *J. Geophys. Res.*, 114, D11201, doi:10.1029/2008JD010870.

Eckhardt, S., A. Stohl, S. Beirle, N. Spichtinger, P. James, C. Forster, C. Junker, T. Wagner, U. Platt, and S. G. Jennings (2003), The North Atlantic Oscillation controls air pollution transport to the Arctic, *Atmos. Chem. Phys.*, 3(5), 1769–1778, doi:10.5194/acp-3-1769-2003.

Engelmann, R., Ansmann, A., Ohneiser, K., Griesche, H., Radenz, M., Hofer, J., Althausen, D., Dahlke, S., Maturilli, M., Veselovskii, I., Jimenez, C., Wiesen, R., Baars, H., Bühl, J., Gebauer, H., Haarig, M., Seifert, P., Wandinger, U., and Macke, A.: Wildfire smoke, Arctic haze, and aerosol effects on mixed-phase and cirrus clouds over the North Pole region during MOSAiC: an introduction, *Atmos. Chem. Phys.*, 21, 13397–13423, <https://doi.org/10.5194/acp-21-13397-2021>, 2021.

Evangeliou, N., Balkanski, Y., Hao, W. M., Petkov, A., Silverstein, R. P., Corley, R., Nordgren, B. L., Urbanski, S. P., Eckhardt, S., Stohl, A., Tunved, P., Crepinsek, S., Jefferson, A., Sharma, S., Nøjgaard, J. K., and Skov, H.: Wildfires in northern Eurasia affect the budget of black carbon in the Arctic – a 12-year retrospective synopsis (2002–2013), *Atmos. Chem. Phys.*, 16, 7587–7604, <https://doi.org/10.5194/acp-16-7587-2016>, 2016.

Fisher, J. A., et al. (2010), Source attribution and interannual variability of Arctic pollution in spring constrained by aircraft (ARCTAS, ARCPAC) and satellite (AIRS) observations of carbon monoxide, *Atmos. Chem. Phys.*, 10(3), 977–996, doi:10.5194/acp-10-977-2010.

Flanner, M. G., Zender, C. S., Randerson, J. T., & Rasch, P. J. (2007). Present-day climate forcing and response from black carbon in snow. *Journal of Geophysical Research*, 112(September 2006), D11202. <https://doi.org/10.1029/2006JD008003>

Garrett, T. J., Zhao, C., and Novelli, P.: Assessing the relative contributions of transport efficiency and scavenging to seasonal variability in Arctic aerosol, *Tellus B*, 62, 190–196, <https://doi.org/10.1111/j.1600-0889.2010.00453.x>, 2010.

Giles, D. M., Sinyuk, A., Sorokin, M. G., Schafer, J. S., Smirnov, A., Slutsker, I., Eck, T. F., Holben, B. N., Lewis, J. R., Campbell, J. R., Welton, E. J., Korkin, S. V., and Lyapustin, A. I.: Advancements in the Aerosol Robotic Network (AERONET) Version 3 database – automated near-real-time quality control algorithm with improved cloud

screening for Sun photometer aerosol optical depth (AOD) measurements, *Atmos. Meas. Tech.*, 12, 169–209, <https://doi.org/10.5194/amt-12-169-2019>, 2019.

Hall, J. V., Loboda, T. V., Giglio, L., McCarty G. W. (2016), A MODIS-based burned area assessment for Russian croplands: Mapping requirements and challenges. *Remote Sensing of Environment*, Vol. 184, 506-521. <https://doi.org/10.1016/j.rse.2016.07.022>

Hesarakis S, O'Neill NT, Lesins G, Saha A, Martin RV, Fioletov VE, Baibakov K, Abboud I. Comparisons of a chemical transport model with a four-year (April to September) analysis of fine-and coarse-mode aerosol optical depth retrievals over the Canadian Arctic. *Atmosphere-Ocean*. 2017 Oct 20;55(4-5):213-29.

Hogan, T.F. and T.E. Rosmond: The description of the Navy Operational Global Atmospheric Prediction System's spectral forecast model. *Mon. Wea. Rev.*, 119, 1786-1815, 1991.

Hyer, E. J., J. S. Reid, and J. Zhang, 2011: An over-land aerosol optical depth data set for data assimilation by filtering, correction, and aggregation of MODIS Collection 5 optical depth retrievals. *Atmospheric Measurement Techniques*, European Geophysical Union, 379-408.

IPCC Chapter 6, Szopa, S., V. Naik, B. Adhikary, P. Artaxo, T. Berntsen, W.D. Collins, S. Fuzzi, L. Gallardo, A. Kiendler-Scharr, Z. Klimont, H. Liao, N. Unger, and P. Zanis, 2021: Short-Lived Climate Forcers. In *Climate Change 2021: The Physical Science Basis. Contribution of Working Group I to the Sixth Assessment Report of the Intergovernmental Panel on Climate Change* [Masson-Delmotte, V., P. Zhai, A. Pirani, S.L. Connors, C. Péan, S. Berger, N. Caud, Y. Chen, L. Goldfarb, M.I. Gomis, M. Huang, K. Leitzell, E. Lonnoy, J.B.R. Matthews, T.K. Maycock, T. Waterfield, O. Yelekçi, R. Yu, and B. Zhou (eds.)]. Cambridge University Press, Cambridge, United Kingdom and New York, NY, USA, pp. 817–922, doi:10.1017/9781009157896.008.

Jacob, D. J., J. H. Crawford, H. Maring, A. D. Clarke, J. E. Dibb, L. K. Emmons, R. A. Ferrare, C. A. Hostetler, P. B. Russell, and H. B. Singh (2010), The arctic research of the composition of the troposphere from aircraft and satellites (ARCTAS) mission: Design, execution, and first results, *Atmos. Chem. Phys.*, 10(11), 5191–5212.

Kang S., Y. Zhang, Y. Qian, and H. Wang. 2020. "A review of black carbon in snow and ice and its impact on the cryosphere." *Earth - Science Reviews* 210. PNNL-SA-154137. [doi:10.1016/j.earscirev.2020.103346](https://doi.org/10.1016/j.earscirev.2020.103346)

Khan, A. L., S. Wagner, R. Jaffe, P. Xian, M. Williams, R. Armstrong, and D. McKnight (2017), Dissolved black carbon in the global cryosphere: Concentrations and chemical signatures, *Geophys. Res. Lett.*, 44, 6226–6234, doi:10.1002/2017GL073485.

Kaku, K. C., Reid, J. S., Hand, J. L., Edgerton, E. S., Holben, B. N., Zhang, J., & Holz, R. E.: Assessing the challenges of surface-level aerosol mass estimates from remote sensing during the SEAC⁴RS and SEARCH campaigns: Baseline surface observations and remote sensing in the southeastern United States. *Journal of Geophysical Research: Atmospheres*, 123, 7530–7562. <https://doi.org/10.1029/2017JD028074>, 2018.

Korontzi, S., J. McCarty, T. Loboda, S. Kumar, and C. Justice (2006), Global distribution of agricultural fires in croplands from 3 years of Moderate Resolution Imaging Spectroradiometer (MODIS) data, *Global Biogeochem. Cycles*, 20, GB2021, doi:10.1029/2005GB002529.

Leck, C. and Svensson, E.: Importance of aerosol composition and mixing state for cloud droplet activation over the Arctic pack ice in summer, *Atmos. Chem. Phys.*, 15, 2545–2568, <https://doi.org/10.5194/acp-15-2545-2015>, 2015.

Levy, R. C., Remer, L. A., Kleidman, R. G., Mattoo, S., Ichoku, C., Kahn, R., and Eck, T. F.: Global evaluation of the Collection 5 MODIS dark-target aerosol products over land, *Atmos. Chem. Phys.*, 10, 10399–10420, <https://doi.org/10.5194/acp-10-10399-2010>, 2010.

Lund Myhre, C., Toledano, C., Myhre, G., Stebel, K., Yttri, K. E., Aaltonen, V., Johnsrud, M., Frioud, M., Cachorro, V., de Frutos, A., Lihavainen, H., Campbell, J. R., Chaikovsky, A. P., Shiobara, M., Welton, E. J., and Tørseth, K.: Regional aerosol optical properties and radiative impact of the extreme smoke event in the European Arctic in spring 2006, *Atmos. Chem. Phys.*, 7, 5899–5915, <https://doi.org/10.5194/acp-7-5899-2007>, 2007.

Lynch, P., J. S. Reid, D. L. Westphal, J. Zhang, T. Hogan, E. J. Hyer, C. A. Curtis, D. Hegg, Y. Shi, J. R. Campbell, J. Rubin, W. Sessions, J. Turk and A. Walker: An 11-year Global Gridded Aerosol Optical Thickness Reanalysis (v1.0) for Atmospheric and Climate Sciences. *Geosci. Model Dev.*, 9, 1489–1522, doi:10.5194/gmd-9-1489-2016, 2016.

Macias Fauria, M, E. A. Johnson, Large-scale climatic patterns control large lightning fire occurrence in Canada and Alaska forest regions. *J. Geophys. Res.* **111**, G04008 (2006).

Markowicz, K. M., et al. (2016), Impact of North American intense fires on aerosol optical properties measured over the European Arctic in July 2015, *J. Geophys. Res. Atmos.*, 121, 14,487–14,512, doi:10.1002/2016JD025310.

Markowicz, K.M., Lisok, J., Xian, P., Simulation of long-term direct aerosol radiative forcing over the arctic within the framework of the iAREA project, *Atmospheric Environment* (2021), doi: <https://doi.org/10.1016/j.atmosenv.2020.117882>.

Mauritsen, T., Sedlar, J., Tjernström, M., Leck, C., Martin, M., Shupe, M., Sjogren, S., Sierau, B., Persson, P. O. G., Brooks, I. M., and Swietlicki, E.: An Arctic CCN-limited cloud-aerosol regime, *Atmos. Chem. Phys.*, 11, 165–173, <https://doi.org/10.5194/acp-11-165-2011>, 2011.

McCarty, J. L., Aalto, J., Paunu, V.-V., Arnold, S. R., Eckhardt, S., Klimont, Z., Fain, J. J., Evangeliou, N., Venäläinen, A., Tchebakova, N. M., Parfenova, E. I., Kupiainen, K., Soja, A. J., Huang, L., and Wilson, S.: Reviews & Syntheses: Arctic Fire Regimes and Emissions in the 21st Century, *Biogeosciences Discuss.* [preprint], <https://doi.org/10.5194/bg-2021-83>, in review, 2021.

O'Neill, N.T., T.F.Eck, B.N.Holben, A.Smirnov, O.Dubovik, and A.Royer (2001) Bimodal size distribution influences on the variation of Angstrom derivatives in spectral and optical depth space, *J. Geophys. Res.*, 106, 9787-9806.

O'Neill, N. T., Eck, T. F., Smirnov, A., Holben, B. N., and Thulasiraman S. (2003) Spectral discrimination of coarse and fine mode optical depth. *J. Geophys. Res.*, 108, D05212, doi:10.1029/2002JD002975.

Peterson, D. A., E. J. Hyer, J. R. Campbell, J. E. Solbrig and M. D. Fromm (2017), A conceptual model for development of intense pyroconvection in western North America. *Mon. Wea. Rev.*, **145**, 2235-2255, DOI: 10.1175/MWR-D-16-0232.1.

Peterson, D. A., J. R. Campbell, E. J. Hyer, M. D. Fromm, G. P. Kablick, J. H. Cossuth, and M. T. Deland (2018), Wildfire-driven thunderstorms cause a volcano-like stratospheric injection of smoke. *NPJ Clim. and Atmos. Sci.*, 1:30; <https://doi.org/10.1038/s41612-018-0039-3>.

Prenni, A. J., Harrington, J. Y., Tjernström, M., DeMott, P. J., Avramov, A., Long, C. N., Kreidenweis, S. M., Olsson, P. Q., and Verlinde, J.: Can ice-nucleating aerosols affect arctic seasonal climate?, *B. Am. Meteorol. Soc.*, 88, 541–550, <https://doi.org/10.1175/BAMS-88-4-541>, 2007.

Quinn, P. K., et al. (2008), Short-lived pollutants in the Arctic: Their climate impact and possible mitigation strategies, *Atmos. Chem. Phys.*, 8(6), 1723–1735, doi:10.5194/acp-8-1723-2008.

Randerson, J. T., and Coauthors, 2006: The impact of boreal forest fire on climate warming. *Science*, 314, 1130–1132, doi:[10.1126/science.1132075](https://doi.org/10.1126/science.1132075).

Ranjbar, K., O'Neill, N. T., Lutsch, E., McCullough, E. M., AboEl-Fetouh, Y., Xian, P., et al. (2019). Extreme smoke event over the high Arctic. *Atmospheric Environment*, 218, 117002. <https://doi.org/10.1016/j.atmosenv.2019.117002>

Ranjbar, K., O'Neill, N. T., and Aboel-Fetouh, Y.: Comment on “Short-cut transport path for Asian dust directly to the Arctic: a case Study” by Huang et al. (2015) in *Environ. Res. Lett.*, *Atmos. Chem. Phys.*, 22, 1757–1760, <https://doi.org/10.5194/acp-22-1757-2022>, 2022.

Reid, J. S., Hyer, E. J., Prins, E. M., Westphal, D. L., Zhang, J., Wang, J., Christopher, S. A., Curtis, C. A., Schmidt, C. C., Eleuterio, D. P., Richardson, K. A., and Hoffman, J. P.: Global Monitoring and Forecasting of Biomass-Burning Smoke: Description of and Lessons from the Fire Locating and Modeling of Burning Emissions (FLAMBE) Program, *IEEE J. Sel. Top. Appl.*, 2, 144–162, JSTARS-2009-00034, 2009.

Reid, J. S., Koppmann, R., Eck, T. F., and Eleuterio, D. P.: A review of biomass burning emissions part II: intensive physical properties of biomass burning particles, *Atmos. Chem. Phys.*, 5, 799–825, <https://doi.org/10.5194/acp-5-799-2005>, 2005.

Rinke, A., Maturilli, M., Graham, R. M., Hatthes, H., Handorf, D., Cohen, L., Hudson, S. R. and Moore, J. C., (2017), Extreme cyclone events in the Arctic: Wintertime variability and trends. *Environ. Res. Lett.* **12** 094006

Saha, A., et al. (2010), Pan-Arctic sunphotometry during the ARCTAS-A campaign of April 2008, *Geophys. Res. Lett.*, 37, L05803, doi:10.1029/2009GL041375.

Sand, M., T. K. Berntsen, Ø. Seland, and J. E. Kristjánsson (2013), Arctic surface temperature change to emissions of black carbon within Arctic or midlatitudes, *J. Geophys. Res. Atmos.*, 118, 7788–7798, doi:10.1002/jgrd.50613.

Serreze, M.C. and R.G. Barry, 2011: Processes and impacts of Arctic amplification: A research synthesis. *Global and Planetary Change*, **77** (1– 2), 85–96, doi:10.1016/j.gloplacha.2011.03.004.

Serreze, M.C., Francis, J.A. The Arctic Amplification Debate. *Climatic Change* **76**, 241–264 (2006). <https://doi.org/10.1007/s10584-005-9017-y>

Sharma, S., M. Ishizawa, D. Chan, D. Lavoué, E. Andrews, K. Eleftheriadis, and S. Maksyutov (2013), 16-year simulation of Arctic black carbon: Transport, source

contribution, and sensitivity analysis on deposition, *J. Geophys. Res. Atmos.*, 118, 943–964, doi:10.1029/2012JD017774.

Shi, Y., J. Zhang, J. S. Reid, E. J. Hyer, and N. C. Hsu, 2013: Critical evaluation of the MODIS Deep Blue aerosol optical depth product for data assimilation over North Africa. *Atmospheric Measurement Techniques*, **6**, 949–969.

Shi, Y., J. Zhang, J. S. Reid, B. Holben, E. J. Hyer, and C. Curtis, 2011: An analysis of the collection 5 MODIS over-ocean aerosol optical depth product for its implication in aerosol assimilation. *Atmos. Chem. Phys.*, **11**, 557–565.

Shindell, D. and Faluvegi, G.: Climate response to regional radiative forcing during the twentieth century, *Nat. Geosci.*, 2, 294–300, <https://doi.org/10.1038/ngeo473>, 2009.

Schlosser, J. S., R. A. Braun, T. Bradley, H. Dadashazar, A. B. MacDonald, A. A. Aldhaif, M. A. Aghdam, A. H. Mardi, P. Xian, and A. Sorooshian (2017), Analysis of aerosol composition data for western United States wildfires between 2005 and 2015: Dust emissions, chloride depletion, and most enhanced aerosol constituents, *J. Geophys. Res. Atmos.*, 122, 8951–8966, doi:10.1002/2017JD026547.

Skiles S. M., Flanner, M., Cook, J. M., Dumont, M. and Painter, T. (2018) Radiative forcing by light-absorbing particles in snow. *Nature Climate Change*, 8, 964–971. <https://doi.org/10.1038/s41558-018-0296-5>

Sogacheva, L., Popp, T., Sayer, A. M., Dubovik, O., Garay, M. J., Heckel, A., Hsu, N. C., Jethva, H., Kahn, R. A., Kolmonen, P., Kosmale, M., de Leeuw, G., Levy, R. C., Litvinov, P., Lyapustin, A., North, P., Torres, O., and Arola, A.: Merging regional and global aerosol optical depth records from major available satellite products, *Atmos. Chem. Phys.*, 20, 2031–2056, <https://doi.org/10.5194/acp-20-2031-2020>, 2020.

Stohl, A., et al. (2006), Pan-Arctic enhancements of light absorbing aerosol concentrations due to North American boreal forest fires during summer 2004, *J. Geophys. Res.*, 111, D22214, doi:10.1029/2006JD007216.

Stohl, A., et al. (2007), Arctic smoke—Record high air pollution levels in the European Arctic due to agricultural fires in eastern Europe in spring 2006, *Atmos. Chem. Phys.*, 7(2), 511–534, doi:10.5194/acp-7-511-2007.

Stone, R. S., G. P. Anderson, E. P. Shettle, E. Andrews, K. Loukachine, E. G. Dutton, C. Schaaf, and M. O. Roman III (2008), Radiative impact of boreal smoke in the Arctic: Observed and modeled, *J. Geophys. Res.*, 113, D14S16,

doi:10.1029/2007JD009657.

Tomasi, C., Vitale, V., Lupi, A., Di Carmine, C., Campanelli, M., Herber, A., Treffeisen, R., Stone, R. S., Andrews, E., Sharma, S., Radionov, V., von Hoyningen-Huene, W., Stebel, K., Hansen, G. H., Myhre, C. L., Wehrli, C., Aaltonen, V., Lihavainen, H., Virkkula, A., Hillamo, R., Ström, J., Toledano, C., Cachorro, V. E., Ortiz, P., de Frutos, A. M., Blindheim, S., Frioud, M., Gausa, M., Zielinski, T., Petelski, T., & Yamanouchi, T. (2007). Aerosols in polar regions: a historical overview based on optical depth and in situ observations. *Journal of Geophysical Research, Atmospheres*, 112, D16. <https://doi.org/10.1029/2007JD008432>.

Torres, O., Bhartia, P. K., Taha, G., Jethva, H., Das, S., Colarco, P., Krotkov, N., Omar, A., and Ahn, C.: Stratospheric Injection of Massive Smoke Plume From Canadian Boreal Fires in 2017 as Seen by DSCOVR-EPIC, CALIOP, and OMPS-LP Observations, *J. Geophys. Res.-Atmos.*, 125, e2020JD032579, <https://doi.org/10.1029/2020JD032579>, 2020.

Tosca, M, J. Campbell, M. Garay, S. Lolli, F. Seidel, J. Marquis, and O. Kalashnikova (2017), Attributing accelerated summertime warming in the southeast United States to recent reductions in aerosol burden: indications from vertically-resolved observations. *Remote Sens.*, 9, 674, doi:10.3390/rs9070674.

Wang, Y., J. Jiang, H. Su, S. Choi, L. Huang, J. Guo and Y. Yung: Elucidating the Role of Anthropogenic Aerosols in Arctic Sea Ice Variations. *J. Climate*, 31(1), 99-114, 2018. <https://doi.org/10.1029/2006JD007234>

Warneke, C., Froyd, K. D., Brioude, J., Bahreini, R., Brock, C. A., Cozic, J., et al. (2010). An important contribution to springtime Arctic aerosol from biomass burning in Russia. *Geophysical Research Letters*, 37, L01801. <https://doi.org/10.1029/2009GL041816>

Wendisch, M., Macke, A., Ehrlich, A., Lupkes, C., Mech, M., Chechin, D., et al. (2019). The Arctic cloud puzzle: Using ACLOUD/PASCAL multiplatform observations to unravel the role of clouds and aerosol particles in Arctic amplification. *Bulletin of the American Meteorological Society*, 100, 841–871. <https://doi.org/10.1175/BAMS-D-18-0072.1>

Wex, H., Huang, L., Zhang, W., Hung, H., Traversi, R., Becagli, S., Sheesley, R. J., Moffett, C. E., Barrett, T. E., Bossi, R., Skov, H., Hünnerbein, A., Lubitz, J., Löffler, M., Linke, O., Hartmann, M., Herenz, P., and Stratmann, F.: Annual variability of ice-nucleating particle concentrations at different Arctic locations, *Atmos. Chem. Phys.*, 19, 5293–5311, <https://doi.org/10.5194/acp-19-5293-2019>, 2019.

Xian, P., J. S. Reid, J. F. Turk, E. J. Hyer and D. L. Westphal: Impact of models versus satellite measured tropical precipitation on regional smoke optical thickness in an aerosol transport model, *Geophys. Res. Lett.*, 36, L16805, doi:10.1029/2009GL038823, 2009.

Xian, P., Reid J. S., Hyer, E., Sampson, C.R., Rubin, J., Ades M., et. al., Current state of the global operational aerosol multi-model ensemble: an update from the International Cooperative for Aerosol Prediction (ICAP), 2019, Quarterly J. of the Royal Met. Soc. <https://doi.org/10.1002/qj.3497>

Yang, Y., Wang, H., Smith, S. J., Easter, R. C., and Rasch, P. J.: Sulfate Aerosol in the Arctic: Source Attribution and Radiative Forcing, *J. Geophys. Res.-Atmos.*, 123, 1899–1918, <https://doi.org/10.1002/2017JD027298>, 2018.

Yumimoto, K., Tanaka, T. Y., Oshima, N., and Maki, T.: JRAero: the Japanese Reanalysis for Aerosol v1.0, *Geosci. Model Dev.*, 10, 3225–3253, <https://doi.org/10.5194/gmd-10-3225-2017>, 2017.

Zamora, L. M., Kahn, R. A., Cubison, M. J., Diskin, G. S., Jimenez, J. L., Kondo, Y., McFarquhar, G. M., Nenes, A., Thornhill, K. L., Wisthaler, A., Zelenyuk, A., and Ziemba, L. D.: Aircraftmeasured indirect cloud effects from biomass burning smoke in the Arctic and subarctic, *Atmos. Chem. Phys.*, 16, 715–738, <https://doi.org/10.5194/acp-16-715-2016>, 2016.

Zhang, J. L., and J. S. Reid, 2006: MODIS aerosol product analysis for data assimilation: Assessment of over-ocean level 2 aerosol optical thickness retrievals. *J. Geophys. Res.-Atmos.*, 111.

Zhang, J. and Reid, J. S.: A decadal regional and global trend analysis of the aerosol optical depth using a data-assimilation grade over-water MODIS and Level 2 MISR aerosol products, *Atmos. Chem. Phys.*, 10, 18879–18917, doi:10.5194/acpd-10-18879-2010, 2010.

Zhang, J., Reid, J. S., Alfaro-Contreras, R., and Xian, P.: Has China been exporting less particulate air pollution over the past decade?, *Geophys. Res. Lett.*, 44, 2941– 2948, doi:[10.1002/2017GL072617](https://doi.org/10.1002/2017GL072617), 2017

Zhang, J. L., J. S. Reid, D. L. Westphal, N. L. Baker, and E. J. Hyer, 2008: A system for operational aerosol optical depth data assimilation over global oceans. *J. Geophys. Res.*, 113, D10208, doi:[10.1029/2007JD009065](https://doi.org/10.1029/2007JD009065).

1037

1038 Zhao, C., & Garrett, T. J. (2015). Effects of Arctic haze on surface cloud radiative
1039 forcing. *Geophysical Research Letters*, 42, 557–564.

1040 <https://doi.org/10.1002/2014GL062015>

1041

1042 Zhang, Z.; Wang, L.; Xue, N.; Du, Z. Spatiotemporal Analysis of Active Fires in the
1043 Arctic Region during 2001–2019 and a Fire Risk Assessment Model. *Fire* **2021**, 4, 57.

1044 <https://doi.org/10.3390/fire4030057>

1045

1046